

Efficient Implementation of Third-order Tensor Methods with Adaptive Regularization for Unconstrained Optimization

Coralia Cartis¹, Raphael Hauser¹, Yang Liu¹, Karl Welzel¹,
and Wenqi Zhu¹

¹Mathematical Institute, University of Oxford*[†]

{coralia.cartis, raphael.hauser, yang.liu, karl.welzel, wenqi.zhu}@maths.ox.ac.uk

3rd January 2025

Abstract

High-order tensor methods that employ Taylor-based local models of positive integer degree p within adaptive regularization frameworks have recently garnered significant research interest for both convex and nonconvex optimization problems. The well-known p th-order adaptive regularization (AR p) method has demonstrated optimal worst-case global convergence rates and local convergence rates. At each iteration of this method, a local model of the objective function, consisting of a p th-order Taylor approximation and a $(p + 1)$ th-order regularization term, is minimized. However, for $p \geq 2$, the subproblem typically contains multiple local minima. It is recommended to solve the subproblem globally when $p = 2$, as the global minimizer is guaranteed to be a descent direction. However, for any $p \geq 3$, it remains an open question how to efficiently minimize the subproblem and which minimizer to select. In this context, designing efficient AR p variants is a critical area of interest, especially for $p \geq 3$. In this paper, we extend the interpolation-based updating strategies, originally introduced by [Gould, Porcelli and Toint, *Comput Optim Appl*, Vol. 53, 2012, pp. 1–22] for $p = 2$, to cases where $p \geq 3$.

*The order of the authors is alphabetical; Yang Liu and Karl Welzel are the primary contributors.

[†]This work was supported by the Hong Kong Innovation and Technology Commission (InnoHK Project CIMDA).

This updating strategy enables the regularization parameter to adjust adaptively based on interpolation models. We propose a novel prerejection mechanism that rejects unwanted subproblem minimizers prior to any function evaluations, thereby reducing computational costs for $p \geq 3$. Numerical results illustrate how the proposed interpolation-based updating strategy and the prerejection mechanism for $p = 3$ enhance the overall numerical performance.

1. Introduction

In this paper, we consider the unconstrained nonconvex optimization problem,

$$\min_{\mathbf{x} \in \mathbb{R}^d} f(\mathbf{x})$$

where $f: \mathbb{R}^d \rightarrow \mathbb{R}$ and $f \in \mathcal{C}^{p,1}(\mathbb{R}^d)$ which means that f is p times continuously differentiable ($p \geq 1$), bounded below and the p th derivative of f is globally Lipschitz continuous. Recent research, including [7, 9, 10, 13, 14, 19], has demonstrated that certain optimization algorithms can achieve both p th-order local convergence and optimal worst-case global complexity bounds [15] for nonconvex functions. In these methods, a local model $m_k(\mathbf{s})$ is constructed to approximate $f(\mathbf{x} + \mathbf{s})$ based on a regularized p th-order Taylor expansion. Recall the p th-order Taylor expansion of $f(\mathbf{x}_k + \mathbf{s})$ at \mathbf{x}_k can be written as

$$t_k(\mathbf{s}) = t_{\mathbf{x}_k}^p(\mathbf{s}) = f(\mathbf{x}_k) + \sum_{j=1}^p \frac{1}{j!} \nabla^j f(\mathbf{x}_k) [\mathbf{s}]^j, \quad (1)$$

where k is the iteration counter, $\nabla^j f(\mathbf{x}_k) \in \mathbb{R}^{\otimes j d}$ is a j th-order tensor, $\mathbb{R}^{\otimes j d}$ denotes the j -fold tensor product of \mathbb{R}^d and $\nabla^j f(\mathbf{x}_k) [\mathbf{s}]^j$ is the j th derivative of f at \mathbf{x}_k along direction $\mathbf{s} \in \mathbb{R}^d$.¹ To ensure that the local model m_k is bounded below, a $(p+1)$ st-order regularization term scaled by $\sigma_k \geq 0$ is added to t_k . The model m_k is given by

$$m_k(\mathbf{s}) = m_{\mathbf{x}_k, \sigma_k}^p(\mathbf{s}) = t_k(\mathbf{s}) + \frac{\sigma_k}{p+1} \|\mathbf{s}\|^{p+1}. \quad (2)$$

The iterate \mathbf{x}_k is then updated by approximately minimizing this model to find a step \mathbf{s}_k , and setting $\mathbf{x}_{k+1} = \mathbf{x}_k + \mathbf{s}_k$, provided that a sufficient decrease in the objective function is achieved. This process continues until an approximate local minimizer of f is found.

Inside the p th-order adaptive regularization framework (AR p) [7, 13, 14], the regularization parameter σ_k is adjusted adaptively to ensure progress towards optimality over the iterations. Under Lipschitz continuity assumptions on $\nabla^p f$, the AR p algorithm requires no more than $\mathcal{O}(\varepsilon^{-(p+1)/p})$ evaluations of f and its derivatives to compute an approximate first-order local minimizer that satisfies $\|\nabla f(\mathbf{x}_k)\| \leq \varepsilon^2$, which is optimal for this function class [9, 15]. This result demonstrates that as we increase the order p , the evaluation complexity bound improves. The same holds for the rate of local convergence.

¹This notation is equivalent to the multi-index notation for the multidimensional Taylor expansion

$$t_{\mathbf{x}_k}^p(\mathbf{s}) = \sum_{|\alpha| \leq p} \frac{1}{\alpha!} D^\alpha f(\mathbf{x}_k) \mathbf{s}^\alpha \text{ since } \frac{1}{j!} \nabla^j f(\mathbf{x}_k) [\mathbf{s}]^j = \sum_{|\alpha|=j} \frac{1}{\alpha!} D^\alpha f(\mathbf{x}_k) \mathbf{s}^\alpha.$$

²Unless otherwise stated, $\|\cdot\|$ denotes the Euclidean norm in this paper.

As [19] show, the AR_p method achieves a p th-order local rate if the objective function is strongly convex and σ_k is chosen large enough, depending on the Lipschitz constant of $\nabla^p f$. These results, suggesting superior performance of higher-order methods, motivate us to develop an efficient algorithmic implementation for the AR_p method.

It is widely observed that second-order methods with inexact Hessian information generally exhibit superior practical performance compared to first-order methods [22, 29, 31, 40]. Such observations align with theoretical analyses by the same authors that provide insight into why second-order methods can be expected to have lower outer iteration complexity. A key factor in designing second-order methods that are efficient in practice is being able to solve the subproblems at low computational cost.

While this line of research makes a convincing argument that it pays off to move from first- to second-order methods if the application permits it, it remains unknown whether higher order methods, such as AR_p with $p \geq 3$, have the potential to further improve the practical performance of second-order methods, and this is unclear even for performance measures that ignore the computational cost of subproblem solves. Rather than using overall wall clock time, the relevant literature so far focuses on investigating if higher-order methods can be designed to achieve stable improvement over AR2 in terms of outer iteration complexity. The current paper will also focus on this question in the context of AR_p methods for $p \geq 3$. Before giving further technical details, we illustrate the potential benefits in [Example 1.1](#).

Example 1.1. The following examples demonstrate the potential for superior performance of third-order methods compared to first- or second-order methods. We constructed two functions that incorporate key information about the local shape of the function inside the third-order derivative and report the path of iterates for AR1, AR2, and AR3. The iterates were generated using the AR_p method ([Algorithm 1.1](#)), where the initial σ_0 was set to 50, and we applied a non-decreasing strategy for all candidates, i.e., σ_k was only increased when an iteration was unsuccessful (in the sense of [Procedure 1.2](#)) but never decreased. Note that σ_k remained constant during both “slalom” and “hairpin turn” experiments, i.e., all iterates in [Figure 1](#) are successful. Each subproblem is solved by the Matlab steepest descent algorithm starting at $\mathbf{s}_0 = (-0.1, 0)^\top$ and terminating when $\|\nabla m_k(\mathbf{s})\| < 10^{-9}$. The subproblem starting point is slightly shifted toward the direction of rapid decrease to provide additional opportunities for the subproblem solver to find minimizers with smaller objective function values in each iteration.

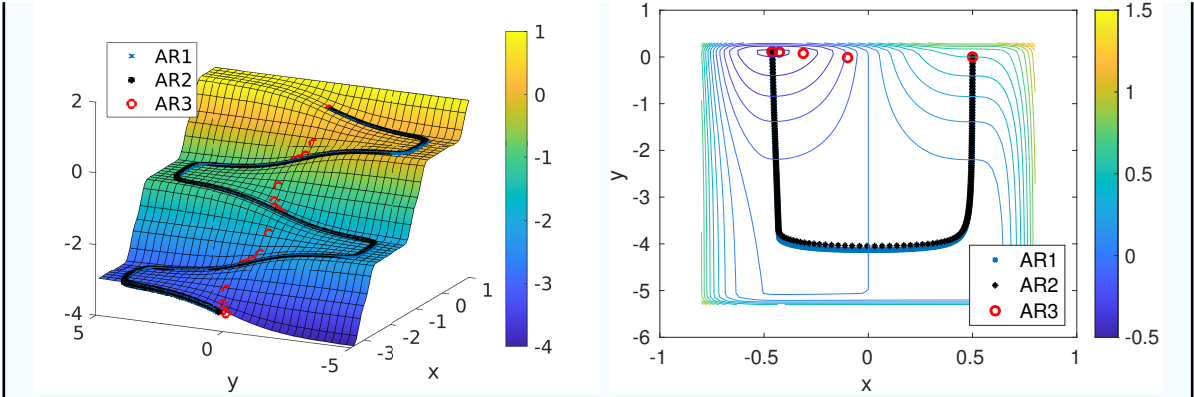


Figure 1: Two examples, namely the “slalom” (left) and “hairpin turn” (right), illustrate the potential benefits of increasing p . The starting point was set to $\mathbf{x}_0 = (0.5, 0)^\top$ for both experiments. By leveraging curvature information, AR2 requires fewer iterations and can turn earlier than AR1. However, AR3 is capable of utilizing higher-order curvature information, resulting in a dramatic decrease of iterations. The total number of iterations for the “slalom” experiment using AR1, AR2, and AR3 were 29 529, 935, and 18, respectively, while the total number of iterations for the “hairpin turn” experiment are 7 630, 230, and 5. For more details about the construction of these functions, see [Appendix A.4](#).

The left image in [Figure 1](#) shows the periodic and unbounded slalom function (40). AR1 and AR2 both take small steps along a curving path. Only in the AR3 method does the local Taylor expansion include crucial information about the curvature in the negative x direction, enabling the iterates to follow the steep ‘downhill’ path. The image on right-hand side of [Figure 1](#) is using the hairpin turn function (39), which has the same structure as one turn of the slalom function but is modified such that it has a global minimum close to $(-0.5, 0)^\top$. Again, knowledge of the third derivative allows AR3 to find the minimizer using significantly fewer iterations than AR1 and AR2. Please see [Appendix A.4](#) for more details on both functions’ construction.

AR p methods are quite well understood theoretically: Nesterov et al. have contributed extensively to the field of convex higher-order methods including AR p [34, 35, 36, 37, 38] and the authors of [7, 9, 10, 14] derived worst-case global complexity bounds for AR p and showed that they are optimal for p th-order methods in the non-convex case.

Somewhat in contrast, the efficient implementation of higher-order methods remains an active area of investigation in which the community has not yet settled on a consensus: Earlier work by Schnabel et al. [18, 42, 43] resulted in a practical tensor algorithm for solving unconstrained optimization problems. Their idea is to construct a fourth order local model based on exact first- and second-order information and choosing the third- and fourth-order term such that the model interpolates previous function values and gradients. This model is used within a trust-region framework to ensure consistent

progress. Recently, [1] introduced a higher-order Newton model with polynomial work per iteration, with adaptive regularization parameter updates provided by [47]. However, since this method is based on semidefinite programming, it does not scale well to problems of medium and large size.

Let us now comment more specifically on the progress on AR_p methods: In the case of $p = 1$ (AR1), the minimizer of the model in (2) is a steepest descent step. The case of $p = 2$ (AR2) recovers the widely researched (adaptive) cubic regularization framework (ARC) [11, 12, 21, 28, 32, 39]. In the ARC framework, efficient iterative algorithms are available for finding the global minimizer of the subproblem [11, 15]. Moreover, specific strategies for choosing the regularization parameter are available [11, 16, 24, 26, 39]. The AR_p algorithm with $p = 3$ was investigated by Birgin et al. [6] who compared the numerical performance of AR2 and AR3 in unconstrained optimization. Solvers for non-convex AR3 subproblems have been proposed in [17, 45, 46] by generalizing a method of Nesterov suggested in [37]. However, for $p \geq 3$, both the minimization of subproblems (2) and an efficient adaptive choice of the regularization parameter remain under-explored areas.

Considering the first of the two issues, the problem of minimizing AR_p subproblems, an important difference between AR2 and AR3 is that the latter problem can have multiple local minima even when the Hessian is positive definite. Although choosing any of the local minimizers provides the optimal worst-case complexity bound, the practical efficiency of the algorithm is highly dependent on the choice. Section 4 of this paper addresses this specific question.

Considering the second issue, the problem of adaptive choice of the regularization parameter, [24] introduced interpolation-based updates for the regularization parameter designed specifically for AR2 implementations. These updates use information from previous iterations to estimate an appropriate regularization parameter for the current iteration and help improve the overall numerical performance of the algorithm. To the best of our knowledge, no efficient updating strategy has as yet been designed specifically for AR_p subproblems with $p \geq 3$. Section 3 of this paper is dedicated to filling this gap.

Finally, we note that avoiding the computational burden of computing the exact third-order tensor is also an active field of investigation with the potential to improve the efficiency of implementations: One approach is to approximate the tensor term by simpler terms, such as in [46], which uses a scalar approximation while solving the AR3 subproblem, and [44], which uses p th-order information to approximate the $(p + 1)$ st-order tensor. We do not further investigate this question in the present paper.

1.1. Contributions

The following are the key contributions of our paper:

- We introduce a Taylor-based initial regularization parameter selection strategy, which adaptively chooses a suitable σ_0 with low computational cost.
- We extend the interpolation-based updating strategy from $p = 2$, originally introduced by [24], to any positive integer $p \geq 3$. This updating strategy allows σ to

change dramatically to a suitable level based on interpolation models, assuming that local information continues to hold at the next iteration.

- Motivated by [6], we identify fundamental differences between the local minima of the subproblems for $p = 2$ and $p \geq 3$. Based on this, we introduce a novel prerejection module capable of “predicting” unsuccessful steps before any function evaluations are carried out for general $p \geq 3$. Numerical experiments with $p = 3$ confirm that this prerejection strategy is efficient.
- Numerical results provided in each section support the efficiency of the proposed modifications of the basic algorithm as demonstrated through convergence dot plots and performance profile plots.

1.2. The AR_p algorithmic framework

Algorithm 1.1: The generic AR_p framework

Input: A starting point $\mathbf{x}_0 \in \mathbb{R}^d$, a tolerance $\varepsilon > 0$, and an initial regularization parameter $\sigma_0 > 0$

```

1 for  $k = 0, 1, \dots$  do
2   if  $k = 0$  or  $\mathbf{x}_k \neq \mathbf{x}_{k-1}$  then
3     Compute  $f(\mathbf{x}_k)$  and  $\nabla f(\mathbf{x}_k)$ 
4     if  $\|\nabla f(\mathbf{x}_k)\| < \varepsilon$  then
5       return approximate local minimizer  $\mathbf{x}_k$ 
6     else
7       Compute  $\nabla^2 f(\mathbf{x}_k), \dots, \nabla^p f(\mathbf{x}_k)$ 
8     end
9   end
10  Construct the local model  $m_k(\mathbf{s}) = t_{\mathbf{x}_k}^p(\mathbf{s}) + \frac{\sigma_k}{p+1}\|\mathbf{s}\|^{p+1}$  and find an
    approximate local minimizer  $\mathbf{s}_k$  that satisfies  $m_k(\mathbf{s}_k) < m_k(\mathbf{0})$  and a
    subproblem termination condition
11  Compute  $\mathbf{x}_{k+1}$  and  $\sigma_{k+1}$  via one of the updating strategies of Table 1
12 end
```

Since we will be discussing various variants of the AR_p algorithm and different updating strategies for σ_k , we present the general AR_p algorithmic framework in Algorithm 1.1. Two key parts are unspecified in this algorithm: the subproblem termination condition on Line 10 and the updating strategy on Line 11.

For the termination condition (TC) we will consider two different options: The first limits the norm of the gradient by an absolute constant $\varepsilon_{\text{sub}} > 0$ as

$$\|\nabla m_k(\mathbf{s}_k)\| \leq \varepsilon_{\text{sub}}, \quad (\text{TC.a})$$

Procedure 1.2: Simple update

Parameters: $0 < \eta_1 \leq \eta_2 < 1$, $0 < \gamma_1 < 1 < \gamma_2$, $\sigma_{\min} > 0$

Defaults: $\eta_1 = 0.01$, $\eta_2 = 0.95$, $\gamma_1 = 0.5$, $\gamma_2 = 3$, $\sigma_{\min} = 10^{-8}$

- 1 Compute the predicted function decrease $\delta_k^{\text{pred}} = t_k(\mathbf{0}) - t_k(\mathbf{s}_k)$
 - 2 Compute the actual function decrease $\delta_k^{\text{act}} = f(\mathbf{x}_k) - f(\mathbf{x}_k + \mathbf{s}_k)$
 - 3 Compute the decrease ratio $\rho_k = \delta_k^{\text{act}} / \delta_k^{\text{pred}}$
 - 4 **if** $\rho_k \geq \eta_2$ **then**
 - 5 | Set $\mathbf{x}_{k+1} = \mathbf{x}_k + \mathbf{s}_k$ and $\sigma_{k+1} = \max\{\gamma_1 \sigma_k, \sigma_{\min}\}$ // very successful step
 - 6 **else if** $\rho_k \geq \eta_1$ **then**
 - 7 | Set $\mathbf{x}_{k+1} = \mathbf{x}_k + \mathbf{s}_k$ and $\sigma_{k+1} = \sigma_k$ // successful step
 - 8 **else**
 - 9 | Set $\mathbf{x}_{k+1} = \mathbf{x}_k$ and $\sigma_{k+1} = \gamma_2 \sigma_k$ // unsuccessful step
 - 10 **end**
-

whereas the second bounds the norm of the gradient depending on the size of the step:

$$\|\nabla m_k(\mathbf{s}_k)\| \leq \theta \|\mathbf{s}_k\|^p \quad (\text{TC.r})$$

for some $\theta > 0$. In the latter case, the subproblem is solved to a higher precision the smaller the step becomes. (TC.r) provides exactly the right amount of accuracy to achieve $O(\varepsilon^{-(p+1)/p})$ global iteration complexity despite solving the subproblem only approximately. We will refer to (TC.a) as the absolute and (TC.r) as the relative subproblem termination condition.

The role of the updating strategy is to determine whether the current step should be accepted ($\mathbf{x}_{k+1} = \mathbf{x}_k + \mathbf{s}_k$) or rejected ($\mathbf{x}_{k+1} = \mathbf{x}_k$) and to update σ_k in such a way to ensure progress, in particular by increasing σ_k whenever the step is rejected. We provide the simplest possible updating strategy with provably optimal worst-case complexity in Procedure 1.2. This approach measures the predicted decrease δ_k^{pred} using the Taylor expansion, and evaluates the success of the step by calculating $\rho_k = \delta_k^{\text{act}} / \delta_k^{\text{pred}}$. Depending on the value of ρ_k , the parameter σ_k is either decreased by a constant, kept unchanged, or increased by a constant. We refer to Algorithm 1.1 using Procedure 1.2 on Line 11 as AR p -Simple, where p as always describes the order of the highest derivative. Throughout the paper we introduce four additional updating strategies that can be used inside Algorithm 1.1 on Line 11. Table 1 gives an overview of all of these variants.

1.3. Implementation details

In this paper, we aim to explore ways to enhance the efficiency of AR p methods. Specifically, we will use AR3 to illustrate the impact of various aspects of AR p algorithms for $p \geq 3$, with numerical experiments presented at the end of each section. First, let us summarize the general setup for these experiments.

Parameter settings Throughout the paper, we set the first-order tolerance for Algorithm 1.1 to $\varepsilon = 10^{-8}$. By default, the subproblem solver will terminate when

Table 1: Overview of all named AR p variants used in this paper

Name	Updating strategy used on Line 11 of Algorithm 1.1
AR p -Simple	Procedure 1.2 (Simple update)
AR p -Simple ⁺	Procedure 1.2 & Procedure 4.1 (Prerejection)
AR p -Interp	Procedure 3.2 (Interpolation update)
AR p -Interp ⁺	Procedure 3.2 & Procedure 4.1 & Remark 4.6
AR p -BGMS	Procedure 4.2 (BGMS update)

$\|\nabla m_k(\mathbf{s})\| \leq 10^{-9}$, that means we use [\(TC.a\)](#) with $\varepsilon_{\text{sub}} = 10^{-9}$. Such strict requirement for the subproblem step is chosen to make the algorithm’s performance less dependent on any specific subproblem solver used. In our implementation, AR2 subproblems are solved using MCM [[11](#), [Algorithm 6.1](#)]. MCM is a factorization-based solver specifically designed for the AR2 subproblem and can compute its global minimizer with high accuracy. Since AR2 is capable of handling nonlinear, nonconvex functions, we use our AR2 implementation as the local solver for subproblems of all AR3 variants listed in [Table 1](#) throughout the experiments in this paper. To be precise, we use AR2-Simple as a subproblem solver with the default parameters, starting at $\mathbf{s}_0 = \mathbf{0}$ and $\sigma_0 = 10^{-8}$. The subsubproblems (the subproblems of our inner subproblem solver AR2-Simple) are solved using MCM until [\(TC.a\)](#) is satisfied with $\varepsilon_{\text{sub}} = 10^{-10}$. In addition to terminating when $\|\nabla f(\mathbf{x}_k)\|$ is sufficiently small, the algorithm and the subproblem solvers also terminate after a maximum of 1000 iterations or when numerical issues are detected.

Problem set The problem set used in this paper contains the 35 unconstrained minimization problems from Moré, Garbow, and Hillstom’s (MGH) test set [[33](#)], as implemented by [[4](#)]. However, most of the problems in the MGH test set have small dimensions ($2 \leq d \leq 40$), while we would also like to evaluate the algorithms on both large-scale and ill-conditioned problems. Therefore, we provide additional test functions, including the multidimensional Rosenbrock function ([31](#)), a nonlinear least-squares function ([32](#)) and four regularized third-order polynomials ([30](#)). We construct one well-conditioned regularized third-order polynomial and three ill-conditioned regularized third-order polynomial (with either an ill-conditioned Hessian, an ill-conditioned tensor³, or both an ill-conditioned Hessian and tensor). For more details, see [Appendix A](#). Finally, unless otherwise specified, our problem set is chosen by including half of the MGH test problems (those with odd labels) along with the six constructed problems mentioned above, resulting in a total of 24 problems. The starting points for all test problems are set to their default values, while the starting points for the six additional constructed problems are provided in [Appendix A](#). The selection of our testing set is guided by the following considerations: Firstly, since open source libraries contain only a limited number of test functions with third order terms, we added additional examples of our own.

³By “ill-conditioned tensor”, we refer to the construction of the tensor via a canonical polyadic (CP) decomposition [[27](#)] with an ill-conditioned super-diagonal core.

Secondly, to prevent over-fitting, we withhold half of the MGH test problems until the final benchmark at the end. Lastly, we ensure that the test set includes high-dimensional and ill-conditioned problems. On that basis, we believe that the set of 24 problems is representative despite its small size.

The remainder of this paper is organized as follows: in [Section 2](#), we first explore the performance of [Algorithm 1.1](#) with various σ_0 options to highlight the significance of choosing the right starting value of the regularization parameter. Based on these results, we then select the optimal σ_0 setting for the rest of the paper. In [Section 3](#), we introduce and examine an interpolation-based updating strategy. Following this, we present a novel prerejection framework in [Section 4](#). Comparisons of different subproblem termination criteria are discussed in [Section 5](#). Finally, in [Section 6](#), we provide a comprehensive benchmark comparing second- and third-order methods as well as our implementation and the work of [\[6\]](#) on the full set of 35 MGH test problems.

Notation and definitions

We end this section by declaring the notation and definitions used throughout the paper. Vectors and matrices will always be denoted by bold lower-case and bold upper-case letters, respectively, e.g., \mathbf{v} and \mathbf{V} . We use regular lower-case and upper-case letters to denote scalar constants, e.g., d or L . The transpose of a real vector \mathbf{v} is denoted by \mathbf{v}^\top . The inner product of two vectors \mathbf{v} and \mathbf{y} is denoted by $\langle \mathbf{v}, \mathbf{y} \rangle = \mathbf{v}^\top \mathbf{y}$. $\|\mathbf{v}\|$ and $\|\mathbf{V}\|$ denote vector- and matrix- ℓ_2 -norms of a vector \mathbf{v} and a matrix \mathbf{V} respectively. A superscript p either denotes the power p or a quantity using p th-order information, while a subscript k denotes the iteration counter of outer iterations of the AR p algorithm. The first p derivatives of f at \mathbf{x}_k are denoted as $\nabla f(\mathbf{x}_k), \nabla^2 f(\mathbf{x}_k), \dots, \nabla^p f(\mathbf{x}_k)$. The application of a p -tensor \mathbf{T} as a multilinear map to vectors $\mathbf{s}_1, \dots, \mathbf{s}_m$, where $m \leq p$, is written as $\mathbf{T}[\mathbf{s}_1, \dots, \mathbf{s}_m]$, and $\mathbf{T}[\mathbf{s}]^m$ represents the special case when $\mathbf{s} = \mathbf{s}_1 = \dots = \mathbf{s}_m$. In both cases the result is a $(p - m)$ -tensor. In particular, when $m = p$ we get a scalar. The minimum function value of any objective f is denoted by f^* .

2. Choosing the initial regularization parameter σ_0

The choice of regularization parameter σ is crucial for the performance of the AR p algorithm. It can be understood as roughly equivalent to the inverse of a trust-region radius in trust-region methods. Choosing σ too large results in successful but small steps, while choosing too small a value leads to large but unsuccessful steps. In this section, we utilize AR3-Simple ([Algorithm 1.1](#) combined with [Procedure 1.2](#)) to demonstrate the impact of adjusting the initial regularization parameter σ_0 and the general behaviour of the method. This straightforward experiment allows us to describe the visualizations we use throughout the paper in detail.

We consider $\sigma_0 = 10^{-8}$, $\sigma_0 = 1$ and $\sigma_0 = 10^8$ as well as a simple and cost-effective method for approximating the “right” value of σ_0 using one additional function evaluation. The function is evaluated at an offset \mathbf{y} , whose entries are randomly chosen from

a standard normal distribution, and σ_0 is computed as follows:

$$\sigma_0 = \max \left\{ (p+1) \frac{|f(\mathbf{x}_0 + \mathbf{y}) - t_{\mathbf{x}_0}^p(\mathbf{y})|}{\|\mathbf{y}\|^{p+1}}, \sigma_{\min} \right\}, \quad (3)$$

where $t_{\mathbf{x}_0}^p$ is defined as in (1). The idea behind this approach is that σ_0 is chosen to compensate for the error in the Taylor approximation, which is why this method is referred to as **Taylor** in the plots below. It also has a connection to the Lipschitz constant L_p of the p th derivative. We know from [14, Lemma 2.1] that $|f(\mathbf{x}_0 + \mathbf{y}) - t_{\mathbf{x}_0}^p(\mathbf{y})| \leq \frac{L_p}{(p+1)!} \|\mathbf{y}\|^{p+1}$, leading to $\sigma_0 = \sigma_{\min}$ or $\sigma_0 \leq \frac{L_p}{p!}$. While this approximation cannot compute the exact Lipschitz constant, it provides a value that is within the correct order of magnitude in most cases.

2.1. Numerical illustrations

We use two different types of graphs to visualize our numerical results: one type focuses on individual test functions to illustrate the effect of specific features introduced in different algorithmic variants, while the second type compares the overall performance of algorithms across a range of test problems. We introduce them below alongside the interpretation of the resulting graphs for the choice of σ_0 .

2.1.1. Convergence dot plots

To illustrate how the progress of AR3 towards the function minimizer interacts with the regularization parameter σ_k , we designed a custom plot, which we refer to as a “convergence dot plot”. In this plot, e.g. [Figure 2](#), each iteration k is represented by a dot. The position on the horizontal axis is determined by $f(\mathbf{x}_k) - f^*$ and the vertical position by σ_k . Both axes are log-scaled and the x- and y-coordinates of the dots are rounded up to 10^{-25} and 10^{-10} respectively, if necessary. The type of dot indicates the oracle calls at the tentative iterate $\mathbf{x}_k + \mathbf{s}_k$: If the step \mathbf{s}_k is accepted, meaning $\mathbf{x}_{k+1} = \mathbf{x}_k + \mathbf{s}_k$ and both the function and all derivatives are evaluated at this point, the dot is represented by a filled diamond. If the step \mathbf{s}_k is rejected, only the function value at $\mathbf{x}_k + \mathbf{s}_k$ is computed before the algorithm decides to remain at the current iterate ($\mathbf{x}_{k+1} = \mathbf{x}_k$), and the dot takes the form of a filled circle. Lastly, if the step is preredicted, meaning that neither the function value nor any derivatives are evaluated at $\mathbf{x}_k + \mathbf{s}_k$, the dot is shown as an empty circle. Since we postpone the discussion of prerediction mechanisms until [Section 4](#), the first few plots will not include any empty circles. A special case occurs at the very last iterate, where no tentative step \mathbf{s}_k is computed. There are no further evaluations and the value σ_k is computed but not used. We still include this iterate in the plot, because it nicely illustrates the convergence of $f(\mathbf{x}_k)$ to f^* , but we use a triangle as a marker.

Since the x-axis represents the function value and is oriented such that smaller function values are on the right, any successful iteration will produce a new dot to the right of the current one. Similarly, on the y-axis, larger values of σ_k are positioned higher up, so unsuccessful iterations will produce a new dot above the current one. In other words,

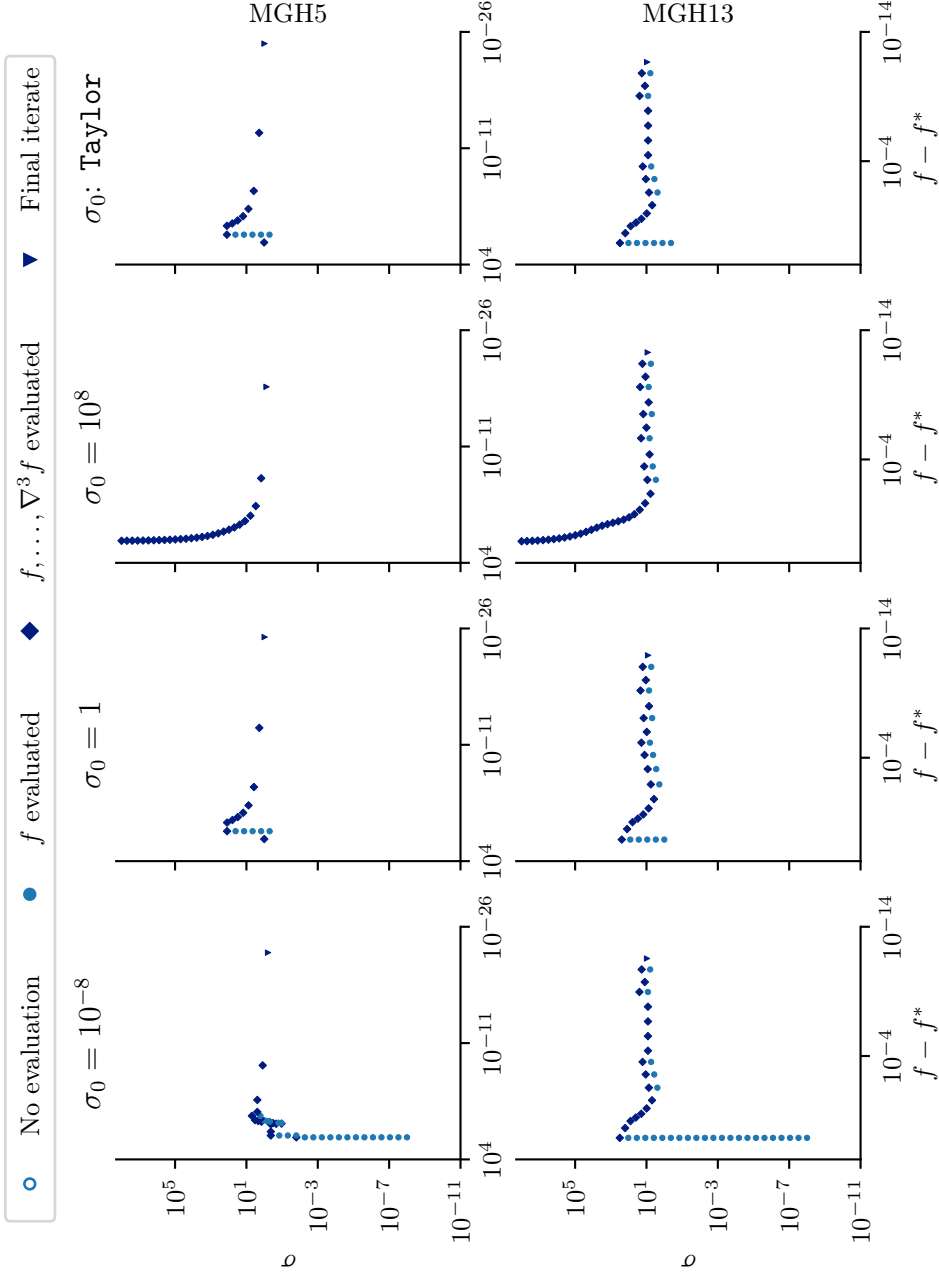


Figure 2: The convergence dot plot shows the impact of different σ_0 values for AR3-Simple using (TC.a) with $\varepsilon_{\text{sub}} = 10^{-9}$. An extremely small σ_0 results in more unsuccessful iterations (blue circles), while an extremely large σ_0 leads to many successful iterations (dark blue diamonds) with small step sizes, resulting in slow convergence. Taylor is able to automatically adjust σ_0 to a suitable value, providing the best performance.

to follow the sequence of iterations in order, one should read bottom-to-top within each vertical line of dots and left-to-right across the plot. The total number of function evaluations required to determine \mathbf{x}_k can be established by counting how many of the dots corresponding to iterations 0 to $k-1$ are filled (either circle or diamond) and adding one for the function evaluation at \mathbf{x}_0 . Similarly, the number of derivative evaluations is one larger than the number of diamond-shaped dots among iterations 0 to $k-1$.

Figure 2 presents the convergence dot plots for problems 5 and 13 from the MGH test set, corresponding to the ‘‘Beale’’ function [3] and the ‘‘Powell singular’’ [41] function, respectively. We will keep them as running examples for all numerical illustrations, as the plots are generally straightforward to interpret and display the typical behaviour of our method. These two functions exhibit different local convergence behaviours, which can be observed from this plot. Since the x-axis is log-scaled, equispaced diamond dots indicate that the successful iterates are converging linearly with respect to the function value. When the distance between these dots increases as the algorithm progresses, this corresponds to superlinear convergence.

For MGH5, there is a clear superlinear convergence of the function value to its minimum in each case. This aligns with the theory predicting that for (locally) strongly convex functions with Lipschitz continuous p th derivatives, the local convergence rate of AR p methods is of p th order [19]. Therefore, we should expect third-order convergence asymptotically. In contrast, the MGH13 function was constructed by Powell such that the Hessian is singular at the minimizer, meaning that second-order methods only converge at a linear rate. For this function, the third derivative at the minimizer is zero, so even with additional derivative information, the local convergence rate remains linear.⁴

Returning to the influence of σ_0 on the algorithm’s behaviour, the figure clearly illustrates the point made earlier: there is an optimal value or ‘‘sweet spot’’ for σ_0 (and σ_k in general). When σ_0 is excessively large (e.g., $\sigma_0 = 10^8$), all iterations are successful, but the progress is minuscule until σ_k is reduced to an appropriate level. Conversely, when σ_0 is too small (e.g., $\sigma_0 = 10^{-8}$), the initial iterations are all unsuccessful until, once again, the regularization parameter adjusts to the correct level. For the two problems shown in Figure 2 the Taylor approximation computes a σ_0 very close to 1. While this may not be the perfect value, it is at least within a few orders of magnitude of the right value, significantly reducing the number of iterations and function evaluations compared to the two extreme values of σ_0 .

2.1.2. Performance profile plots

We aim to determine whether the conclusions drawn from our two test problems also apply to the entire test set. Performance profile plots are a standard tool for comparing the performance of different algorithms with respect to a given cost [20, 23]. In this work, we follow the approach and notation from [6], considering the value of $\Gamma_i(\tau, \varepsilon_f)$ for each method M_i . This $\Gamma_i(\tau, \varepsilon_f)$ represents ‘‘the proportion of problems for which method

⁴In general, in directions that lie in the null space of $\nabla^2 f(\mathbf{x}_*)$, the third derivative must also be zero at a local minimizer \mathbf{x}_* , so we cannot expect any acceleration of the local convergence rate when the Hessian is degenerate.

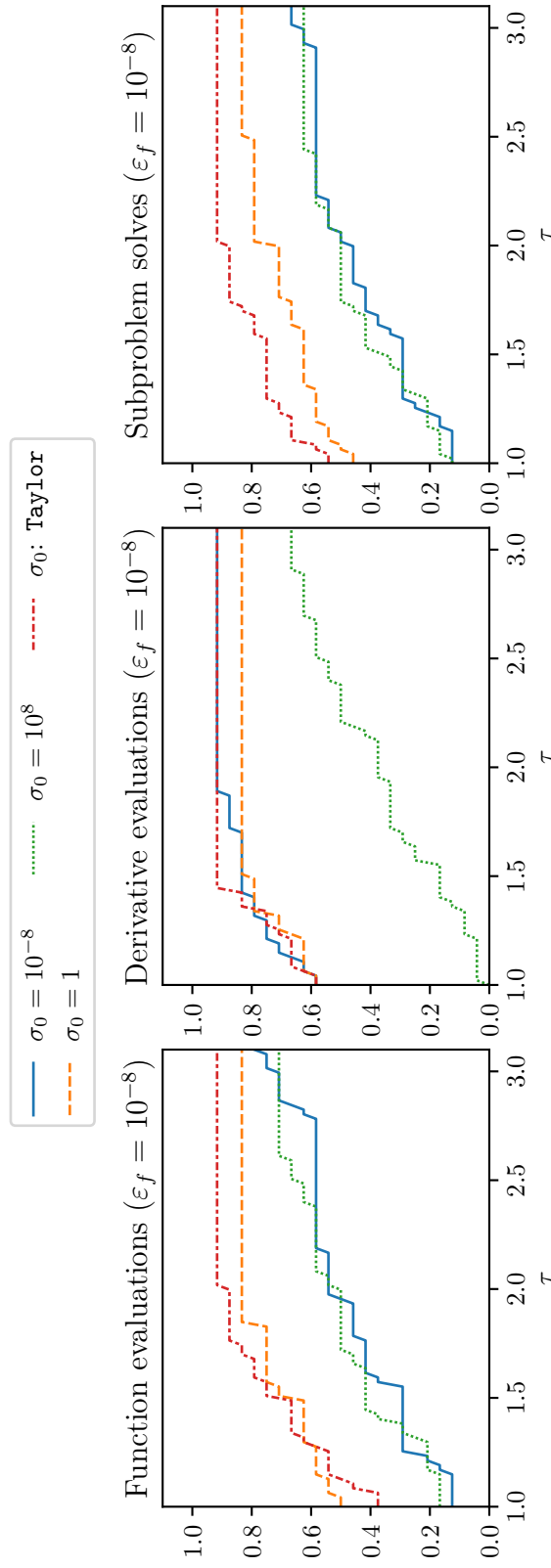


Figure 3: The performance profile plot shows the impact of using different σ_0 values for AR3-Simple using (TC.a) with $\varepsilon_{\text{sub}} = 10^{-9}$. Although Taylor requires one extra function evaluation, it provides the most favourable and stable performance across all three measurements, particularly in subproblem solves.

M_i was able to find an ε_f -approximation to a solution with a cost up to τ times the cost required by the most efficient method.” In this context, an ε_f -approximate solution refers to an iterate \mathbf{x}_k during the algorithm’s run for which

$$\frac{f(\mathbf{x}_k) - f^*}{\max\{1, |f^*|\}} < \varepsilon_f. \quad (4)$$

Since the minimum function value f^* is often unknown, we use the smallest function value found by any of the methods as a practical proxy.

As described in [Section 1.3](#), our test set consists of 24 problems, including 18 odd-numbered MGH problems and six additional large-dimensional problems. In the main paper, we report performance profile plots using the number of function evaluations, derivative evaluations and subproblem solves as the cost metrics, with $\varepsilon_f = 10^{-8}$ as the required function value accuracy. Additional performance profiles for different values of ε_f and τ can be found in [Appendix C](#).

Analysing [Figure 3](#), we observe that extreme values of σ_0 require significantly more function evaluations and subproblem solves compared to a more reasonable choice, such as $\sigma_0 = 1$. The very large σ_0 also results in more frequent derivative evaluations due to many successful iterations with minimal progress. Since the `Taylor` method of estimating σ_0 is competitive across all metrics and adapts to the scaling of the problem, we use it for the remainder of the paper.

3. An interpolation-based update for AR_p

After establishing that the correct choice of the regularization parameter is critical for an efficient AR_p method, we consider the update mechanism for σ_k next. [\[24\]](#) introduced a method for updating σ_k based on a one-dimensional interpolation of the objective function. While their work specifically addresses the case of $p = 2$, we are motivated by this approach to introduce an interpolation-based update for any arbitrary $p \geq 2$. The primary advantage of the interpolation-based strategy is its ability to adapt more quickly to the optimal level of σ in many situations, utilizing only the information that is already available and avoiding costly computations. Given that the update of the regularization parameter is crucial for the efficiency of AR_p methods, having such a strategy available is essential for AR_p numerical studies.

3.1. Derivation

The general structure presented in [Procedure 3.1](#) is similar to the simple update in [Procedure 1.2](#): a decrease ratio ρ_k is computed, and σ_k is adjusted by a constant factor as long as $\rho_k \in (0, 1)$. More sophisticated rules are applied only when the step is either extremely successful ($\rho_k \geq 1$) or extremely unsuccessful ($\rho_k < 0$). An important difference is that under [Procedure 3.1](#) the predicted function decrease is calculated on the basis of the decrease in m_k , which is strictly smaller than the decrease in t_k used under [Procedure 1.2](#). The criterion used under [Procedure 3.1](#) therefore increases the likelihood

Procedure 3.1: Interpolation update (general structure)

Parameters: $0 < \eta_1 \leq \eta_2 < 1$, $0 < \gamma_1 < 1 < \gamma_2$, $\sigma_{\min} > 0$

- 1 Compute the predicted function decrease $\delta_k^{\text{pred}} = m_k(\mathbf{0}) - m_k(\mathbf{s}_k)$
- 2 Compute the actual function decrease $\delta_k^{\text{act}} = f(\mathbf{x}_k) - f(\mathbf{x}_k + \mathbf{s}_k)$
- 3 Compute the decrease ratio $\rho_k = \delta_k^{\text{act}} / \delta_k^{\text{pred}}$
- 4 **if** $\rho_k \geq 1$ **then** // extremely successful step
- 5 | Set $\mathbf{x}_{k+1} = \mathbf{x}_k + \mathbf{s}_k$ and determine σ_{k+1} by interpolation
- 6 **else if** $\rho_k \geq \eta_2$ **then** // very successful step
- 7 | Set $\mathbf{x}_{k+1} = \mathbf{x}_k + \mathbf{s}_k$ and $\sigma_{k+1} = \max\{\gamma_1\sigma_k, \sigma_{\min}\}$
- 8 **else if** $\rho_k \geq \eta_1$ **then** // successful step
- 9 | Set $\mathbf{x}_{k+1} = \mathbf{x}_k + \mathbf{s}_k$ and $\sigma_{k+1} = \sigma_k$
- 10 **else if** $\rho_k \geq 0$ **then** // unsuccessful step
- 11 | Set $\mathbf{x}_{k+1} = \mathbf{x}_k$ and $\sigma_{k+1} = \gamma_2\sigma_k$
- 12 **else** // extremely unsuccessful step
- 13 | Set $\mathbf{x}_{k+1} = \mathbf{x}_k$ and determine σ_{k+1} by interpolation
- 14 **end**

of a step being considered extremely successful, and this has a positive impact on the practical performance.

There is also a significant difference from a theoretical perspective: While both ways of measuring the predicted function decrease offer the same global complexity guarantees for AR2⁵ [7, 12, 13], the same cannot be said for $p \geq 3$. Both procedures still give convergence, but only the simple update [Procedure 1.2](#) yields a provably optimal global complexity rate. The use of [Procedure 3.1](#) is therefore driven by practical performance considerations rather than theoretical guarantees.

The interpolation-based updates in the extremely successful and extremely unsuccessful cases are derived using three key simplifications:

- (S1) *Consistent regularization*: An alternative value of the regularization parameter $\tilde{\sigma}_k$, that would have been a good choice for the current iteration, is also assumed to be a good choice for the next iteration.
- (S2) *Ray-based minimization*: Any minimizer $\tilde{\mathbf{s}}_k$ for this counterfactual choice of $\tilde{\sigma}_k$ is assumed to satisfy $\tilde{\mathbf{s}}_k = \alpha \mathbf{s}_k$ for some $\alpha > 0$.
- (S3) *Interpolation along the ray*: Along the ray $\{\alpha \mathbf{s}_k \mid \alpha \geq 0\}$, the objective function is well approximated by the interpolating polynomial p_f defined below.

(S1) allows us to use the information already gathered about the regularized Taylor expansion and its minimizer at the current iteration for the next iteration, even though,

⁵Note that the same complexity guarantees are obtained under slightly different assumptions on the subproblem solution. When measuring the predicted decrease using the regularized model, one needs to assume that \mathbf{s}_k has a smaller model value than the Cauchy point and that $\|\nabla^2 f(\mathbf{x}_k)\|$ stays bounded. When using the Taylor approximation, it suffices to assume that $\|\nabla m_k(\mathbf{s}_k)\| \leq \theta \|\mathbf{s}_k\|^2$ for some $\theta \geq 0$.

in theory, there is no guarantee that the optimal values of σ_k and σ_{k+1} will be similar if the current iteration is successful. (S2) implies that we only need to consider the relevant functions on the ray extending from the origin through \mathbf{s}_k . Let

$$t_{\rightarrow}(\alpha) = t_{\mathbf{x}_k}^p(\alpha \mathbf{s}_k / \|\mathbf{s}_k\|) \quad \text{and} \quad m_{\sigma, \rightarrow}(\alpha) = m_{\mathbf{x}_k, \sigma}^p(\alpha \mathbf{s}_k / \|\mathbf{s}_k\|) \quad \text{for } \alpha \in [0, \infty) \quad (5)$$

be the current Taylor expansion and model along the ray pointing in the direction of \mathbf{s}_k . $t_{\rightarrow}(\alpha)$ and $m_{\sigma, \rightarrow}(\alpha)$ are one-dimensional polynomials of order p and $p + 1$, respectively. The interpolating polynomial $p_f(\alpha) \approx f(\mathbf{x}_k + \alpha \mathbf{s}_k / \|\mathbf{s}_k\|)$ is defined as the unique polynomial of degree $p + 1$ that satisfies

$$p_f(0) = f(\mathbf{x}_k), \quad p_f^{(j)}(0) = \nabla^j f(\mathbf{x}_k) [\mathbf{s}_k / \|\mathbf{s}_k\|]^j \quad \text{and} \quad p_f(\|\mathbf{s}_k\|) = f(\mathbf{x}_k + \mathbf{s}_k), \quad (6)$$

incorporating all the information gathered about the objective function along the ray. It is straightforward to show that $p_f(\alpha)$ can be explicitly written as

$$p_f(\alpha) = f(\mathbf{x}_k) + \sum_{j=1}^p \frac{1}{j!} \nabla^j f(\mathbf{x}_k) [\mathbf{s}_k / \|\mathbf{s}_k\|]^j \alpha^j + \left[\frac{f(\mathbf{x}_k + \mathbf{s}_k) - t_k(\mathbf{s}_k)}{\|\mathbf{s}_k\|^{p+1}} \right] \alpha^{p+1} \quad (7)$$

with coefficients that are easy to compute. (S3) enables us to use p_f instead of f and avoid additional evaluations of the objective function.

Let us now describe the concept behind the interpolation-based updates, beginning with the extremely unsuccessful case, which is the most straightforward. Since the step was unsuccessful, a different regularization parameter $\tilde{\sigma}_k$ should have been chosen such that the corresponding step $\tilde{\mathbf{s}}_k$ would have been successful, satisfying

$$\tilde{\rho}_k = \frac{f(\mathbf{x}_k) - f(\mathbf{x}_k + \tilde{\mathbf{s}}_k)}{m_{\mathbf{x}_k, \tilde{\sigma}_k}^p(\mathbf{0}) - m_{\mathbf{x}_k, \tilde{\sigma}_k}^p(\tilde{\mathbf{s}}_k)} \geq \eta_1. \quad (8)$$

Using the simplifications described earlier, we therefore search for the smallest $\sigma > \sigma_k$ such that a minimizer α of $m_{\sigma, \rightarrow}$ satisfies

$$\frac{p_f(0) - p_f(\alpha)}{m_{\sigma, \rightarrow}(0) - m_{\sigma, \rightarrow}(\alpha)} \geq \eta_1. \quad (9)$$

The extremely successful case splits into two scenarios: In the first scenario, where $m_k(\mathbf{s}_k) \geq f(\mathbf{x}_k + \mathbf{s}_k) \geq t_k(\mathbf{s}_k)$, we aim to find the largest $\sigma < \sigma_k$ such that the difference between the regularized model and the objective function is reduced by a factor of $\beta \in (0, 1)$ at the minimizer α . This can be expressed as

$$m_{\sigma, \rightarrow}(\alpha) - p_f(\alpha) \leq \beta(m_{\sigma_k, \rightarrow}(\|\mathbf{s}_k\|) - p_f(\|\mathbf{s}_k\|)) = \beta(m_k(\mathbf{s}_k) - f(\mathbf{x}_k + \mathbf{s}_k)). \quad (10)$$

In the second scenario, where $f(\mathbf{x}_k + \mathbf{s}_k) < t_k(\mathbf{s}_k)$, the highest-order coefficient of p_f is negative, meaning the polynomial is not lower bounded on $\alpha \in (0, \infty)$ and therefore not useful. Then, instead of using p_f , we resort to the Taylor expansion and simply aim to

decrease the difference between the regularized model and the Taylor expansion by the same factor β :

$$m_{\sigma,\rightarrow}(\alpha) - t_{\rightarrow}(\alpha) \leq \beta(m_{\sigma_k,\rightarrow}(\|\mathbf{s}_k\|) - t_{\rightarrow}(\|\mathbf{s}_k\|)) = \beta(m_k(\mathbf{s}_k) - t_k(\mathbf{s}_k)). \quad (11)$$

In each scenario, we establish a constraint for the new σ and its corresponding minimizer α given by (9), (10) or (11). We will abbreviate this constraint as $c(\alpha, \sigma) \leq 0$. By additionally replacing the constraint that α is a minimizer of $m_{\sigma,\rightarrow}$ with second-order necessary conditions⁶ we arrive at the following ‘‘optimization problems’’.

$$\begin{array}{ccc} \min_{\alpha, \sigma} & \sigma & \max_{\alpha, \sigma} & \sigma \\ \text{s.t.} & m'_{\sigma,\rightarrow}(\alpha) = 0 & \text{s.t.} & m'_{\sigma,\rightarrow}(\alpha) = 0 \\ & m''_{\sigma,\rightarrow}(\alpha) \geq 0 & & m''_{\sigma,\rightarrow}(\alpha) \geq 0 \\ & c(\alpha, \sigma) \leq 0 & \text{or} & c(\alpha, \sigma) \leq 0 \\ & \sigma \geq 0 & & \sigma \geq 0 \\ & \sigma \geq \sigma_k & & \sigma \leq \sigma_k \\ & \alpha > 0 & & \alpha > 0 \end{array} \quad (12)$$

In the unsuccessful case, we need to solve the problem on the left, and in the successful case, the one on the right. We will analyse them simultaneously. The stationarity condition can be rearranged to express σ as a function of α :

$$m'_{\sigma,\rightarrow}(\alpha) = t'_{\rightarrow}(\alpha) + \sigma\alpha^p = 0 \quad \Leftrightarrow \quad \sigma = \frac{-t'_{\rightarrow}(\alpha)}{\alpha^p}. \quad (13)$$

Substituting σ with this expression (and multiplying the inequalities by $\alpha > 0$ as needed) leads to the following equivalent system, that only involves α and polynomial inequalities in α .

$$\begin{array}{ccc} \min_{\alpha} & -\frac{t'_{\rightarrow}(\alpha)}{\alpha^p} & \max_{\alpha} & -\frac{t'_{\rightarrow}(\alpha)}{\alpha^p} \\ \text{s.t.} & t''_{\rightarrow}(\alpha)\alpha - pt'_{\rightarrow}(\alpha) \geq 0 & \text{s.t.} & t''_{\rightarrow}(\alpha)\alpha - pt'_{\rightarrow}(\alpha) \geq 0 \\ & c(\alpha) \leq 0 & \text{or} & c(\alpha) \leq 0 \\ & t'_{\rightarrow}(\alpha) \leq 0 & & t'_{\rightarrow}(\alpha) \leq 0 \\ & t'_{\rightarrow}(\alpha) + \sigma_k\alpha^p \leq 0 & & t'_{\rightarrow}(\alpha) + \sigma_k\alpha^p \geq 0 \\ & \alpha > 0 & & \alpha > 0 \end{array} \quad (14)$$

The inequality $c(\alpha) = c(\alpha, -t'_{\rightarrow}(\alpha)/\alpha^p) \leq 0$ can also be expressed as a polynomial inequality since $m_{\sigma,\rightarrow}(\alpha) = t_{\rightarrow}(\alpha) - \frac{1}{p+1}t'_{\rightarrow}(\alpha)\alpha$. Therefore, we can rewrite (9) to (11)

⁶In [24], it sufficed to demand stationarity of α , since there would only ever be exactly one local minimizer $\alpha > 0$.

as follows:

$$\eta_1 \left(t_{\rightarrow}(0) - t_{\rightarrow}(\alpha) + \frac{1}{p+1} t'_{\rightarrow}(\alpha) \alpha \right) - (p_f(0) - p_f(\alpha)) \stackrel{(9)}{\leq} 0 \quad (15)$$

$$t_{\rightarrow}(\alpha) - \frac{1}{p+1} t'_{\rightarrow}(\alpha) \alpha - p_f(\alpha) - \beta(m_k(\mathbf{s}_k) - f(\mathbf{x}_k + \mathbf{s}_k)) \stackrel{(10)}{\leq} 0 \quad (16)$$

$$\frac{1}{p+1} t'_{\rightarrow}(\alpha) \alpha - \beta(m_k(\mathbf{s}_k) - t_k(\mathbf{s}_k)) \stackrel{(11)}{\leq} 0 \quad (17)$$

In all cases, the feasible set of α is described by a series of polynomial inequalities of order at most p . Since the derivative of the objective in (14) is given by

$$\frac{-t''_{\rightarrow}(\alpha) \alpha + p t'_{\rightarrow}(\alpha)}{\alpha^{p+1}}, \quad (18)$$

the objective is monotonic over the feasible set, meaning that the optimal value will be attained at the boundary. It is therefore sufficient to compute the roots of all polynomial left-hand sides in (14), determine which of them satisfy all other inequalities, and then choose the one with the smallest or largest value of $\sigma = -t'_{\rightarrow}(\alpha)/\alpha^p$. It is important to note that the strict inequality $\alpha > 0$ does not cause any issues, as for $t'_{\rightarrow}(\alpha) \neq 0$, the value of σ converges to $\pm\infty$ as α approaches zero, making it either non-optimal or in violation of the bound on σ . In [24], the authors analyse the inequalities in (14) in the context of a quadratic t_{\rightarrow} and derive more explicit formulas. However, the fundamental process still involves solving polynomial equations and choosing the appropriate root α to compute σ from.

Since the α^* and corresponding σ^* computed from solving (14) are based on simplifying assumptions, it is important to safeguard the results. Moreover, there may be instances where no feasible solutions to (14) exist, meaning that α^* and σ^* cannot be determined. In such cases, a fallback procedure is necessary. We adopt the approach from [24], which involves enforcing a minimum and maximum increase in the extremely unsuccessful case and falling back to a simple decrease by a constant factor if $\alpha^* > \alpha_{\max} \|\mathbf{s}_k\|$ in the successful case. The full algorithm is shown in [Procedure 3.2](#).

3.2. Numerical illustrations

For the new parameters in [Procedure 3.2](#), we use the default values suggested in [24], except for γ_1 and γ_2 . The increase and decrease of σ_k when $\rho_k \in (0, 1)$ are kept consistent between the simple and the interpolation-based update to ensure a fair comparison.

[Figure 4](#) presents the convergence dot plots for AR3-Simple, and the interpolation-based update strategy we just described, labelled AR3-Interp ([Algorithm 1.1](#) combined with [Procedure 3.2](#)). For MGH5, we observe that AR3-Interp significantly reduces the overall number of iterations as well as the number of function and derivative evaluations by adapting σ_k much more aggressively than AR3-Simple. However, the other example illustrates that there are cases where the interpolation-based update is less efficient than the simple one, because it decreases σ_k too quickly. In these cases, while the number

Procedure 3.2: Interpolation update

Parameters: $0 < \eta_1 \leq \eta_2 < 1$, $0 < \gamma_{\min} < \gamma_1 < 1 < \gamma_2 < \gamma_{\max}$, $0 < \beta < 1$,
 $\alpha_{\max} > 1$, $\chi_{\min} > 0$, $\sigma_{\min} > 0$

Defaults: $\eta_1 = 0.01$, $\eta_2 = 0.95$, $\gamma_{\min} = 10^{-1}$, $\gamma_1 = 0.5$, $\gamma_2 = 3$, $\gamma_{\max} = 10^2$,
 $\beta = 10^{-2}$, $\alpha_{\max} = 2$, $\chi_{\min} = 10^{-8}$, $\sigma_{\min} = 10^{-8}$

```
1 Compute the predicted function decrease  $\delta_k^{\text{pred}} = m_k(\mathbf{0}) - m_k(\mathbf{s}_k)$ 
2 Compute the actual function decrease  $\delta_k^{\text{act}} = f(\mathbf{x}_k) - f(\mathbf{x}_k + \mathbf{s}_k)$ 
3 Compute the decrease ratio  $\rho_k = \delta_k^{\text{act}} / \delta_k^{\text{pred}}$ 
4 if  $\rho_k \geq 1$  then // extremely successful step
5   Set  $\mathbf{x}_{k+1} = \mathbf{x}_k + \mathbf{s}_k$ 
6   Compute  $\chi_k = m_k(\mathbf{s}_k) - \max\{f(\mathbf{x}_k + \mathbf{s}_k), t_k(\mathbf{s}_k)\}$ 
7   if  $\chi_k \geq \chi_{\min}$  then
8     if  $f(\mathbf{x}_k + \mathbf{s}_k) \geq t_k(\mathbf{s}_k)$  then
9       | Compute  $\alpha^*$  and  $\sigma^*$  from (14)-max using (16) as the constraint  $c$ 
10      else
11        | Compute  $\alpha^*$  and  $\sigma^*$  from (14)-max using (17) as the constraint  $c$ 
12      end
13      Set  $\sigma_{k+1} = \begin{cases} \max\{\sigma^*, \sigma_{\min}\} & \text{if } (\alpha^*, \sigma^*) \text{ exists and } \alpha^* \leq \alpha_{\max} \|\mathbf{s}_k\| \\ \max\{\gamma_{\min} \sigma_k, \sigma_{\min}\} & \text{otherwise} \end{cases}$ 
14    else
15      | Set  $\sigma_{k+1} = \max\{\gamma_1 \sigma_k, \sigma_{\min}\}$ 
16    end
17 else if  $\rho_k \geq \eta_2$  then // very successful step
18   | Set  $\mathbf{x}_{k+1} = \mathbf{x}_k + \mathbf{s}_k$  and  $\sigma_{k+1} = \max\{\gamma_1 \sigma_k, \sigma_{\min}\}$ 
19 else if  $\rho_k \geq \eta_1$  then // successful step
20   | Set  $\mathbf{x}_{k+1} = \mathbf{x}_k + \mathbf{s}_k$  and  $\sigma_{k+1} = \sigma_k$ 
21 else if  $\rho_k \geq 0$  then // unsuccessful step
22   | Set  $\mathbf{x}_{k+1} = \mathbf{x}_k$  and  $\sigma_{k+1} = \gamma_2 \sigma_k$ 
23 else // extremely unsuccessful step
24   | Set  $\mathbf{x}_{k+1} = \mathbf{x}_k$ 
25   | Compute  $\alpha^*$  and  $\sigma^*$  from (14)-min using (15) as the constraint  $c$ 
26   | Set  $\sigma_{k+1} = \begin{cases} \min\{\max\{\sigma^*, \gamma_2 \sigma_k\}, \gamma_{\max} \sigma_k\} & \text{if } (\alpha^*, \sigma^*) \text{ exists} \\ \gamma_2 \sigma_k & \text{otherwise} \end{cases}$ 
27 end
```

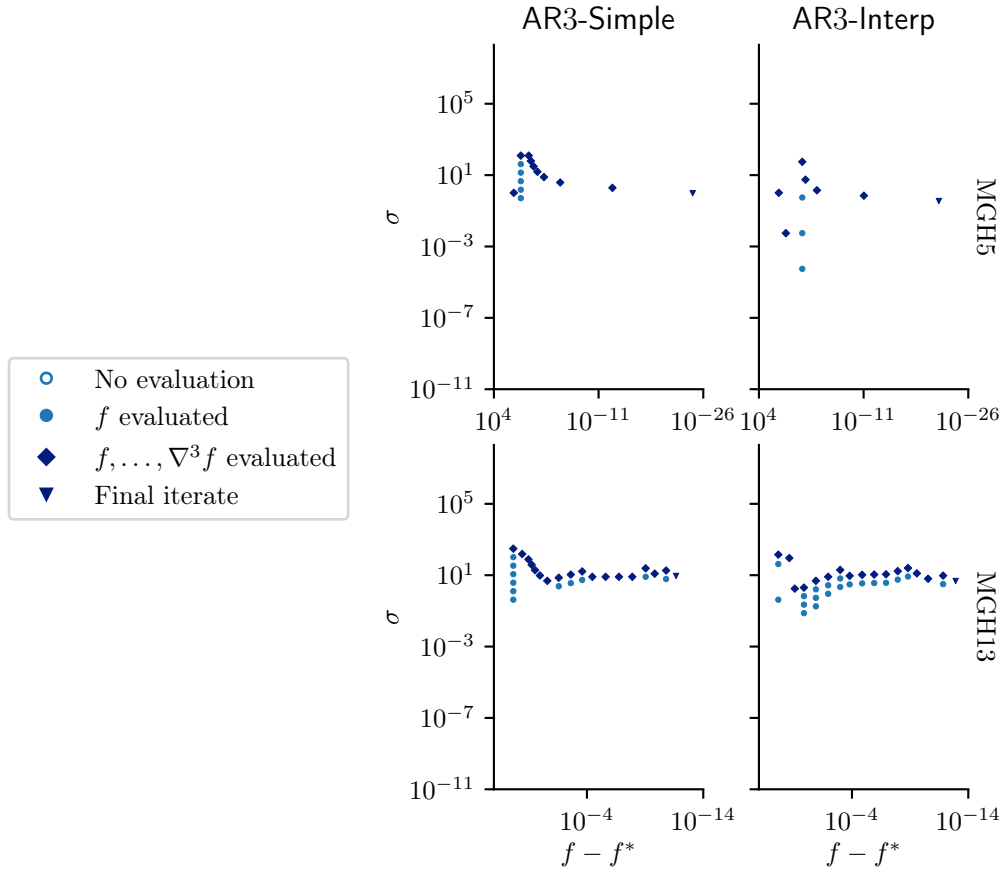


Figure 4: The convergence dot plot illustrates the effectiveness of the interpolation-based strategy. In the experiments the subproblem is solved to a high accuracy using (TC.a) with $\varepsilon_{\text{sub}} = 10^{-9}$ and σ_0 is chosen according to (3). As expected, AR3-Interp changes the regularization parameter more aggressively in many cases. Compared to AR3-Simple, this strategy enhanced performance for MGH5 but caused additional unsuccessful steps for MGH13 by decreasing σ_k too rapidly.

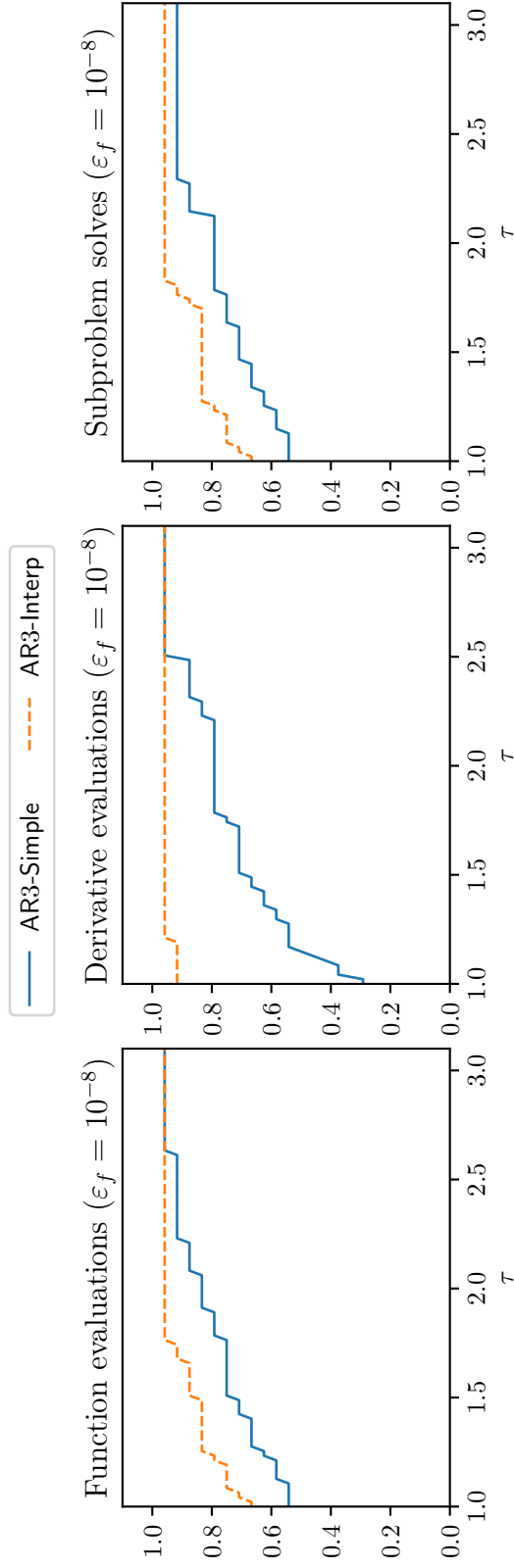


Figure 5: The performance profile plot illustrates the effectiveness of the interpolation-based strategy. In the experiments the subproblem is solved to a high accuracy using (TC.a) with $\varepsilon_{\text{sub}} = 10^{-9}$ and σ_0 is chosen according to (3). On our selection of test problems, AR3-Interp performs significantly better than AR3-Simple, especially on the number of derivative evaluations.

of derivative evaluations decreases, the number of function evaluations increases due to the smaller σ_k causing more unsuccessful iterations.

To assess the overall impact of switching from AR3-Simple to AR3-Interp, we examine the performance profile curves in Figure 5. These curves suggest that, on average, the new updating strategy reduces the number of function evaluations, derivative evaluation and subproblem solves. The most striking improvement is seen in the number of derivative evaluations, or equivalently the number of successful iterations, where AR3-Interp outperforms AR3-Simple on almost all test problems.

4. A prerejection framework

The performance of Algorithm 1.1 can be further enhanced by avoiding function evaluations when a step is unlikely to decrease the objective function. In this section, we introduce a novel prerejection mechanism that rejects steps based on the Taylor expansion along the subspace spanned by the step. This mechanism is motivated by the fundamentally different behaviour of minimizers in the AR3 subproblem when σ changes, compared to minimizers in the AR2 subproblem. The following subsections will discuss this difference, define various types of local minimizers, provide conditions to characterize these minimizers in the one-dimensional case, and propose a new prerejection heuristic based on this analysis.

4.1. Discontinuity in the AR p subproblem solutions

As p increases, the AR p subproblem of minimizing the regularized model in (2) becomes increasingly challenging to solve. For $p = 1$ we are searching for the minimum of a quadratically regularized linear function. The solution in this case is always a scaled negative gradient, and the scaling factor can be easily computed from the regularization parameter.

For $p = 2$, the local model can become non-convex and may have multiple local minima. However, it is still possible to solve the optimization problem thanks to the characterization of its global minimum [15, Theorem 8.2.8]. Moreover, this global minimizer is guaranteed to be a descent direction, that is, it satisfies $\nabla f(\mathbf{x}_k)^\top \mathbf{s}_k \leq 0$. Given this, solvers for the AR2 subproblem always aim to find the global minimizer [15], which can be efficiently computed because the structure of the global minimizer is similar to that of the trust-region subproblem.

For $p \geq 3$, many of the properties that hold for lower-order methods no longer apply. The AR p subproblem becomes significantly more challenging to solve, there is no simple characterization for any of its minimizers, and the global minimizer does not even have to be a descent direction (see Example B.1).

Notably, both optimal complexity guarantees [15] and local convergence results [19] do not impose restrictions on which minimizer should be chosen. This is because when σ is sufficiently large, any local or global minimizer will provide a sufficient decrease, and the updates will be accepted. From an efficiency standpoint, it is preferable to maintain

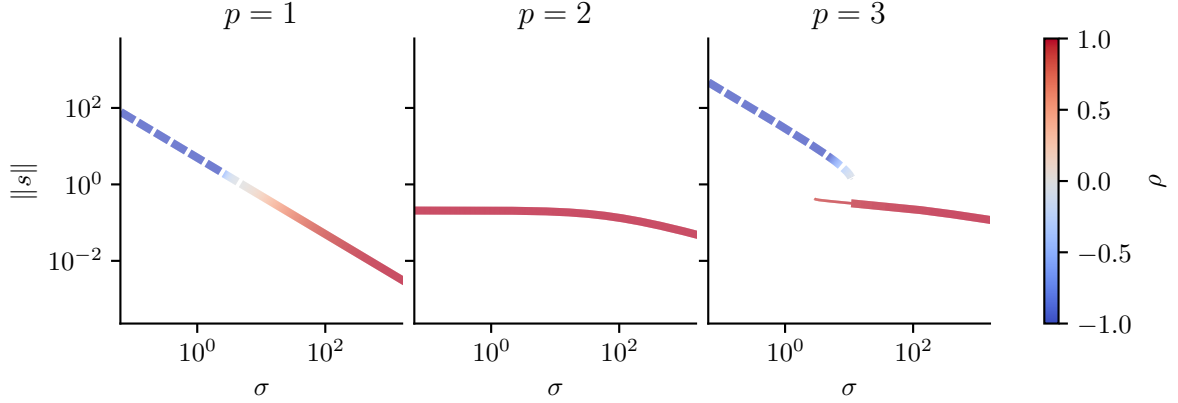


Figure 6: All local and global minimizers of the AR_p subproblems as a function of σ . The models are constructed at $x = 0$ for $f(x) = 3x^4 - 10x^3 + 12x^2 - 5x$. Non-global minimizers are drawn using thin lines. The values of ρ are capped to $[-1, 1]$ and negative values are drawn using a dashed line.

σ at a lower level to allow for larger steps. However, when the third derivative of f at \mathbf{x}_k is nonzero, the third-order Taylor expansion is always nonconvex and does not have a lower bound. In the case of small σ , the global minimizer of the model is a large step in the negative tensor direction regardless of the local behaviour of the model. This indicates that understanding the minimizers of the model and their dependence on σ is important for an efficient implementation of AR3.

Figure 6 illustrates how the local minimizers of AR_p subproblems for $p \in \{1, 2, 3\}$ change as σ changes for one specific objective function and expansion point. The colour of the lines corresponds to ρ , the success measure employed in the simple update (Procedure 1.2). In the case of $p = 3$, for this example, no minimizer changes continuously as σ increases from zero to infinity. Instead, there are two distinct branches: one branch corresponds to a minimizer that exists only for small values of σ , and the other corresponds to a local minimizer that exists only for large values of σ , with some overlap in the middle. During this overlap, the global minimizer of the model switches from one branch to the other. As indicated by the colour, the local minimizers on the first branch would result in unsuccessful steps ($\rho \leq 0$), whereas the minimizers on the second branch yield successful steps (ρ close to 1). Note that this example does not necessarily represent the typical behaviour of AR3 model minimizers but rather is an example of a new phenomenon: a discontinuity in the minimizer paths as σ changes. The function is carefully chosen such that the third-order Taylor expansion is strictly monotonically decreasing but becomes very flat around the minimizer of f . This leads to the behaviour seen in Figure 6, where initially there is only a single stationary point. However, once σ becomes large enough, a local maximum forms near the flat part of the Taylor expansion, leading to two minimizers. As σ increases further, the local maximum merges with the “original minimizer”, becomes a saddle point, and eventually vanishes. See Figure 7b for a graph of the function and the models for different values of σ .

4.2. Persistent and transient minimizers

We introduce some definitions that help describe the discontinuity phenomenon shown in [Figure 6](#). To simplify the notation, we drop the subscript k in this section and write $t: \mathbb{R}^d \rightarrow \mathbb{R}$ for the p th-order polynomial representing the Taylor expansion and $m_\sigma(\mathbf{s}) = t(\mathbf{s}) + \frac{\sigma}{p+1} \|\mathbf{s}\|^{p+1}$ for the corresponding regularized model.

Definition 4.1 (Minimizer curve). *Let $I \subset \mathbb{R}_{\geq 0}$ be an interval. A minimizer curve of t is a continuous function $\psi: I \rightarrow \mathbb{R}^d$ such that $\psi(\sigma)$ is a local minimizer of m_σ for any $\sigma \in I$. It is called maximal if ψ cannot be extended to any minimizer curve on a strictly larger interval than I .*

Definition 4.2 (Persistent/transient minimizer). *Let $\psi: I \rightarrow \mathbb{R}^d$ be a maximal minimizer curve of t . We say*

1. ψ is c -persistent for $c \geq 0$ if the minimizer curve persists as σ increases from c to ∞ , i.e., if $(c, \infty) \subset I$.
2. ψ is persistent if it is c -persistent for some $c \geq 0$.
3. ψ is transient if it is not persistent.
4. ψ is bounded if $\sup_{\sigma \in I} \|\psi(\sigma)\| < \infty$.

A local minimizer of m_σ is persistent/transient/bounded if it lies on a minimizer curve with such a property.

The fundamental difference between persistent and transient minimizers lies in their relationship with the local behaviour of the Taylor expansion t . Specifically, we know that $\lim_{\sigma \rightarrow \infty} \psi(\sigma) = \mathbf{0}$ holds for any persistent minimizer curve. In contrast, for any transient curve, $\|\psi(\sigma)\|$ is bounded away from zero (see [Theorem B.2](#)). Thus, transient minimizers disappear when σ becomes sufficiently large, whereas persistent minimizers follow the local descent path of the objective function. With this in mind, our proposed prerejection heuristic considers all transient minimizers as not useful and rejects them without evaluating the objective function.

However, it must be acknowledged that this approach may not always be the optimal decision. For instance, when $\nabla^p f$ is Lipschitz continuous with constant L_p and $\sigma \geq \frac{p+1}{p!} L_p$, the AR p model overestimates the objective function everywhere [[13](#), Lemma 2.1]. In this scenario, choosing the global minimizer of the model, whether transient or persistent, is the optimal choice as it provides the largest guaranteed function decrease. Moreover, selecting any local minimum guarantees the optimal global complexity of the AR p algorithm. Therefore, it is not recommended applying the prerejection framework when σ_k is already known to be sufficiently large. Still, in practice, the Lipschitz constant

is usually unknown, and prerejection serves as a practical tool to guide the selection of a minimizer without evaluating the function value.

Given that our algorithm is adaptive, in practice, σ is rarely large enough to cause the model to overestimate the function everywhere. Therefore, the global minimizer of the AR p subproblem, which might be transient, can be far from the expansion point and may not represent the local behaviour of the Taylor model. Our prerejection heuristic thus is designed with the practical consideration that transient minimizers are often not beneficial. In our experience, the prerejection mechanism described later in this section very rarely rejects steps that would otherwise have been successful.

To illustrate [Definition 4.2](#), we describe the different cases shown in [Figure 6](#) using these definitions. For $p = 1$, there is a single maximal minimizer curve, which is persistent but not bounded. This contrasts with the maximal minimizer curve for $p = 2$, which is both persistent and bounded. In the $p = 3$ case, there are two maximal minimizer curves: one is persistent, and the other is transient.⁷

The example in [Figure 6](#) is specifically chosen to show this behaviour, but it is worth mentioning that the need to deal with transient minimizers only arises for $p \geq 3$. For the AR1 subproblem of minimizing $\nabla f(\mathbf{x}_k)^\top \mathbf{s} + \frac{\sigma}{2} \|\mathbf{s}\|^2$, as alluded to earlier, there is only a single local and global minimizer for any σ and it takes the form $\mathbf{s} = -\sigma^{-1} \nabla f(\mathbf{x}_k)$ which is continuous in σ . Therefore, there is always a single maximal minimizer curve and it is always globally persistent. In the AR2 subproblem, there can be more than one maximal minimizer curve, and some of these curves can indeed be transient, but crucially any global minimizer of the model will always be a persistent one, ensuring the existence of a globally persistent minimizer curve (see [Theorem B.3](#)). Because solvers have been developed that can compute a global minimum of the AR2 subproblem (e.g. Algorithm 6.1 in [\[11\]](#)), the presence of transient minimizers does not impact the outer loop of the algorithm. The situation changes for $p = 3$. As shown in [Figure 6](#), there are instances when no minimizer curve is globally persistent. In other words, as long as σ is sufficiently small, any subproblem solver will find a transient minimizer.

4.3. Detecting transient minimizers in one dimension

In this section, we will refer to any $\mathbf{s} \in \mathbb{R}^n$ that is a local minimizer of m_σ for some $\sigma \geq 0$ as a *minimizer of the model m* . According to the definition provided above, determining whether a given minimizer is transient would require following its associated minimizer curve as σ increases to infinity to see whether it eventually disappears. Although continuation methods could potentially achieve this for arbitrary dimensions d , such an approach would involve numerous expensive calculations, and it would be unclear at what point to stop the process and determine that the minimizer is persistent. Fortunately, in the one-dimensional case, we can determine whether a given minimizer is transient efficiently ([Theorem 4.3](#) and [Remark 4.4](#)). In this scenario, it is possible to compute an interval such that all points within the interval are persistent minimizers,

⁷The persistent minimizer curve is defined on (c_1, ∞) with $c_1 = \frac{176}{25} - \frac{28\sqrt{14}}{25} \approx 2.849$ and the transient one on $(0, c_2)$ with $c_2 = \frac{176}{25} + \frac{28\sqrt{14}}{25} \approx 11.231$.

and all points outside the interval are either not minimizers of the model or are transient minimizers. Moreover, whenever this interval is bounded, the unique persistent minimizer curve is also bounded, and vice versa. This insight will serve as the foundation for a rejection heuristic introduced in [Section 4.4](#).

Theorem 4.3. *Let t be a one-dimensional polynomial of order p such that^a $t'(0) < 0$ and define*

$$\mathcal{R}_+ = \{\alpha > 0 \mid t'(\alpha) = 0 \text{ or } t''(\alpha)\alpha - pt'(\alpha) = 0\}. \quad (19)$$

If \mathcal{R}_+ is empty, then the persistent minimizers are exactly $\alpha \in (0, \infty)$. If \mathcal{R}_+ is non-empty and its smallest entry $\bar{\alpha}$ is a simple root of either polynomial, then all persistent minimizers are contained in $(0, \bar{\alpha}]$, and all points in $(0, \bar{\alpha})$ are persistent minimizers.

^aThe case of $t'(0) > 0$ follows similarly as explained in [Remark 4.5](#)

Proof. For any tuple $(\alpha, \sigma) \in \mathbb{R} \times \mathbb{R}_{\geq 0}$ such that α is a local minimizer of m_σ , the second-order necessary conditions imply

$$t'(\alpha) + \sigma|\alpha|^{p-1}\alpha = m'_\sigma(\alpha) = 0 \quad (20a)$$

$$t''(\alpha) + p\sigma|\alpha|^{p-1} = m''_\sigma(\alpha) \geq 0 \quad (20b)$$

$$\sigma \geq 0. \quad (20c)$$

Since $t'(0) < 0$, we know that $\alpha \neq 0$, and we can rewrite (20a) as follows:

$$\sigma = \frac{-t'(\alpha)}{|\alpha|^{p-1}\alpha}. \quad (21)$$

By combining (20) and (21), we get the following system, which is equivalent to (20):

$$\sigma = \frac{-t'(\alpha)}{|\alpha|^{p-1}\alpha} \quad (22a)$$

$$t''(\alpha) + p\frac{-t'(\alpha)}{\alpha} \geq 0 \quad (22b)$$

$$\frac{-t'(\alpha)}{\alpha} \geq 0 \quad (22c)$$

Notably, the last two inequalities do not involve σ , which means we can use them to identify which α can be minimizers of the model. According to [Theorem B.2](#), any persistent minimizer lies on a continuous curve of minimizers that converges to zero. Conversely, if there exists a point α that is not a minimizer for any σ , we know that all minimizers beyond that value in the direction away from zero must be transient.

For α close enough to zero, say $\alpha \in (-\beta, \beta)$ for some $\beta > 0$, we know that $t'(\alpha)$ is negative, implying that in this region, the only solutions to (22c) are positive. Using the reasoning above, we know that there are no minimizers $\alpha \in (-\beta, 0)$, and so all persistent

minimizers must be positive. For positive minimizers we can simplify the conditions. They must satisfy:

$$\alpha > 0 \tag{23a}$$

$$-t'(\alpha) \geq 0 \tag{23b}$$

$$t''(\alpha)\alpha - pt'(\alpha) \geq 0 \tag{23c}$$

according to (22b) and (22c).

Since t is a p th-order polynomial, (23b) and (23c) are polynomial inequalities of order $p - 1$, and they are satisfied for α small enough because $t'(0) < 0$. If \mathcal{R}_+ is non-empty, by the definition of $\bar{\alpha}$, it is the smallest α such that one of the two conditions is satisfied with equality. Furthermore, since we assume it is a simple root of one of the two polynomials, there must be a sign change in one of them. This means there are no minimizers $\alpha \in (\bar{\alpha}, \bar{\alpha} + \beta)$ for some $\beta > 0$. Using the same argument as above, all persistent minimizers must therefore be in $(0, \bar{\alpha}]$. If \mathcal{R}_+ is empty, on the other hand, we have already shown that all persistent minimizers are in $(0, \infty)$. This is the first part of the claim.

For the second part, let $\bar{\alpha} = \infty$ if \mathcal{R}_+ is empty. Using the definition of $\bar{\alpha}$ again, all $\alpha \in (0, \bar{\alpha})$ satisfy (23b) and (23c) strictly and are strict local minimizers of the corresponding m_σ . To show that they are all persistent, let ψ be the minimizer curve defined by $\psi(\sigma(\alpha)) = \alpha$ for $\alpha \in (0, \bar{\alpha})$ where

$$\sigma(\alpha) = \frac{-t'(\alpha)}{|\alpha|^{p-1}\alpha}. \tag{24}$$

We need to prove that ψ is a well-defined function, that it is continuous, and that its domain is unbounded from above. Note first that $\sigma(\alpha)$ is continuously differentiable for positive α and that the derivative of $\sigma(\alpha)$ is

$$\sigma'(\alpha) = \frac{-t''(\alpha)\alpha + pt'(\alpha)}{|\alpha|^{p+1}} \stackrel{(23c)}{<} 0. \tag{25}$$

This means that the function is strictly monotonically decreasing and, therefore, a one-to-one mapping between $(0, \bar{\alpha})$ and its range. Moreover, as α converges to zero, $-t'(\alpha)$ converges to a positive constant and $|\alpha|^{p-1}\alpha$ converges to zero and so its range is unbounded from above. If $\bar{\alpha} < \infty$, this shows that $\psi: (\sigma(\bar{\alpha}), \infty) \rightarrow (0, \bar{\alpha})$ defines (part of) a persistent minimizer curve, which contains all points in $(0, \bar{\alpha})$. When $\bar{\alpha} = \infty$, then $\lim_{\alpha \rightarrow \bar{\alpha}} \sigma(\alpha) = 0$ because $t'(\alpha) = O(\alpha^{p-1})$ as $\alpha \rightarrow \infty$, so that $\psi: (0, \infty) \rightarrow (0, \infty)$ is a persistent minimizer curve, which contains all points in $(0, \infty)$. This completes the second part of the claim. \square

Remark 4.4. Note that the assumption that $\bar{\alpha}$ is a simple root, if it exists, holds for a generic p th-order polynomial t , since a generic polynomial has only simple roots. In this case, determining the interval of persistent minimizers only requires solving for the roots of two $(p - 1)$ st-order polynomials and identifying the smallest

positive root $\bar{\alpha}$, which can be done very efficiently.

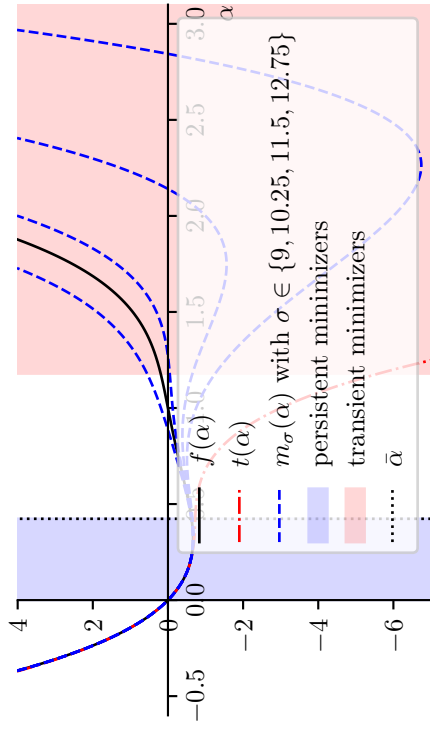
Remark 4.5. The same approach applies if $t'(0) > 0$, as one can simply analyse $\tilde{t}(\alpha) = t(-\alpha)$ with $\tilde{t}'(0) < 0$ and then reverse the signs for the resulting interval.

To illustrate the idea of persistent and transient minimizers we consider the one-dimensional function $f(x) = 3x^4 - 10x^3 + 12x^2 - 5x$ from Figure 6 and its Taylor expansion at $x = 0$ again. Figure 7b shows how the AR3 local model changes as σ varies. The right valley and its local minimizer disappear as σ increases, exactly as shown by Figure 6. Using Theorem 4.3 one can analyse that only $\alpha \in [\alpha_{\text{left}}, \alpha_{\text{right}}] := [(4 - \sqrt{7/2})/5, (4 + \sqrt{7/2})/5] \approx [0.426, 1.174]$ are never minimizers of the model for any value of σ . Therefore, all points to the right of that interval, namely $\alpha > \alpha_{\text{right}}$, are transient minimizers marked in red, and all points to the left up to zero, i.e., $\alpha \in (0, \alpha_{\text{left}})$, are persistent minimizers marked in blue. $\bar{\alpha} = \alpha_{\text{left}}$ in this case. Figure 7a shows the AR2 models for the same function and expansion point. Since the function is locally convex around the expansion point, the second-order Taylor expansion is a convex quadratic with a bounded minimizer even when $\sigma = 0$. This unique model minimizer slowly shifts towards zero when σ increases as also shown by Figure 6. In this case, all possible minimizers are persistent for the AR2 model.

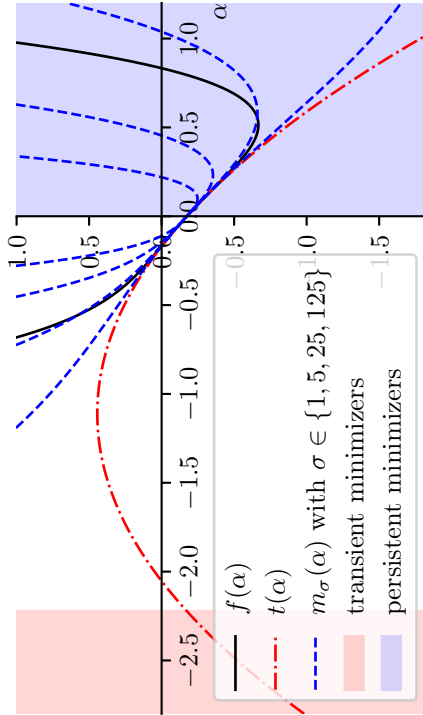
The locally nonconvex case is depicted by Figures 7c and 7d. Here, we consider essentially the same fourth-degree polynomial as before but rotated and expanded at a different point ($x = 5/6$). Both AR2 and AR3 have transient minimizers that correspond to ascent directions and all $\alpha \in (0, \infty)$ are persistent.

4.4. Rejecting directionally transient minimizers

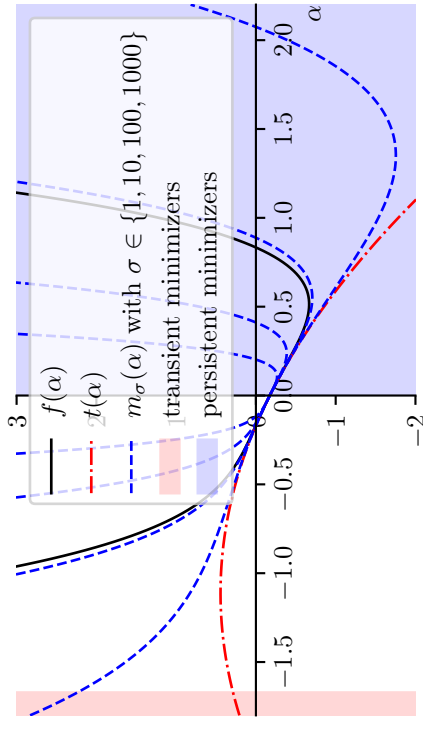
As motivated at the beginning of the section, transient minimizers are unlikely to accurately predict the behaviour of the objective function. To our knowledge, no AR p subproblem solver in the literature is designed to identify whether a persistent minimizer exists and return one. As a practical heuristic, we instead take the step \mathbf{s}_k found by a generic unconstrained nonconvex optimization algorithm applied to the subproblem, consider the one-dimensional subspace spanned by $\mathbf{0}$ and \mathbf{s}_k and determine whether the step is a persistent minimizer along this subspace. If $\alpha = \|\mathbf{s}_k\|$ is persistent for $t_{\rightarrow}(\alpha) = t_{\mathbf{x}_k}^p(\alpha \mathbf{s}_k / \|\mathbf{s}_k\|)$, we classify the step as *directionally persistent*, otherwise as *directionally transient*. According to this definition, a step is automatically directionally transient if it is not a descent direction, i.e., if $\nabla f(\mathbf{x}_k)^\top \mathbf{s}_k \geq 0$. Any directionally transient step is rejected without evaluating the objective function at the potential new iterate, and σ_k is increased by a constant factor. For any directionally persistent step, the function is evaluated, and σ_k is updated as before. The implementation of this heuristic is described in Procedure 4.1. It can be combined with any existing updating strategy on Line 9. We denote AR p variants that have been enhanced with our prerejection heuristic with a superscript $+$, so AR3-Simple and AR3-Interp become AR3-Simple $^+$ and AR3-Interp $^+$.



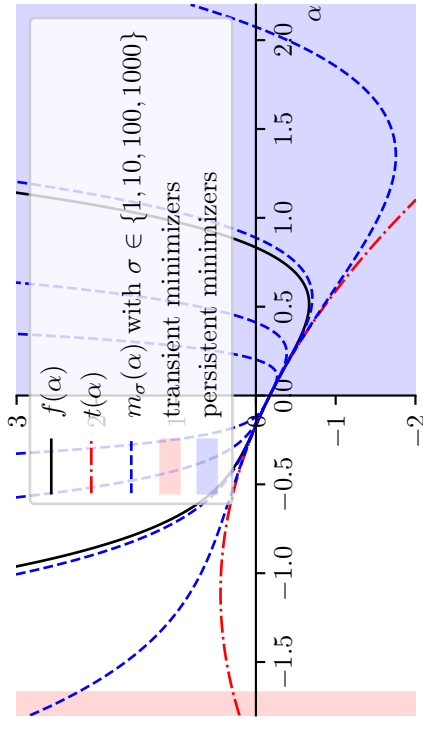
(a) AR2 models for $f(x) = 3x^4 - 10x^3 + 12x^2 - 5x$



(b) AR3 models for $f(x) = 3x^4 - 10x^3 + 12x^2 - 5x$



(c) AR2 models for $f(x) = 3x^4 - \frac{1}{2}x^2 - \frac{10}{9}x - \frac{25}{144}$



(d) AR3 models for $f(x) = 3x^4 - \frac{1}{2}x^2 - \frac{10}{9}x - \frac{25}{144}$

Figure 7: Illustration of AR2 and AR3 subproblem models for different σ . The regions where (22) is satisfied are shaded blue and red, depending on whether the corresponding points are persistent or transient minimizers.

Remark 4.6. When combining [Procedure 4.1](#) and [Procedure 3.2](#) into AR3-Interp⁺ we also adapt the interpolation-based search inside [Procedure 3.2](#) to only consider directionally persistent minimizers. This done by simply adding the “constraint” $\alpha \leq \bar{\alpha}$ to [\(14\)](#), for $\bar{\alpha}$ calculated on [Line 7](#) of [Procedure 4.1](#).

Procedure 4.1: Transient minimizer prerejection-enhanced update

Parameters: $\gamma_2 > 0$
Defaults: $\gamma_2 = 3$

```

1 if  $\nabla f(\mathbf{x}_k)^\top \mathbf{s}_k \geq 0$  then                                     // directionally transient
2 |   Set  $\mathbf{x}_{k+1} = \mathbf{x}_k$  and  $\sigma_{k+1} = \gamma_2 \sigma_k$ 
3 end
4 Define  $t_{\rightarrow}(\alpha) = t_{\mathbf{x}_k}^p(\alpha \mathbf{s}_k / \|\mathbf{s}_k\|)$  and  $m_{\sigma, \rightarrow}(\alpha) = m_{\mathbf{x}_k, \sigma}^p(\alpha \mathbf{s}_k / \|\mathbf{s}_k\|)$ 
5 Define  $\xi = \max(0, m'_{\sigma_k, \rightarrow}(\|\mathbf{s}_k\|))$ 
6 Compute the set of roots  $\mathcal{R} = \{\xi - t'_{\rightarrow}(\alpha) = 0\} \cup \{t''_{\rightarrow}(\alpha)\alpha + p(\xi - t'_{\rightarrow}(\alpha)) = 0\}$ 
7 Select the smallest positive root  $\bar{\alpha} \in \mathcal{R}$  or let  $\bar{\alpha} = \infty$  if there is none
8 if  $\|\mathbf{s}_k\| \leq \bar{\alpha}$  then                                           // directionally persistent
9 |   Compute  $\mathbf{x}_{k+1}$  and  $\sigma_{k+1}$  using some updating strategy
10 else                                                                // directionally transient
11 |   Set  $\mathbf{x}_{k+1} = \mathbf{x}_k$  and  $\sigma_{k+1} = \gamma_2 \sigma_k$ 
12 end

```

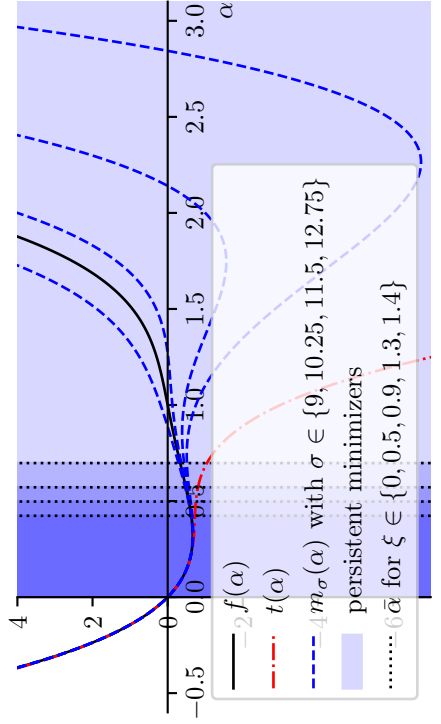
Note that there is a slight modification to the procedure derived in the previous section: the computation of ξ on [Line 5](#) of [Procedure 4.1](#), which aims to resolve an issue with using [Theorem 4.3](#) in practice. When implementing the inequalities in [\(23\)](#) strictly ($\xi = 0$), the method would reject points even if they are extremely close to persistent minimizers as long as they are just outside the interval of persistent minimizers. Since all subproblem solvers return approximate stationary points we must relax the requirements on \mathbf{s}_k slightly to avoid this situation. Instead of requiring α to be a stationary point of $m_{\sigma, \rightarrow}$ in [\(20a\)](#), we require $m'_{\sigma, \rightarrow}(\alpha) \leq \xi$. Given that $\alpha > 0$ is naturally ensured by [Line 1](#) of [Procedure 4.1](#), we can follow the derivation to obtain

$$\sigma \leq \frac{\xi - t'_{\rightarrow}(\alpha)}{\alpha^p} \quad (26)$$

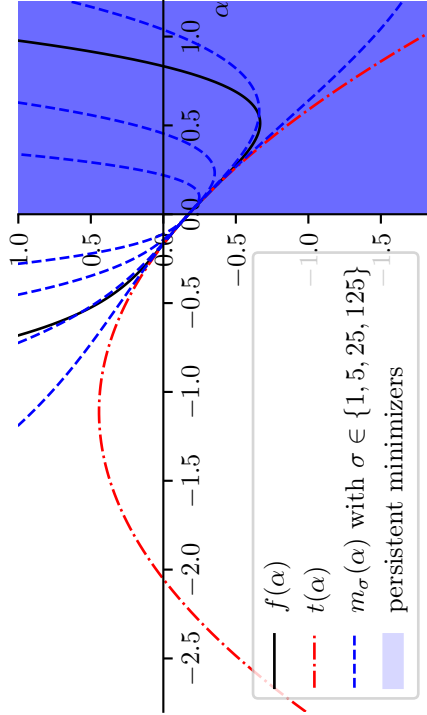
which means [\(23b\)](#) and [\(23c\)](#) need to be adapted as

$$\xi - t'_{\rightarrow}(\alpha) \geq 0 \quad \text{and} \quad t''_{\rightarrow}(\alpha)\alpha + p(\xi - t'_{\rightarrow}(\alpha)) \geq 0. \quad (27)$$

By choosing $\xi = \max(0, m'_{\sigma_k, \rightarrow}(\|\mathbf{s}_k\|))$, we make sure that ξ is never negative and that the relaxed stationarity condition $m'_{\sigma, \rightarrow}(\alpha) \leq \xi$ is satisfied at $\alpha = \|\mathbf{s}_k\|$ for the current regularization parameter σ_k . In other words, since \mathbf{s}_k is considered to be an approximate stationary point by the subproblem solver, we relax [\(20a\)](#) just enough such that $\alpha = \|\mathbf{s}_k\|$ is also considered “stationary enough” by [Procedure 4.1](#).

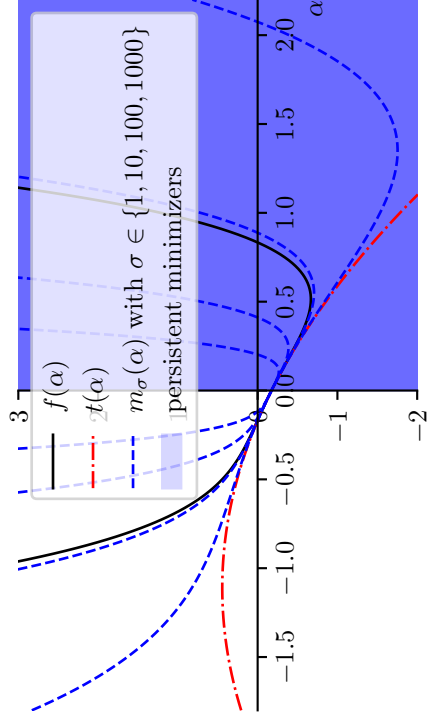


(a) AR2 models for $f(x) = 3x^4 - 10x^3 + 12x^2 - 5x$



(b) AR3 models for $f(x) = 3x^4 - 10x^3 + 12x^2 - 5x$

(c) AR2 models for $f(x) = 3x^4 - \frac{1}{2}x^2 - \frac{10}{9}x - \frac{25}{144}$



(d) AR3 models for $f(x) = 3x^4 - \frac{1}{2}x^2 - \frac{10}{9}x - \frac{25}{144}$

Figure 8: Illustration of AR2 and AR3 subproblem models and the impact of the relaxation parameter ξ in Procedure 4.1. The persistent minimizer regions ($0, \bar{\alpha}$) are shaded in blue with regions overlapping for different values of ξ . The graphs clearly demonstrate how increasing ξ relaxes the requirements on α .

Figure 8 shows the same cases as Figure 7 but focuses on the effect of ξ on the value of $\bar{\alpha}$. Consider Figure 8b as an example. As ξ increases, the blue region, representing the interval $(0, \bar{\alpha}]$ expands until at $\xi = 1.4$, $\bar{\alpha}$ becomes $+\infty$. The depth of the coloured region indicates the shared areas resulting from different choices of ξ ; for example, the darkest region corresponds to $\xi = 0$, as it is mutually contained by all provided ξ values. The same expansion of the blue region can also be observed in Figure 8a. For Figures 8c and 8d the persistent minimizer region is already unbounded for $\xi = 0$, so any further relaxation does not change anything.

Note that, as explained above, ξ is chosen depending on

$$m'_{\sigma_k, \rightarrow}(\|\mathbf{s}_k\|) = \nabla m_k(\mathbf{s}_k)^\top (\mathbf{s}_k / \|\mathbf{s}_k\|) \leq \|\nabla m_k(\mathbf{s}_k)\|, \quad (28)$$

which in turn depends on the termination criterion for the subproblem solver. In the following experiments, the subproblem solver is terminated using (TC.a) with $\varepsilon_{\text{sub}} = 10^{-9}$, so that the conditions on α are only relaxed very little. The values of ξ in Figure 8 are chosen much larger for illustration purposes.

4.5. Numerical illustrations

In Figure 9, we can observe in detail how the prerejection mechanism enhances performance. For MGH5, the total number of function evaluations for AR3-Interp is nearly double compared to AR3-Interp⁺. In the case of MGH13, it was previously shown in Figure 4 that AR3-Interp used more function evaluations than AR3-Simple. However, when using the prerejection framework, AR3-Interp⁺ avoids additional function evaluations, resulting in the same number of function evaluations as AR3-Simple⁺. The prerejection framework effectively rejects unnecessary function evaluations in unsuccessful cases, as demonstrated for MGH13 in Figure 4.

In Figure 10, we observe that the performance of algorithms with our prerejection Procedure 4.1 is promising in terms of function evaluations. Both AR3-Simple and AR3-Interp are enhanced by incorporating Procedure 4.1. The number of derivative evaluations remains identical for AR3-Simple and is similar for AR3-Interp, indicating that the additional prerejection framework does not increase the number of successful iterations while effectively reducing the number of function evaluations in unsuccessful iterations. This suggests that our prerejection mechanism optimizes the overall process by cutting down unnecessary function evaluations without negatively impacting the convergence behaviour.

4.6. Comparison with BGMS step control strategy

BGMS is a method that incorporates both an updating strategy and a heuristic prerejection framework, as detailed in [6, Algorithm 4.1]. BGMS introduces several novel features, including:

- *Zero regularization attempt*: After every successful iteration the new Taylor expansion is constructed and minimized without regularization ($\sigma = 0$). Only when

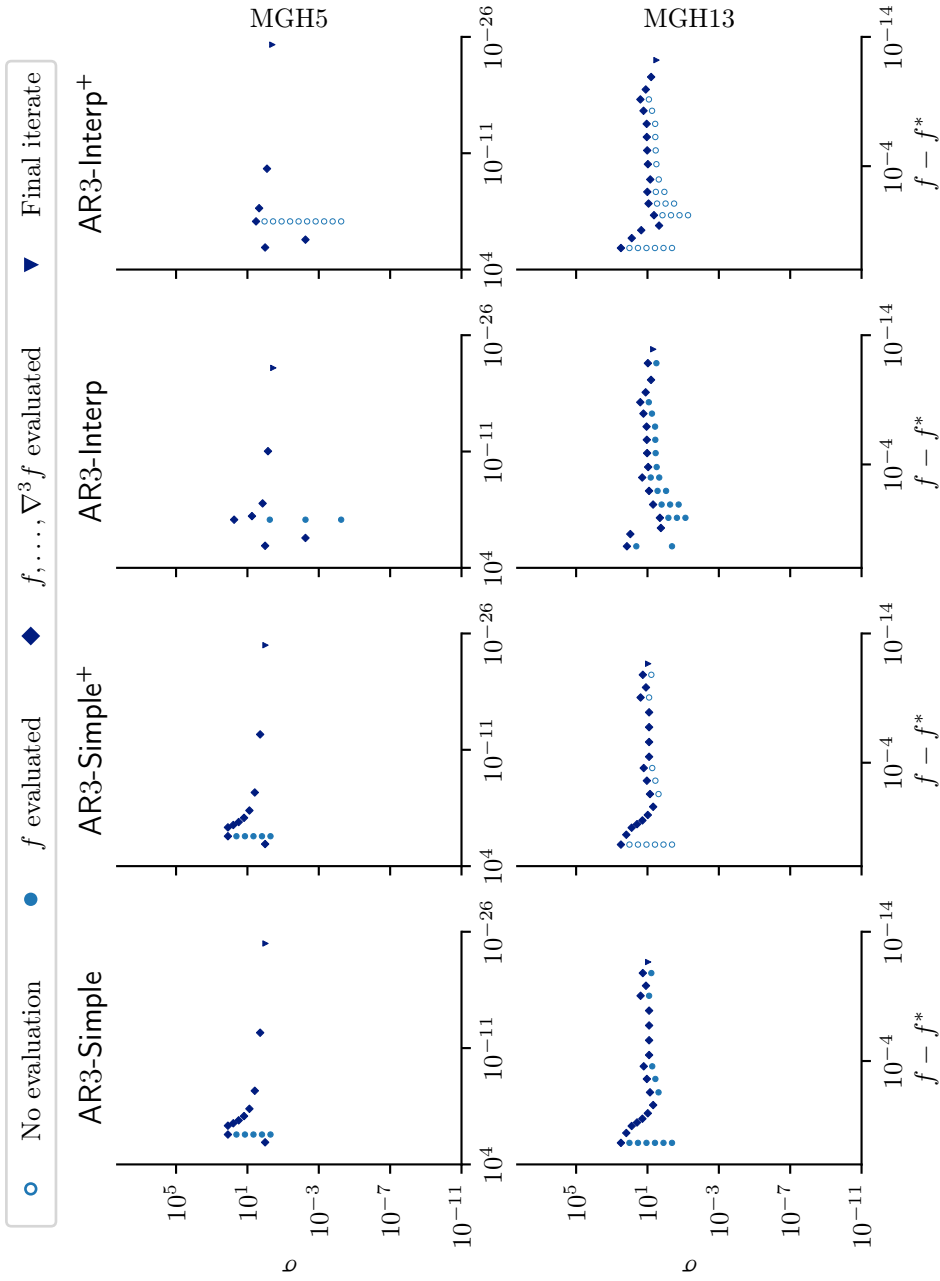


Figure 9: The convergence dot plot illustrates the impact of including prejection. The prejection framework demonstrates its ability to effectively “predict” unsuccessful iterations and avoid the corresponding function evaluations in both AR3-Simple+ and AR3-Interp+. Additionally, we do not observe any cases where prejection incorrectly rejects a successful iteration, which would have resulted in a large σ or more iterations.

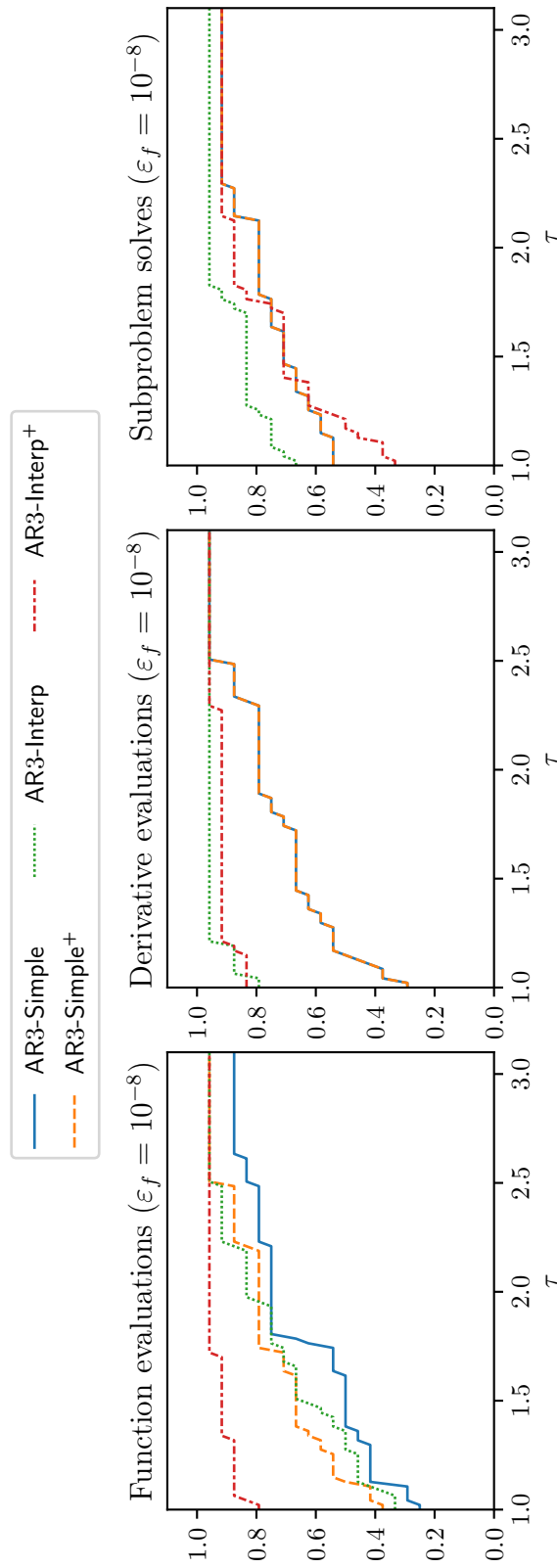


Figure 10: The performance profile plot illustrates the impact of including prejection. AR3-Interp⁺ shows exceptional efficiency in avoiding unnecessary function evaluations, although it increases the number of subproblem solves. However, the enhancement in saving function evaluations persists without causing any additional solves for AR3-Simple⁺.

Procedure 4.2: BGMS update (Algorithm 4.1 in [6])

Parameters: $\hat{\eta}_1, \hat{\eta}_2 > 0$, $J \in \mathbb{N}$, $\alpha > 0$, $0 < \gamma_1 < 1 < \gamma_2$, $\sigma_{\min} > 0$

Defaults: $\hat{\eta}_1 = 10^3$, $\hat{\eta}_2 = 3$, $J = 20$, $\alpha = 10^{-8}$, $\gamma_1 = 0.5$, $\gamma_2 = 10$, $\sigma_{\min} = 10^{-8}$

Note: The procedure requires two additional variables: j_k and σ_k^{ini} . Before the first iteration, the initial regularization parameter computed in (3) is stored in σ_0^{ini} , and σ_0 and j_0 are set zero.

```

1 if  $\sigma_k = 0$  and no  $\mathbf{s}_k$  could be found then
2   | Set  $j_{k+1} = j_k + 1$ ,  $\mathbf{x}_{k+1} = \mathbf{x}_k$ , and  $\sigma_{k+1} = \sigma_k^{\text{ini}}$ 
3 else
4   | if  $j_k \geq J$  or  $\left(\frac{t_k(\mathbf{0}) - t_k(\mathbf{s}_k)}{\max\{1, |t_k(\mathbf{0})|\}} \leq \hat{\eta}_1$  and  $\frac{\|\mathbf{s}_k\|_\infty}{\max\{1, \|\mathbf{x}_k\|_\infty\}} \leq \hat{\eta}_2\right)$  then
5     | if  $f(\mathbf{x}_k + \mathbf{s}_k) \leq f(\mathbf{x}_k) - \alpha \|\mathbf{s}_k\|^{p+1}$  then
6       | Set  $j_{k+1} = 0$ ,  $\mathbf{x}_{k+1} = \mathbf{x}_k + \mathbf{s}_k$ , and  $\sigma_{k+1} = 0$ 
7     | else
8       | Set  $j_{k+1} = j_k + 1$ ,  $\mathbf{x}_{k+1} = \mathbf{x}_k$ , and  $\sigma_{k+1} = \begin{cases} \sigma_k^{\text{ini}} & \text{if } \sigma_k = 0 \\ \gamma_2 \sigma_k & \text{otherwise} \end{cases}$ 
9     | end
10  | else
11    | Set  $j_{k+1} = j_k + 1$ ,  $\mathbf{x}_{k+1} = \mathbf{x}_k$ , and  $\sigma_{k+1} = \begin{cases} \sigma_k^{\text{ini}} & \text{if } \sigma_k = 0 \\ \gamma_2 \sigma_k & \text{otherwise} \end{cases}$ 
12  | end
13 end
14 Set  $\sigma_{k+1}^{\text{ini}} = \max\{\gamma_1 \sigma_k, \gamma_1 \sigma_k^{\text{ini}}, \sigma_{\min}\}$ 

```

no minimizer can be found or the step is not successful, the method switches to a nonzero regularization parameter.

- *Prerejection of long and overly optimistic steps:* Whenever one of

$$\frac{t_k(\mathbf{0}) - t_k(\mathbf{s}_k)}{\max\{1, |t_k(\mathbf{0})|\}} \leq \hat{\eta}_1 \quad \text{and} \quad \frac{\|\mathbf{s}_k\|_\infty}{\max\{1, \|\mathbf{x}_k\|_\infty\}} \leq \hat{\eta}_2 \quad (29)$$

is violated, the step is rejected without evaluating the function at $\mathbf{x}_k + \mathbf{s}_k$.

- *Safeguarded prerejection:* The prerejection can only be activated J times in a row, otherwise $f(\mathbf{x}_k + \mathbf{s}_k)$ is evaluated even when (29) is violated. The authors report best results for $J = 20$, in which case this safeguard is almost never used, and can be understood as a device to ensure optimal complexity despite the heuristic.

These features allow BGMS to significantly reduce the total number of function evaluations. Specifically, the first inequality in (29) rejects steps with large predicted decreases, while the second inequality rejects steps with large entries. Therefore, (29) serves to “reject unuseful steps” [6] without compromising the theoretical results.

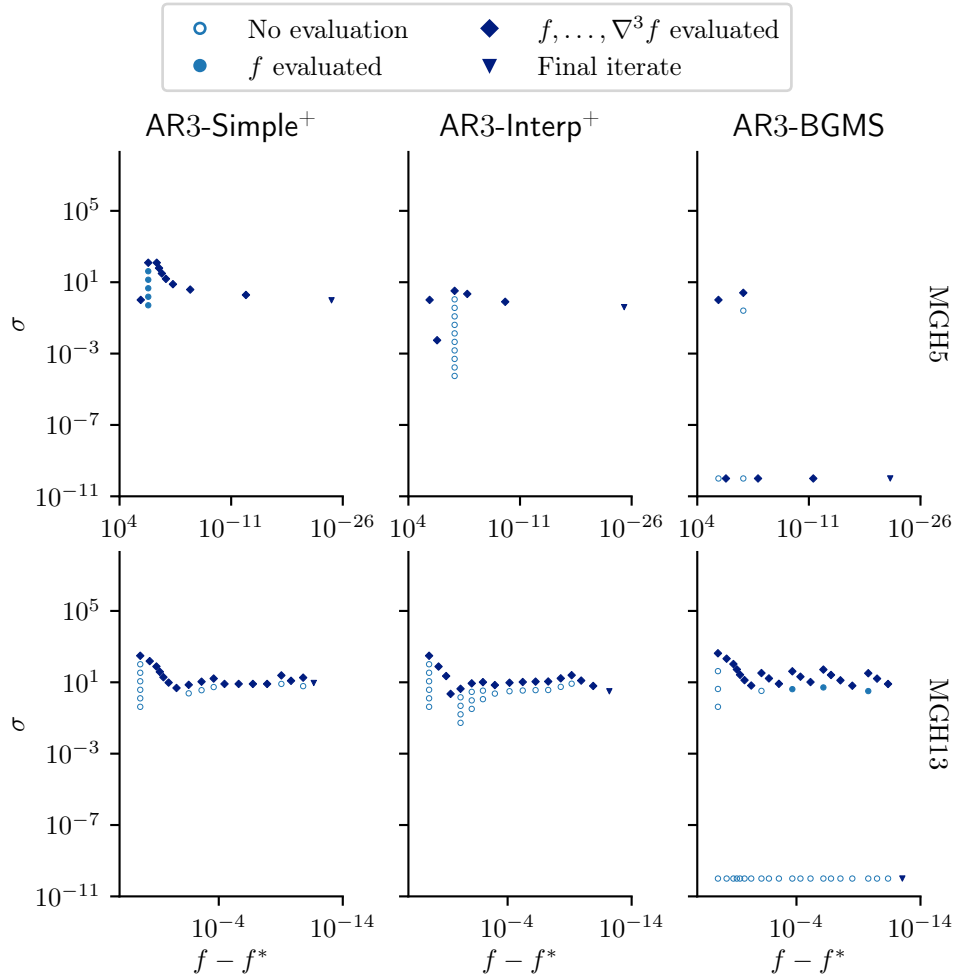


Figure 11: The convergence dot plot highlights the differences between the three update strategies. Note that prerejection is enabled for all three methods. AR3-BGMS demonstrates its unique ability to leverage large step-size trials with $\sigma_k = 0$ on MGH5. However, these attempts fail on MGH13, though fortunately, such steps are prerejected by their prerejection framework.

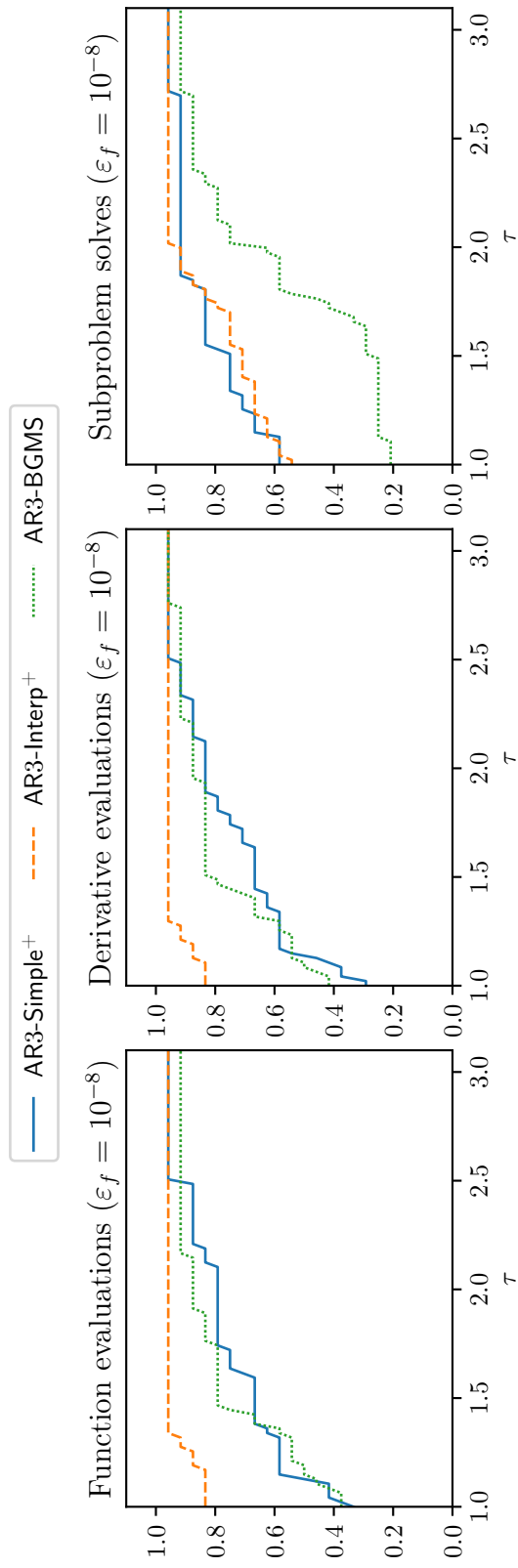


Figure 12: The performance profile plot highlights the differences between the three update strategies. Note that prerejection is enabled for all three methods. AR3-Interp+ outperforms the other two methods in terms of function evaluations and derivative evaluations. AR3-BGMS is comparable to AR3-Simple+ but is less efficient in subproblem solves.

Figures 11 and 12 compare the simple and interpolation-based updating strategies enhanced by Procedure 4.1 with the updating strategy and prerejection framework in Procedure 4.2. AR3-BGMS represents our implementation of the BGMS update. In particular, it uses the same subproblem solver as AR3-Simple and AR3-Interp (see Section 1.3) to ensure a fair comparison. For the parameter settings of AR3-BGMS, we adhere to the parameters recommended in [6].

The convergence dot plots in Figure 11 clearly show the attempts at calculating a minimizer of the unregularized Taylor expansion with dots at the bottom of the graph. Note that iterations where $\sigma_k = 0$ are plotted as if $\sigma_k = 10^{-10}$ to make them visible on the log-scaled axis.⁸ For MGH5, we observe that the zero regularization idea is highly effective. Three iterations successfully make use of the minimizer of the unregularized Taylor expansion and AR3-BGMS terminates after six iterations, which is the same number required by AR3-Interp⁺. In contrast, for MGH13, the zero regularization attempts are never successful. Additionally, there are unsuccessful iterations where the function is evaluated, unlike in AR3-Interp⁺, indicating that the prerejection mechanism in AR3-BGMS is less efficient compared to the one discussed in this section.

The performance profile plots in Figure 12 demonstrate that AR3-Interp⁺ dominates the other two methods in terms of both function evaluations and derivative evaluations. While AR3-BGMS generally outperforms AR3-Simple⁺ across most problems, it lags in the subproblem solving plot due to its attempts without regularization after every successful iteration.

5. Subproblem termination conditions

So far all experiments used (TC.a) with $\varepsilon_{\text{sub}} = 10^{-9}$ to decide when to terminate the search for a subproblem minimizer. In order to investigate the impact of the subproblem termination condition on the performance of the algorithm, we compare this condition, which we consider a very accurate solution of the subproblem, with (TC.r) for $\theta \in \{10^{-2}, 10^0, 10^2, 10^4\}$. For larger steps, the latter condition allows for significantly more inexactness in the solution, which can also lead to extra relaxation in the prerejection procedure Procedure 4.1. Additional experiments, conducted to compare variants using the “generalized norm” termination condition [25], are discussed in Appendix E.

5.1. Numerical illustrations

As shown in Figure 13, when θ becomes large enough, such as $\theta = 100$, AR3-Interp⁺ converges without any unsuccessful iterations for MGH5 and MGH13, and σ_k is maintained at a lower level compared to smaller θ values. However, for $\theta = 10^4$, the early termination of the subproblem solver leads to slower progress and additional iterations for MGH13. This suggests that the optimal parameter value is around $\theta = 100$ in our case. In general, the optimal choice of θ will depend on both the test set and the sub-

⁸As $10^{-10} < \sigma_{\text{min}} = 10^{-8}$ there is no risk of confusion.

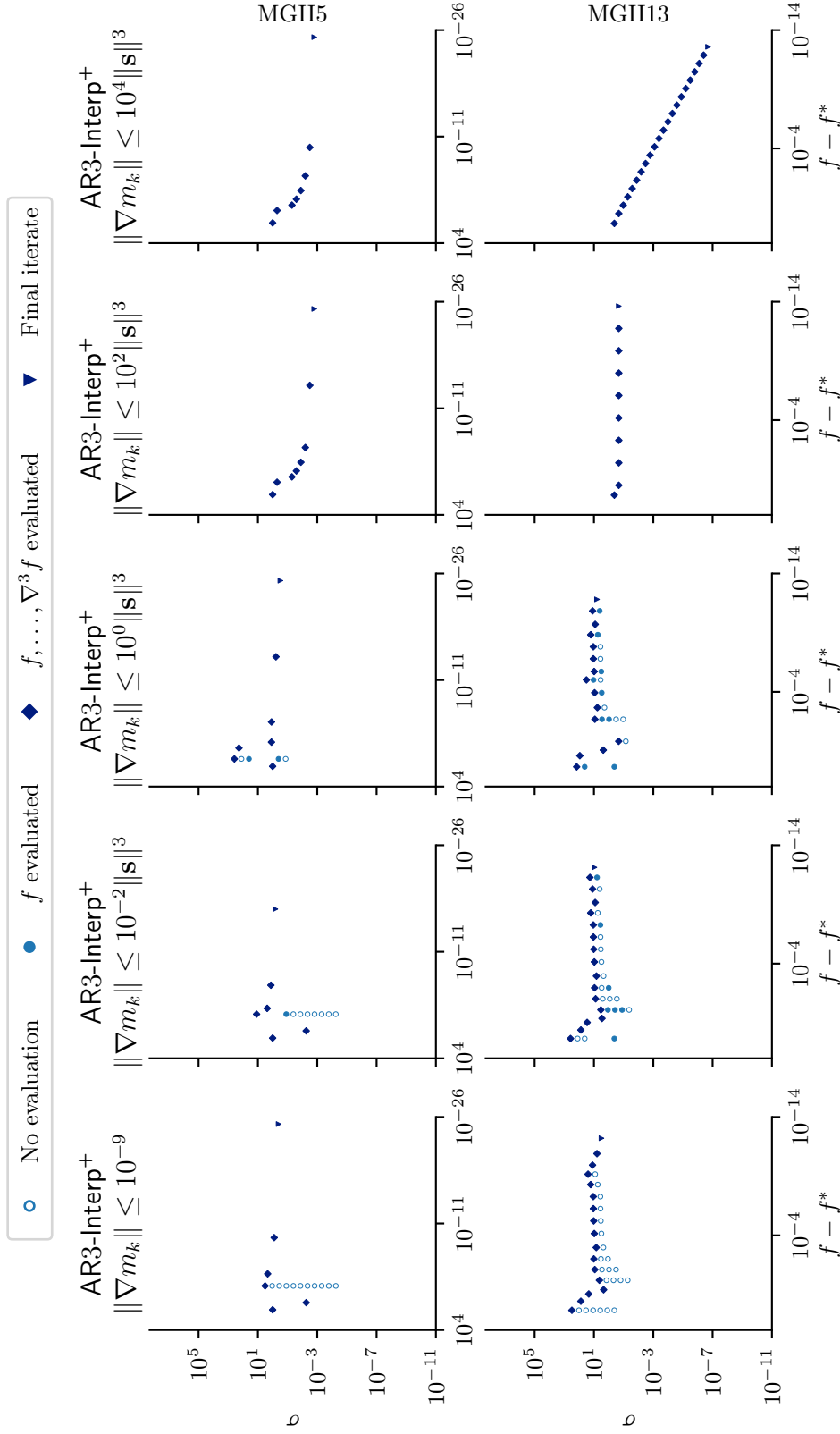


Figure 13: The convergence dot plot shows the differences between different subproblem termination conditions, namely (TC.a) with $\varepsilon_{\text{sub}} = 10^{-9}$ and (TC.r) with $\theta \in \{10^{-2}, 10^0, 10^2, 10^4\}$. More inexact solves more often lead to successful iterations when σ_k is small, sometimes at the expense of fast progress.

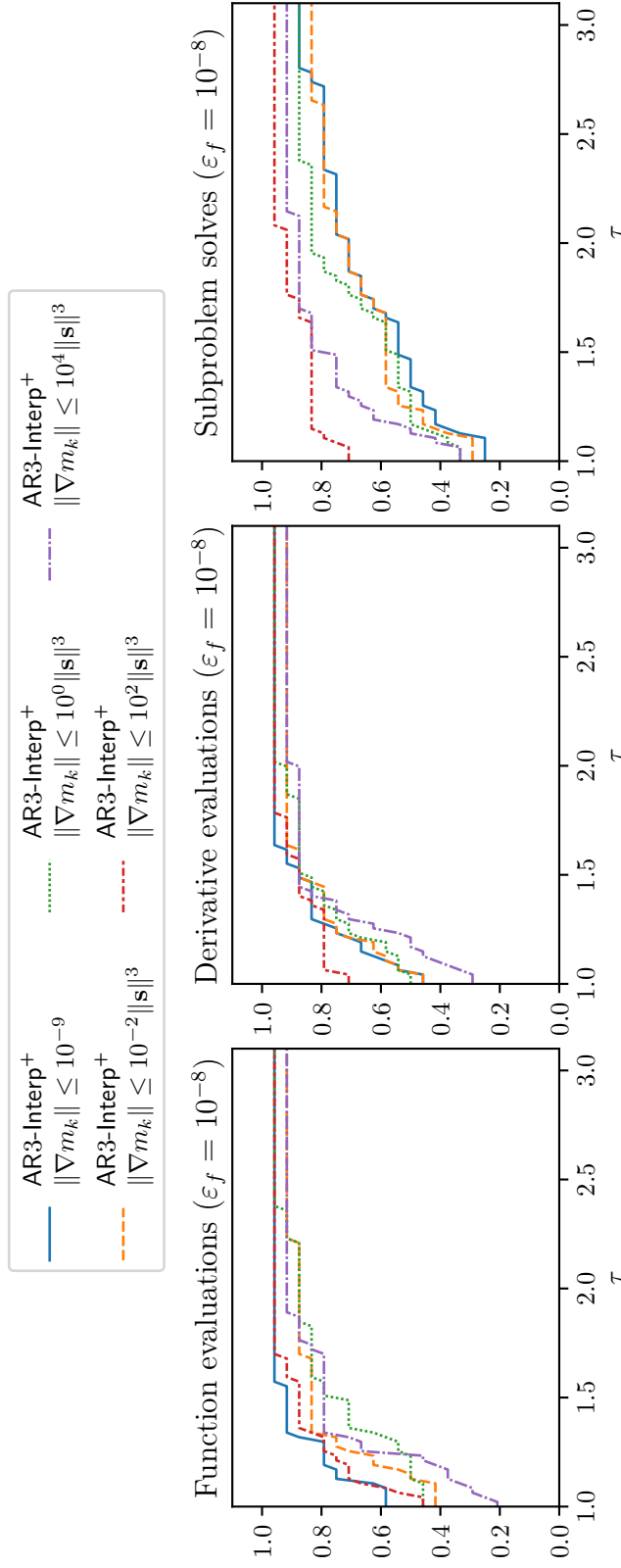


Figure 14: The performance profile plot shows the differences between different subproblem termination conditions, namely (TC.a) with $\varepsilon_{\text{sub}} = 10^{-9}$ and (TC.r) with $\theta \in \{10^{-2}, 10^0, 10^2, 10^4\}$. For all metrics, $\theta = 100$ is among the best performing variants.

problem solver and its parameters, since the solvers' path towards the model minimizer becomes relevant for less stringent termination conditions.

We observed that for larger θ values, our prerejection mechanism was rarely activated and did neither reduce nor increase the number of function evaluations significantly. However, since the optimal θ may not be known in advance, it is still advisable to keep prerejection enabled to avoid unnecessary unsuccessful function evaluations where possible, as illustrated in the left three columns of [Figure 13](#).

The conclusions from the convergence dot plots also hold for the other functions in our test set. Comparing [\(TC.r\)](#) and [\(TC.a\)](#), [Figure 14](#) shows that the number of derivative evaluations does not change significantly, while the number of subproblem solves decreases, indicating a higher percentage of iterations are successful. The added inexactness allows the subproblem solver to terminate earlier and select a point which is not close to a stationary point of the model but nonetheless leads to a successful iteration. Again, the value of $\theta = 100$ consistently performs the best for [\(TC.r\)](#) on function evaluations, derivative evaluations, and subproblem solves and is competitive or outperforms [\(TC.a\)](#) with $\varepsilon_{\text{sub}} = 10^{-9}$. Therefore, we view [AR3-Interp⁺](#) using [\(TC.r\)](#) and $\theta = 100$ as the most successful of all variants considered so far and will benchmark it in the following section.

6. Benchmarking

After determining the best-performing AR3 variant overall, we need to compare it to efficient AR p algorithms found in the literature. Firstly, we benchmark against a second-order method, namely [AR2-Interp](#). For $p = 2$, [Procedure 3.2](#) matches the suggested updating strategy in [\[24\]](#), which was found to outperform simpler updating rules. Therefore, the method can be considered an efficient variant of AR2. We do not use [AR2-Interp⁺](#) because the addition of prerejection would not make a difference. As explained in [Section 1.3](#), we use a very accurate solver which finds the global minimizer of the AR2 subproblems, and this global minimizer is always persistent by [Theorem B.3](#). This means that no step \mathbf{s}_k computed in this way would ever be prerejected. The optimal termination condition for [AR2-Interp](#) was determined to be [\(TC.r\)](#) with $\theta = 0.01$ (see [Appendix D](#)).

Secondly, we compare our contender to the AR3 algorithm used in [\[6\]](#), which we will refer to as [AR3-BGMS/Gencan](#) as it uses [Procedure 4.2](#) to update the regularization parameter and [Gencan](#) [\[2, 5, 8\]](#) as the subproblem solver. Lastly, we also include [AR3-BGMS](#), which is our implementation of the same updating strategy paired with our standard subproblem solver, to give some context on the differences caused by the subproblem solver and other implementation details. For both BGMS variants we report their results using [\(TC.r\)](#) with $\theta = 100$ as this is the subproblem termination condition used in [\[6\]](#).

We included all 35 problems from the MGH test set in the following performance profile plot. As all previous experiments were performed on a set of test functions that included only half of the MGH test set, the selection of [AR3-Interp⁺](#) with [\(TC.r\)](#) and $\theta = 100$ as the best variant is not the result of fine-tuning for this test set.

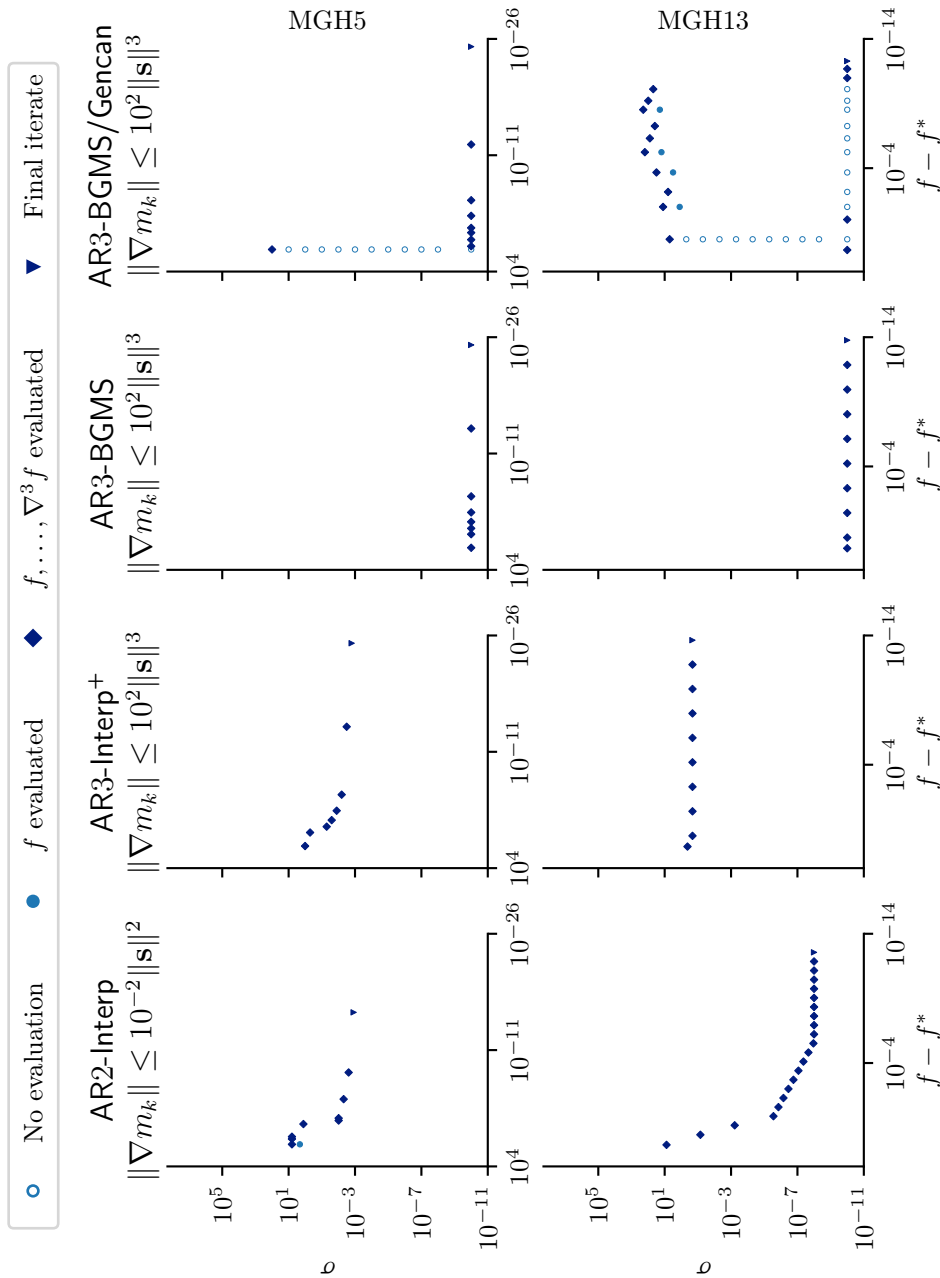


Figure 15: The convergence dot plot compares AR2-Interp, AR3-Interp⁺, AR3-BGMS and AR3-BGMS/Gencan using (TC.r). The second-order method shows slower asymptotic convergence for both MGH5 and MGH13. There are clear differences between AR3-BGMS and AR3-BGMS/Gencan caused by differing solvers for the AR3 subproblems.

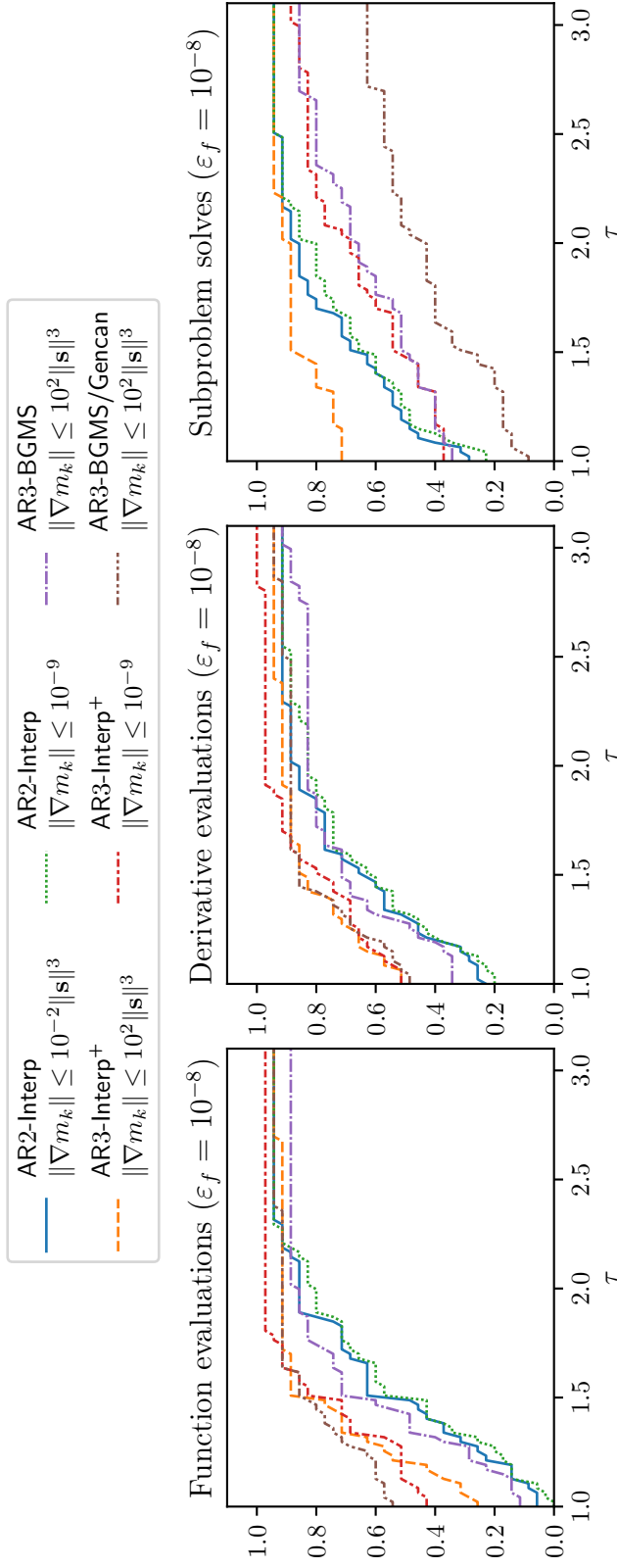


Figure 16: The performance profile plot compares AR2-Interp, AR3-Interp⁺, AR3-BGMS and AR3-BGMS/Gencan using (TC.a) and (TC.r) on the full 35 MGH test problems. AR3-Interp⁺ using the relative subproblem termination condition clearly outperforms the AR2-Interp variants on all metrics and is competitive with AR3-BGMS/Gencan in terms of function and derivative evaluations, while using far fewer subproblem solves.

The convergence dot plot in [Figure 15](#) clearly shows the difference in asymptotic convergence between AR2 and AR3. In the case of MGH5, both AR2-Interp and AR3-Interp⁺ exhibit superlinear local convergence, but the acceleration of convergence from one step to the next is greater for AR3. Similarly, for MGH13 both methods have linear convergence of the function value to its optimum, but the rate is higher for AR3, even when comparing to the slightly slower convergence of AR3-Interp⁺ with (TC.a) shown in [Figure 13](#). The graph in [Figure 15](#) also shows how the solver used for the AR3 subproblem can have a great impact on the number of iterations and the convergence speed, given that the left two columns differ quite significantly, especially for MGH13.

Turning to the performance profile plots in [Figure 16](#), we see that in terms of function and derivative evaluations both AR2-Interp variants (using (TC.a) and (TC.r)) are outperformed by the AR3 methods. This agrees with the findings by [\[6\]](#) as well as the global complexity results for AR p [\[7, 13, 14\]](#) that third-order methods can exploit the access to third derivatives to speed up the computation of a minimizer. Within the AR3 methods, AR3-BGMS/Gencan generally uses less function and derivative evaluations but more subproblem solves than AR3-BGMS, which highlights the need to consider the subproblem solver as a central component of AR p algorithms, especially when allowing for approximate solutions. Overall, the combination of modifications to the basic AR3 algorithm suggested in this paper (AR3-Interp⁺) is among the best-performing variants for function evaluations, derivative evaluations, and subproblem solves and therefore an efficient AR3 implementation.

7. Conclusion

In this paper, we introduced a series of practical algorithms under the general AR p algorithmic framework for nonconvex unconstrained optimization problems. Our approach incorporates an adaptive interpolation-based regularization parameter updating strategy and a prerejection step control strategy. Specifically, we proposed an inexpensive heuristic for choosing a reasonable σ_0 , and extended the interpolation-based updating strategy from [\[24\]](#) to cases where $p \geq 3$. Numerical results demonstrate the effectiveness and robustness of the proposed methods. Next, we closely examined the fundamental differences in AR p subproblems when $p \geq 3$ and introduced a novel prerejection module that efficiently rejects directionally transient minimizers of the subproblem, which demonstrated great efficiency by the numerical results. Furthermore, we examined the performance differences between absolute and relative termination conditions. Numerical results show that the proposed prerejection framework significantly improves efficiency and provides a reliable guide on “predicting” steps leading to unsuccessful iterations before any function evaluations, with both absolute and relative termination conditions. Finally, we combined the best of our proposed strategies and conducted a benchmark experiment, which confirmed that our AR3 variants are more efficient and competitive than the AR2 variants in both function and derivative evaluations, while also offering improvements in implementation efficiency. Additional detailed experimental results are provided in the appendix.

References

- [1] Amir Ali Ahmadi, Abraar Chaudhry, and Jeffrey Zhang. Higher-order Newton methods with polynomial work per iteration. *Advances in Mathematics*, 452:109808, August 2024.
- [2] Marina Andretta, Ernesto G. Birgin, and José Mario Martínez. Practical active-set Euclidian trust-region method with spectral projected gradients for bound-constrained minimization. *Optimization*, 54(3):305–325, June 2005.
- [3] Evelyn Martin Lansdowne Beale. On an iterative method of finding a local minimum of a function of more than one variable. Technical Report 25, Statistical Techniques Research Group, Princeton University, Princeton, N.J., 1958.
- [4] E. G. Birgin, J. L. Gardenghi, J. M. Martínez, and S. A. Santos. Third-order derivatives of the moré, garbow, and hillstrom test set problems. Technical Report MCDO010418, Department of Computer Science, University of São Paulo, São Paulo, SP, Brazil, 2018.
- [5] E. G. Birgin and J. M. Martínez. A Box-Constrained Optimization Algorithm with Negative Curvature Directions and Spectral Projected Gradients. In Goetz Alefeld and Xiaojun Chen, editors, *Topics in Numerical Analysis*, volume 15, pages 49–60. Springer Vienna, Vienna, 2001.
- [6] Ernesto G Birgin, JL Gardenghi, José Mario Martínez, and Sandra A Santos. On the use of third-order models with fourth-order regularization for unconstrained optimization. *Optimization Letters*, 14(4):815–838, 2020.
- [7] Ernesto G Birgin, JL Gardenghi, José Mario Martínez, Sandra Augusta Santos, and Ph L Toint. Worst-case evaluation complexity for unconstrained nonlinear optimization using high-order regularized models. *Mathematical Programming*, 163(1):359–368, 2017.
- [8] Ernesto G. Birgin and José Mario Martínez. Large-Scale Active-Set Box-Constrained Optimization Method with Spectral Projected Gradients. *Computational Optimization and Applications*, 23(1):101–125, October 2002.
- [9] Yair Carmon, John C Duchi, Oliver Hinder, and Aaron Sidford. Lower bounds for finding stationary points I. *Mathematical Programming*, 184(1):71–120, 2020.
- [10] Yair Carmon, John C Duchi, Oliver Hinder, and Aaron Sidford. Lower bounds for finding stationary points II: first-order methods. *Mathematical Programming*, 185(1):315–355, 2021.
- [11] Coralia Cartis, Nicholas I. M. Gould, and Philippe L. Toint. Adaptive cubic regularisation methods for unconstrained optimization. Part I: motivation, convergence and numerical results. *Mathematical Programming*, 127(2):245–295, April 2011.

- [12] Coralia Cartis, Nicholas I. M. Gould, and Philippe L. Toint. Adaptive cubic regularisation methods for unconstrained optimization. Part II: worst-case function- and derivative-evaluation complexity. *Mathematical Programming*, 130(2):295–319, December 2011.
- [13] Coralia Cartis, Nicholas IM Gould, and Ph L Toint. A concise second-order complexity analysis for unconstrained optimization using high-order regularized models. *Optimization Methods and Software*, 35(2):243–256, 2020.
- [14] Coralia Cartis, Nicholas IM Gould, and Ph L Toint. Sharp worst-case evaluation complexity bounds for arbitrary-order nonconvex optimization with inexpensive constraints. *SIAM Journal on Optimization*, 30(1):513–541, 2020.
- [15] Coralia Cartis, Nicholas IM Gould, and Ph L Toint. Evaluation complexity of algorithms for nonconvex optimization. *MOS-SIAM Series on Optimization.*, 2022.
- [16] Coralia Cartis, Nicholas IM Gould, and Philippe L Toint. Trust-region and other regularisations of linear least-squares problems. *BIT Numerical Mathematics*, 49(1):21–53, 2009.
- [17] Coralia Cartis and Wenqi Zhu. Second-order methods for quartically-regularised cubic polynomials, with applications to high-order tensor methods. *arXiv preprint arXiv:2308.15336*, 2023.
- [18] Ta-Tung Chow. *Derivative and Secant Tensor Methods for Unconstrained Optimization*. PhD thesis, University of Colorado at Boulder, 1989.
- [19] Nikita Doikov and Yurii Nesterov. Local convergence of tensor methods. *Mathematical Programming*, 193(1):315–336, 2022.
- [20] Elizabeth D Dolan and Jorge J Moré. Benchmarking optimization software with performance profiles. *Mathematical programming*, 91(2):201–213, 2002.
- [21] Jean-Pierre Dussault. ARCq: a new adaptive regularization by cubics. *Optimization Methods and Software*, 33(2):322–335, 2018.
- [22] Murat A. Erdogdu and Andrea Montanari. Convergence rates of sub-sampled newton methods. In *Proceedings of the 28th International Conference on Neural Information Processing Systems - Volume 2*, NIPS’15, page 3052–3060, Cambridge, MA, USA, 2015. MIT Press.
- [23] Nicholas Gould and Jennifer Scott. A note on performance profiles for benchmarking software. *ACM Transactions on Mathematical Software (TOMS)*, 43(2):15, 2016.
- [24] Nicholas IM Gould, Margherita Porcelli, and Philippe L Toint. Updating the regularization parameter in the adaptive cubic regularization algorithm. *Computational optimization and applications*, 53:1–22, 2012.

- [25] Serge Gratton and Phillipe Louis Toint. Adaptive regularization minimization algorithms with nonsmooth norms. *IMA Journal of Numerical Analysis*, 43(2):920–949, 2023.
- [26] Andreas Griewank. The modification of Newton’s method for unconstrained optimization by bounding cubic terms. Technical report, Technical report NA/12, 1981.
- [27] Frank L Hitchcock. The expression of a tensor or a polyadic as a sum of products. *Journal of Mathematics and Physics*, 6(1-4):164–189, 1927.
- [28] Jonas Moritz Kohler and Aurelien Lucchi. Sub-sampled cubic regularization for non-convex optimization. In Doina Precup and Yee Whye Teh, editors, *Proceedings of the 34th International Conference on Machine Learning*, volume 70 of *Proceedings of Machine Learning Research*, pages 1895–1904. PMLR, 8 2017.
- [29] Yang Liu and Fred Roosta. Convergence of Newton-MR under inexact Hessian information. *SIAM Journal on Optimization*, 31(1):59–90, 2021.
- [30] Yang Liu and Fred Roosta. A Newton-MR Algorithm With Complexity Guarantees for Nonconvex Smooth Unconstrained Optimization. *arXiv preprint arXiv:2208.07095*, 2022.
- [31] James Martens. Deep learning via hessian-free optimization. In *Proceedings of the 27th International Conference on International Conference on Machine Learning, ICML’10*, page 735–742, Madison, WI, USA, 2010. Omnipress.
- [32] José Mario Martínez and Marcos Raydan. Cubic-regularization counterpart of a variable-norm trust-region method for unconstrained minimization. *Journal of Global Optimization*, 68:367–385, 2017.
- [33] Jorge J Moré, Burton S Garbow, and Kenneth E Hillstom. Testing Unconstrained Optimization Software. *ACM Transactions on Mathematical Software (TOMS)*, 7(1):17–41, 1981.
- [34] Yurii Nesterov. Implementable tensor methods in unconstrained convex optimization. *Mathematical Programming*, 186(1):157–183, 2021.
- [35] Yurii Nesterov. Inexact high-order proximal-point methods with auxiliary search procedure. *SIAM Journal on Optimization*, 31(4):2807–2828, 2021.
- [36] Yurii Nesterov. Superfast second-order methods for unconstrained convex optimization. *Journal of Optimization Theory and Applications*, 191(1):1–30, 2021.
- [37] Yurii Nesterov. Quartic Regularity. *arXiv preprint arXiv:2201.04852*, 2022.
- [38] Yurii Nesterov. Inexact accelerated high-order proximal-point methods. *Mathematical Programming*, 197(1):1–26, January 2023.

- [39] Yurii Nesterov and Boris T Polyak. Cubic regularization of Newton method and its global performance. *Mathematical Programming*, 108(1):177–205, 2006.
- [40] Jorge Nocedal and Stephen J Wright. *Numerical optimization*. Springer, 1999.
- [41] M. J. D. Powell. An Iterative Method for Finding Stationary Values of a Function of Several Variables. *The Computer Journal*, 5(2):147–151, 08 1962.
- [42] Robert B Schnabel and Ta-Tung Chow. Tensor methods for unconstrained optimization using second derivatives. *SIAM Journal on Optimization*, 1(3):293–315, 1991.
- [43] Robert B Schnabel and Paul D Frank. Tensor methods for nonlinear equations. *SIAM Journal on Numerical Analysis*, 21(5):815–843, 1984.
- [44] Karl Welzel and Raphael A. Hauser. Approximating higher-order derivative tensors using secant updates. *SIAM Journal on Optimization*, 34(1):893–917, 2024.
- [45] Wenqi Zhu and Coralia Cartis. Quartic Polynomial Sub-problem Solutions in Tensor Methods for Nonconvex Optimization. In *NeurIPS 2022 Workshop*, 2022.
- [46] Wenqi Zhu and Coralia Cartis. Cubic-quartic regularization models for solving polynomial subproblems in third-order tensor methods. *arXiv preprint arXiv:2312.10283*, 2023.
- [47] Wenqi Zhu and Coralia Cartis. Global convergence of high-order regularization methods with sums-of-squares taylor models. *arXiv preprint arXiv:2404.03035*, 2024.

A. Test functions

A.1. Regularized third-order polynomials

To evaluate the AR3 method on functions with a significant third-order component, we consider functions of the following form:

$$f(\mathbf{x}) = \mathbf{b}^\top \mathbf{x} + \frac{1}{2} \mathbf{x}^\top \mathbf{H} \mathbf{x} + \frac{1}{6} \mathbf{T}[\mathbf{x}]^3 + \|\mathbf{x}\|^c. \quad (30)$$

This formulation allows us to control the conditioning of both the Hessian and the third-order tensor term. In our experiment, we set the regularization exponent to $c = 8$ and the dimension to $d = 100$. The vector $\mathbf{b} \in \mathbb{R}^d$ is randomly generated with entries drawn from a uniform distribution $\mathcal{U}[0, 1]$. For the construction of $\mathbf{H} \in \mathbb{R}^{d \times d}$ and $\mathbf{T} \in \mathbb{R}^{d \times d \times d}$, we first generate unitary matrices $\mathbf{U} = [\mathbf{u}_1, \dots, \mathbf{u}_d] \in \mathbb{R}^{d \times d}$ and $\mathbf{V} = [\mathbf{v}_1, \dots, \mathbf{v}_d] \in \mathbb{R}^{d \times d}$, which are obtained from SVD decompositions of random matrices with entries independently drawn from the standard normal distribution $\mathcal{N}[0, 1]$. We then construct $\mathbf{H} = \sum_{i=1}^d \lambda_i^{\mathbf{H}} \mathbf{u}_i \otimes \mathbf{u}_i$, and $\mathbf{T} = \sum_{i=1}^n \lambda_i^{\mathbf{T}} \mathbf{v}_i \otimes \mathbf{v}_i \otimes \mathbf{v}_i$ using the following settings for $1 \leq i \leq d$,

- Both $\lambda_i^{\mathbf{H}}$ and $\lambda_i^{\mathbf{T}}$ take d values from `linspace(1, 10, d)`, starting from 1 and ending at 10, with equal spacing.
- $\lambda_i^{\mathbf{H}}$ values are taken from `logspace(-6, 6, d)`, i.e., from 10^{-6} to 10^6 , equally spaced on a logarithmic scale. The order is then randomly permuted, and the values are multiplied by a random sign. $\lambda_i^{\mathbf{T}}$ values are taken from `linspace(1, 10, d)` as before.
- $\lambda_i^{\mathbf{H}}$ values are taken from `linspace(1, 10, d)`. $\lambda_i^{\mathbf{T}}$ values are taken from `logspace(-6, 2, d)`, after a random permutation and random sign changes.
- $\lambda_i^{\mathbf{H}}$ and $\lambda_i^{\mathbf{T}}$ values are taken from `logspace(-6, 6, d)` and `logspace(-6, 2, d)` respectively, with random permutations and random sign changes applied to both.

With these settings, we obtain four test problems, including three that are ill-conditioned. The default starting point for all four test problems is $\mathbf{x}_0 = (1, \dots, 1)^\top$.

A.2. Multidimensional Rosenbrock

The multi-dimensional Rosenbrock function, also known as (Rosenbrock's) valley or banana function, is defined as

$$f(\mathbf{x}) = \sum_{i=1}^{d-1} [100(x_i^2 - x_{i+1})^2 + (x_i - 1)^2] \quad (31)$$

for any dimension $d \geq 2$. The global minimum is attained at $\mathbf{x}^* = (1, \dots, 1)^\top$, where $f(\mathbf{x}^*) = 0$. The default starting point is $\mathbf{x}_0 = (0, \dots, 0)^\top$.

A.3. Nonlinear least-squares

We consider a binary classification problem using a nonlinear least-squares function [30] of the form

$$f(\mathbf{x}) = \frac{1}{n} \sum_{i=1}^n (\psi(\mathbf{a}_i, \mathbf{x}) - b_i)^2, \quad \psi(\mathbf{a}_i, \mathbf{x}) = \frac{1}{1 + e^{-\langle \mathbf{a}_i, \mathbf{x} \rangle}} \quad (32)$$

where the dataset $\{\mathbf{a}_i, b_i\}_{i=1}^n$ consists of feature vectors $\mathbf{a}_i \in \mathbb{R}^d$, $i = 1, \dots, n$ and the corresponding labels $b_i \in \{0, 1\}$, $i = 1, \dots, n$. We randomly generate \mathbf{a}_i from a uniform distribution $\mathcal{U}[0, 1]$, and b_i are set to zero or one with equal probability. The default starting point is $\mathbf{x}_0 = (0, \dots, 0)^\top$.

A.4. Slalom and hairpin turn functions

These two functions were constructed such that knowledge of the third derivative is crucial for fast convergence. The idea is that in the direction of rapid decrease, the

function behaves like a saddle point, where the first and second derivative are zero, but the third derivative is not. In the other direction, the function only decreases very slowly. Moreover, we want first- and second-order methods that follow the slow decrease direction to eventually converge to the same point as the fast third-order method. To achieve this, the function must compel the lower-order methods to take a large detour instead of the direct path that the third-order method “sees”. To accomplish these objectives, we define a piecewise function using a few helper functions.

Consider polynomials $q: \mathbb{R} \rightarrow \mathbb{R}$ that satisfy the following conditions:

$$q(0) = 0, \quad q(1) = 1, \quad q'(0) = q'(1) = 0, \quad q''(0) = q''(1) = 0, \quad q'''(0) = q'''(1) = z. \quad (33)$$

The lowest-order family of such polynomials is given by

$$q(x) = -20x^7 + 70x^6 - 84x^5 + 35x^4 + \frac{z}{6}(2x^7 - 7x^6 + 9x^5 - 5x^4 + x^3). \quad (34)$$

We define $h_1(x) = 6x^5 - 15x^4 + 10x^3$, which is the solution for $z = 60$. By (33), we can define a piecewise function that is three times continuously differentiable as

$$h_2(x) = h_1(x + 0.5 - \lfloor x + 0.5 \rfloor) + \lfloor x + 0.5 \rfloor - 0.5, \quad (35)$$

which is the component in the direction of fast decrease. Whenever $x = n + 0.5$ for some integer n , the function has a saddle point with a nonzero third derivative.

Next we need to address the other direction. We want to scale h_2 by another function such that first- and second-order methods remain at the saddle point in the x direction and instead move along the y direction. We define $h_3(x) = -20x^7 + 70x^6 - 84x^5 + 35x^4$, which is the solution of (33) for $z = 0$. Again, by (33), the following piecewise function is three times continuously differentiable:

$$h_4(x, y) = \begin{cases} -h_3(2x + 2)(1 - y) + 1 & -1 \leq x < -0.5, \\ y & -0.5 \leq x \leq 0.5, \\ h_3(2x - 1)(1 - y) + y & 0.5 < x \leq 1. \end{cases} \quad (36)$$

This function continuously interpolates between $h_4(x, y) = y$ for $x \in [-0.5, 0.5]$ and $h_4(x, y) = 1$ for $x \in \{-1, 1\}$.

The two components can then be combined into

$$g(x, y) = h_2(x)h_4\left(x, \frac{2}{1 + e^y}\right), \quad (37)$$

which serves as the main building block for this construction. The region where $(x, y) \in [-1, 1] \times [0, \infty)$ resembles a hairpin turn in the mountains, except that the actual turn is stretched out to infinity. As y increases, the “streets” at $x = 0.5$ and $x = -0.5$ level out at zero, with one decreasing from 0.5 and the other one increasing from -0.5 .

To ensure that the minimizer of this function is close to $(-0.5, 0)$, we bend the function upwards with a fourth-order barrier term. Additionally, we introduce a small slope

$r > 0$ in the x direction so that instead of terminating, our algorithm follows the slight downward slope on the flat part of the function and finds the minimizer. In the plot shown in Figure 1, the value of r is $3 * 10^{-4}$. This results in what we refer to as the “hairpin turn” function.

$$b(x, x_{\min}, x_{\max}) = \begin{cases} (x - x_{\min})^4 & x \leq x_{\min}, \\ 0 & x_{\min} < x < x_{\max}, \\ (x - x_{\max})^4 & x \geq x_{\max}, \end{cases} \quad (38)$$

$$f_{\text{hairpin}}(x, y) = g(x, y) + rx + 50b(x, -0.4, 0.5) + 50b(y, 0, 5). \quad (39)$$

Next, let us describe the “slalom” function. It is constructed by stitching together copies of the function in (37) together at $y = 0$ and periodically in the x direction, ensuring that the new function is continuous and that the downhill slopes on one side match with those on the other. The slalom function is defined as:

$$f_{\text{slalom}}(x, y) = rx + \begin{cases} g(x + 1 - 2\lfloor \frac{x+1}{2} \rfloor, y) + 2\lfloor \frac{x+1}{2} \rfloor & y \leq 0 \\ g(x - 2\lfloor \frac{x}{2} \rfloor - 1, y) + 2\lfloor \frac{x}{2} \rfloor + 1 & y \geq 0 \end{cases} \quad (40)$$

Again, a slight slope in the x direction is added to prevent convergence to saddle points. Note that this function is three times continuously differentiable everywhere except along the $y = 0$ line, where there is a discontinuity in the first derivative.

B. Theorems

Example B.1 (AR3 Minimizer is not a Descent Direction). Consider the one-dimensional Taylor expansion $t(s) = s^3 + s^2 - s$. Clearly, any positive s is a descent direction. At the same time, $\min_{s \geq 0} t(s) = t(\frac{1}{3}) = -\frac{5}{27}$ and $\lim_{s \rightarrow -\infty} t(s) = -\infty$. Therefore, for sufficiently small σ , the global minimizer of the model is negative and not a descent direction.

Theorem B.2. Let $\psi: I \rightarrow \mathbb{R}^d$ be a maximal minimizer curve of a Taylor expansion $t: \mathbb{R}^d \rightarrow \mathbb{R}$ with $\nabla t(\mathbf{0}) \neq \mathbf{0}$. Then the following statements are equivalent:

1. ψ is persistent
2. ψ is persistent and $\lim_{\sigma \rightarrow \infty} \psi(\sigma) = \mathbf{0}$
3. $\inf_{\sigma \in I} \|\psi(\sigma)\| = 0$

Proof. Recall that the model has the form $m_\sigma(\mathbf{s}) = t(\mathbf{s}) + \frac{\sigma}{p+1} \|\mathbf{s}\|^{p+1}$, which means any stationary point \mathbf{s} satisfies

$$\nabla m_\sigma(\mathbf{s}) = \nabla t(\mathbf{s}) + \sigma \|\mathbf{s}\|^{p-1} \mathbf{s} = \mathbf{0}. \quad (41)$$

Rearranging and taking norm gives

$$\sigma = \frac{\|\nabla t(\mathbf{s})\|}{\|\mathbf{s}\|^p} =: \tilde{\sigma}(\mathbf{s}) \quad (42)$$

for $\sigma \geq 0$. This defines a function $\tilde{\sigma}: \mathbb{R} \setminus \{\mathbf{0}\} \rightarrow \mathbb{R}_{\geq 0}$ which satisfies $\tilde{\sigma}(\boldsymbol{\psi}(\sigma)) = \sigma$ for all $\sigma \in I$ for any minimizer curve $\boldsymbol{\psi}$.

To show that any persistent minimizer curve converges to $\mathbf{0}$, we can bound $\tilde{\sigma}$ by

$$\tilde{\sigma}(\mathbf{s}) = \frac{\|\nabla t(\mathbf{s})\|}{\|\mathbf{s}\|^p} \leq \max\{C_1\|\mathbf{s}\|^{-1}, C_2\|\mathbf{s}\|^{-p}\} \quad (43)$$

using the fact that t is a p th-order polynomial, which implies that $\|\nabla t(\mathbf{s})\|/\|\mathbf{s}\|^{p-1}$ is uniformly upper bounded by some constant $C_1 < \infty$ when \mathbf{s} is bounded away from zero and $\|\nabla t(\mathbf{s})\|$ is uniformly upper bounded by some constant $C_2 < \infty$ when \mathbf{s} is close to zero. Therefore,

$$\|\boldsymbol{\psi}(\sigma)\| \leq \max\{C_1\tilde{\sigma}(\boldsymbol{\psi}(\sigma))^{-1}, C_2^{1/p}\tilde{\sigma}(\boldsymbol{\psi}(\sigma))^{-1/p}\} = \max\{C_1\sigma^{-1}, C_2^{1/p}\sigma^{-1/p}\} \rightarrow 0 \quad (44)$$

as $\sigma \rightarrow \infty$ for a persistent minimizer curve $\boldsymbol{\psi}$.

Clearly, if $\boldsymbol{\psi}$ is persistent and converges to $\mathbf{0}$, then it also satisfies $\inf_{\sigma \in I} \|\boldsymbol{\psi}(\sigma)\| = 0$. We only need to show that this latter condition in turn implies persistency. The fact that $\|\boldsymbol{\psi}(\sigma)\|$ is not bounded away from zero means there is a sequence $\sigma_1, \sigma_2, \dots \in I$ such that $\|\boldsymbol{\psi}(\sigma_k)\| \rightarrow 0$ as $k \rightarrow \infty$. We have

$$\sigma_k = \tilde{\sigma}(\boldsymbol{\psi}(\sigma_k)) = \frac{\|\nabla t(\boldsymbol{\psi}(\sigma_k))\|}{\|\boldsymbol{\psi}(\sigma_k)\|^p} \rightarrow \infty \quad (45)$$

since the numerator converges to $\|\nabla t(\mathbf{0})\| > 0$ and the denominator converges to zero. Therefore, $\boldsymbol{\psi}$ must be persistent. \square

Theorem B.3. *Let $t: \mathbb{R}^n \rightarrow \mathbb{R}$ be a quadratic polynomial with $\nabla t(\mathbf{0}) \neq \mathbf{0}$, and let $m_\sigma(\mathbf{s}) = t(\mathbf{s}) + \frac{\sigma}{3}\|\mathbf{s}\|^3$ be the corresponding regularized model. Then every global minimizer of m_σ for any $\sigma \geq 0$ is a persistent minimizer of the model.*

Proof. Without loss of generality, we can assume that

$$m_\sigma(\mathbf{s}) = \mathbf{g}^\top \mathbf{s} + \frac{1}{2} \mathbf{s}^\top \mathbf{H} \mathbf{s} + \frac{\sigma}{3} \|\mathbf{s}\|^3 \quad (46)$$

for some $\mathbf{g} \in \mathbb{R}^n \setminus \{\mathbf{0}\}$ and a symmetric $\mathbf{H} \in \mathbb{R}^{n \times n}$. According to [15, Theorem 8.2.8], any global minimizer \mathbf{s}_* of this model satisfies

$$(\mathbf{H} + \lambda_* \mathbf{I}) \mathbf{s}_* = -\mathbf{g} \quad (47)$$

where $\mathbf{H} + \lambda_* \mathbf{I} \succeq \mathbf{0}$ and $\lambda_* = \sigma \|\mathbf{s}_*\|$. By the positive semidefiniteness of the matrix and the nonnegativity of σ , we know that $\lambda_* \geq \max\{0, -\lambda_{\min}(\mathbf{H})\} =: \lambda_s$.

First, consider the case where $\lambda_* > -\lambda_{\min}(\mathbf{H})$. Using the fact that the matrix in (47) is nonsingular and that $\mathbf{g} \neq \mathbf{0}$, we can define

$$\mathbf{s}_1(\lambda) = -(\mathbf{H} + \lambda\mathbf{I})^{-1}\mathbf{g} \quad \text{and} \quad \sigma_1(\lambda) = \lambda/\|\mathbf{s}_1(\lambda)\| \quad (48)$$

for all $\lambda > -\lambda_{\min}(\mathbf{H})$. Note that according to [15, Theorem 8.2.3], we know that $\pi(\lambda) = \|\mathbf{s}_1(\lambda)\|^{-1}$ has a nonnegative derivative whenever $\lambda > \lambda_s$. Therefore,

$$\sigma'_1(\lambda) = \pi(\lambda) + \lambda\pi'(\lambda) > 0 \quad (49)$$

which means that $\sigma_1(\lambda)$ is strictly monotonically increasing on $[\lambda_*, \infty)$. Moreover, $\sigma_1(\lambda)$ is continuous and converges to infinity as λ approaches infinity. This implies that there exists a $c \geq 0$ such that $\sigma_1: [\lambda_*, \infty) \rightarrow [c, \infty)$ is one-to-one, and that $\boldsymbol{\psi}_1$, defined by

$$\boldsymbol{\psi}_1(\sigma_1(\lambda)) = \mathbf{s}_1(\lambda) \quad \text{for all } \lambda \geq \lambda_*, \quad (50)$$

is part of a persistent minimizer curve which contains $\mathbf{s}_* = \mathbf{s}_1(\lambda_*)$.

Next, consider the case where $\lambda_* = -\lambda_{\min}(\mathbf{H})$. In this case $\mathbf{H} + \lambda_*\mathbf{I}$ is singular. Let V be the nullspace of $\mathbf{H} + \lambda_*\mathbf{I}$ and V_\perp its orthogonal complement. We can decompose \mathbf{s}_* into a sum $\mathbf{v} + \mathbf{w}$ where $\mathbf{v} \in V$ and $\mathbf{w} \in V_\perp$. Assume for now that $\mathbf{v} \neq \mathbf{0}$, the other case will be handled later. Since $\mathbf{g} \neq \mathbf{0}$, we also have $\mathbf{w} \neq \mathbf{0}$, and so

$$\mathbf{s}_2(\alpha) = \alpha\mathbf{v} + \mathbf{w} \quad \text{and} \quad \sigma_2(\alpha) = \lambda_*/\|\mathbf{s}_2(\alpha)\| \quad (51)$$

are well-defined. Clearly, $\|\mathbf{s}_2(\alpha)\|$ is strictly monotonically increasing, and $\sigma_2(\alpha)$ is strictly monotonically decreasing. Therefore, there exists a $c \geq 0$ such that $\sigma_2: [0, \infty) \rightarrow (0, c]$ is one-to-one, and $\boldsymbol{\psi}_2$, defined by

$$\boldsymbol{\psi}_2(\sigma_2(\alpha)) = \mathbf{s}_2(\alpha) \quad \text{for all } \alpha \geq 0, \quad (52)$$

forms part of a minimizer curve which contains $\mathbf{s}_* = \mathbf{s}_2(1)$.

With the given construction, $\boldsymbol{\psi}_2$ is not persistent, because it is only defined on $\sigma \in (0, c]$. However, it is possible to extend $\boldsymbol{\psi}_2$ by composing it with $\boldsymbol{\psi}_1$. Note that since $-\lambda_{\min}(\mathbf{H}) = \lambda_* \geq 0$, the construction of $\boldsymbol{\psi}_1$ in (50) extends to all $\lambda > \lambda_s = \lambda_*$, and $\mathbf{s}_1(\lambda)$ can be equivalently defined as $-(\mathbf{H} + \lambda\mathbf{I})^\dagger\mathbf{g}$, where $(\cdot)^\dagger$ denotes the pseudoinverse of a matrix. Therefore,

$$\lim_{\lambda \rightarrow \lambda_*} \mathbf{s}_1(\lambda) = -(\mathbf{H} - \lambda_*\mathbf{I})^\dagger\mathbf{g} = \mathbf{s}_2(0) \quad \text{and} \quad \lim_{\lambda \rightarrow \lambda_*} \sigma_1(\lambda) = \lambda_*/\|\mathbf{s}_2(0)\| = \sigma_2(0). \quad (53)$$

This implies that the curve defined by following $\boldsymbol{\psi}_2$ for $\sigma \in (0, \sigma_2(0)]$ and $\boldsymbol{\psi}_1$ for $(\sigma_2(0), \infty)$ forms (part of) a persistent minimizer curve that contains \mathbf{s}_* .

To finish the proof, we need to consider the case $\lambda_* = -\lambda_{\min}(\mathbf{H})$ and $\mathbf{v} = \mathbf{0}$ that was skipped before. This case corresponds exactly to $\mathbf{s}_* = -(\mathbf{H} - \lambda_*\mathbf{I})^\dagger\mathbf{g}$. Therefore, in this scenario, it suffices to extend $\boldsymbol{\psi}_1$ by using the limit points of σ_1 and \mathbf{s}_1 as determined in (53), namely map $\lambda_*/\|\mathbf{s}_*\|$ to \mathbf{s}_* . The extended curve is continuous as shown above and (part of) a persistent minimizer curve. \square

Corollary B.4. *Assuming $\bar{\alpha}$ as defined in [Theorem 4.3](#) exists, there is a minimizer curve which is bounded and 0-persistent if and only if $t'(\bar{\alpha}) = 0$.*

Proof. In addition to the assumptions in the statement, assume there exists a bounded and 0-persistent minimizer curve ψ . This implies $\psi: [0, \infty) \rightarrow (0, \bar{\alpha}]$ or $\psi: (0, \infty) \rightarrow (0, \bar{\alpha})$. In both cases, we know from [\(21\)](#) that

$$\frac{t'(\bar{\alpha})}{\bar{\alpha}^p} = \lim_{\sigma \rightarrow 0} \frac{-t'(\psi(\sigma))}{\psi(\sigma)^p} = \lim_{\sigma \rightarrow 0} \sigma = 0. \quad (54)$$

Now consider the case where $t'(\bar{\alpha}) = 0$. Following the same construction as in the proof of [Theorem 4.3](#), we see that $\lim_{\alpha \rightarrow \bar{\alpha}} \sigma(\alpha) = 0$, and therefore, ψ is defined for all $\alpha \in (0, \infty)$, making it 0-persistent. The boundedness of ψ follows from the existence of $\bar{\alpha}$. \square

C. Additional experiments

We report our experiments in each section in detail with respect to different ε_f (including those measures in τ as defined in [Section 2.1.2](#)).

C.1. Choosing the initial regularization parameter σ_0

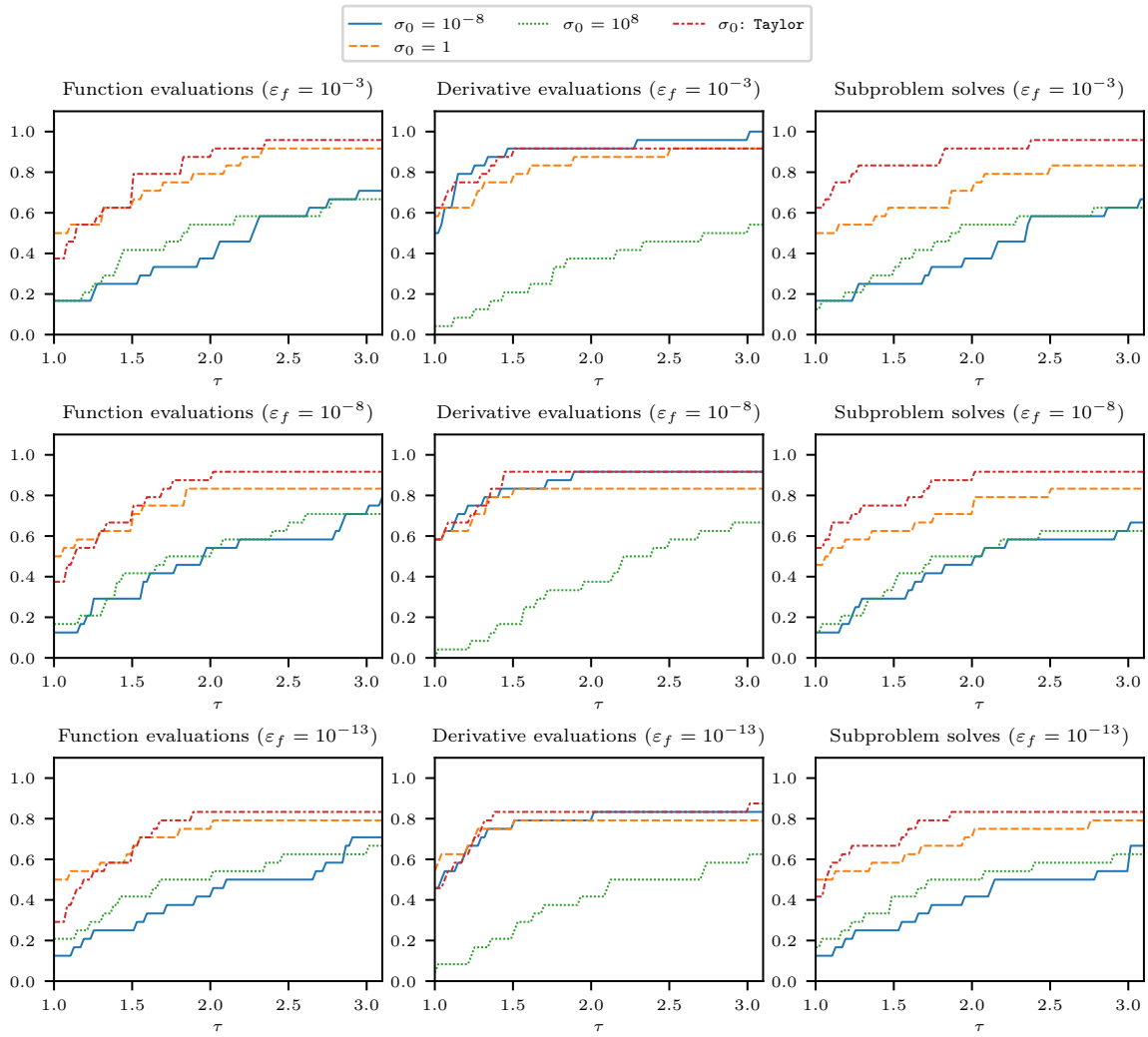


Figure 17: Additional performance profile plots are provided to show the impact of using different σ_0 values with respect to different ϵ_f .

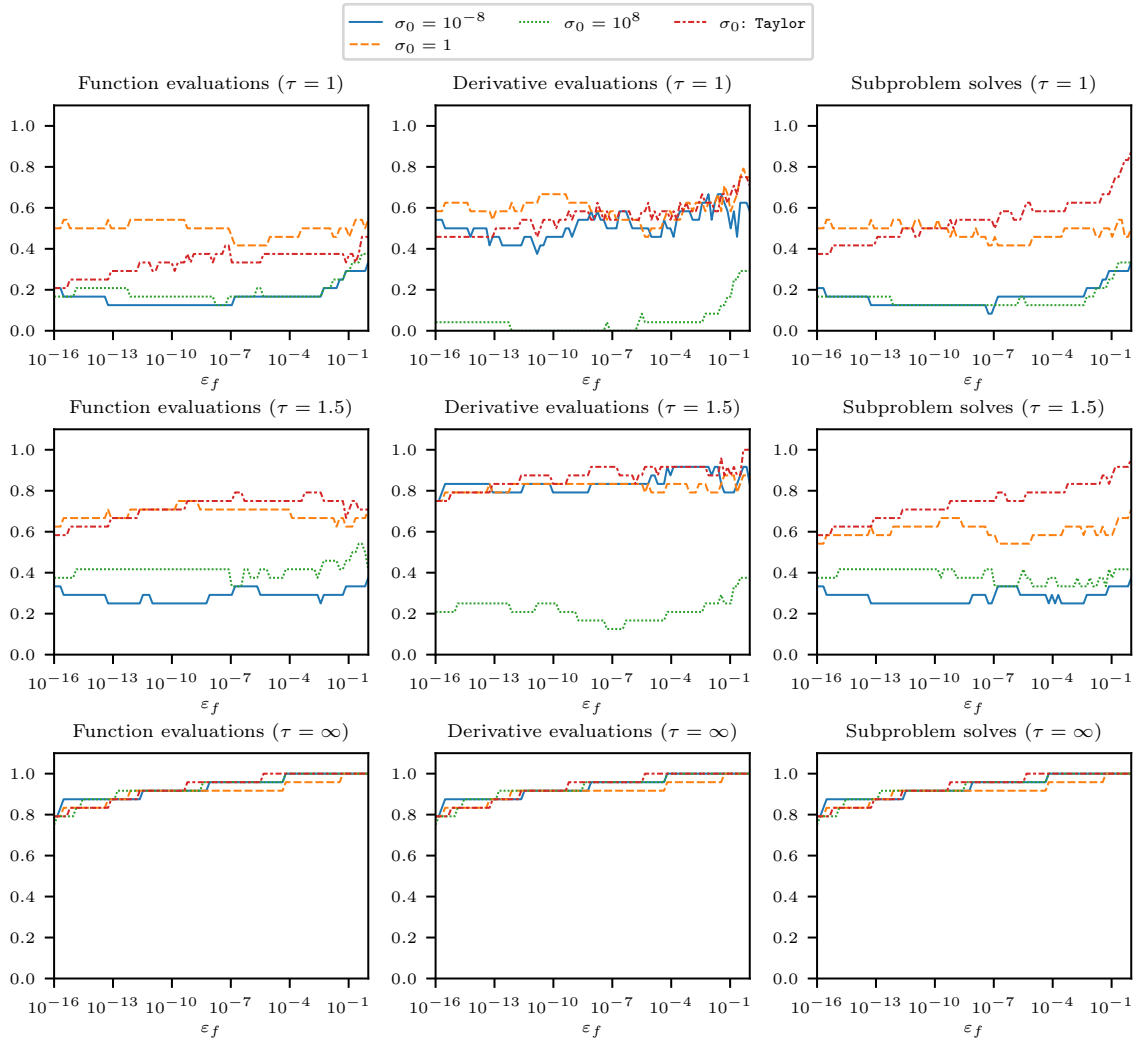


Figure 18: Additional performance profile plots are provided to show the impact of using different σ_0 values with respect to different τ .

C.2. An interpolation-based update for AR p

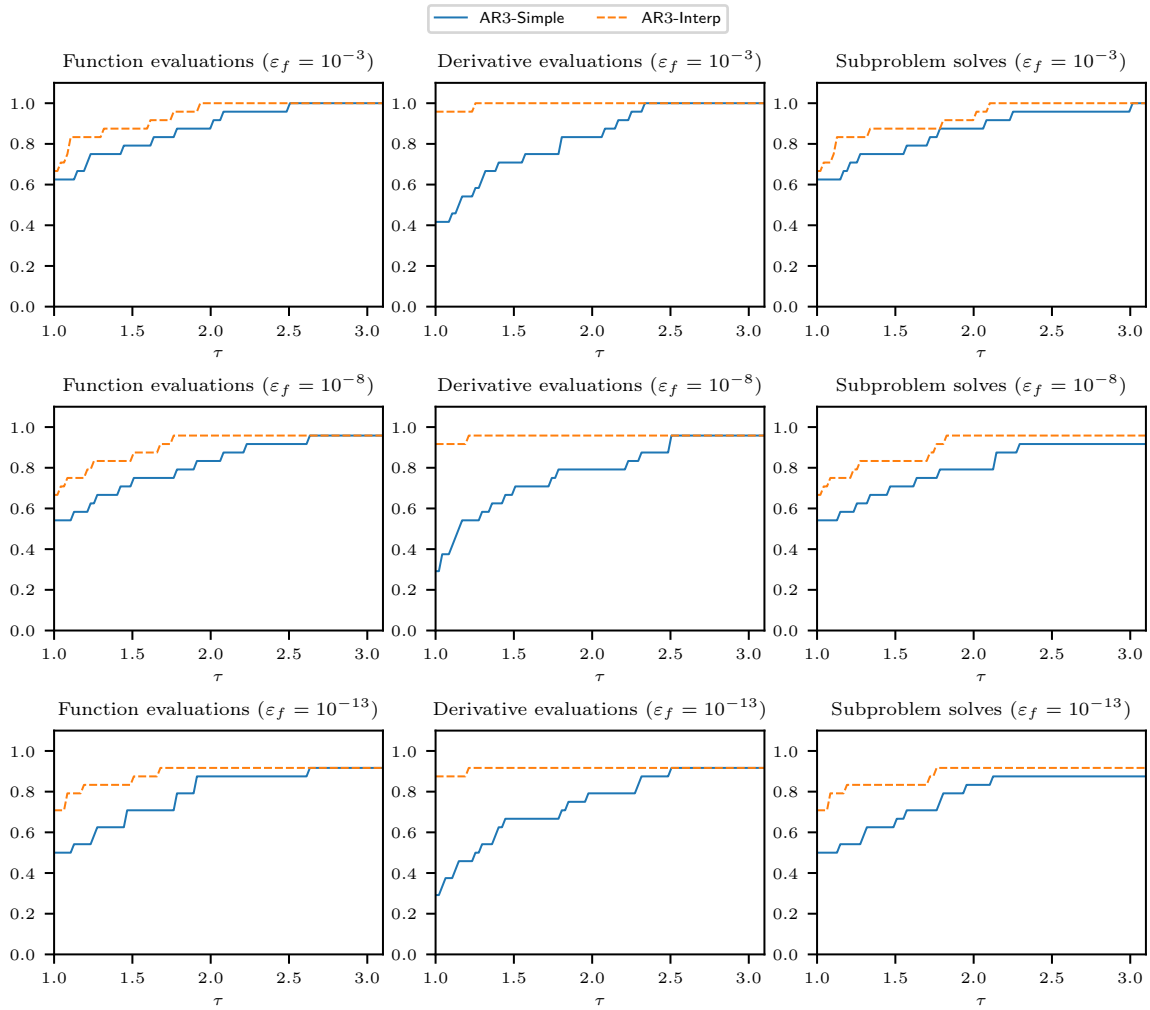


Figure 19: The convergence dot plot illustrates the effectiveness of the interpolation-based strategy with respect to different ε_f .

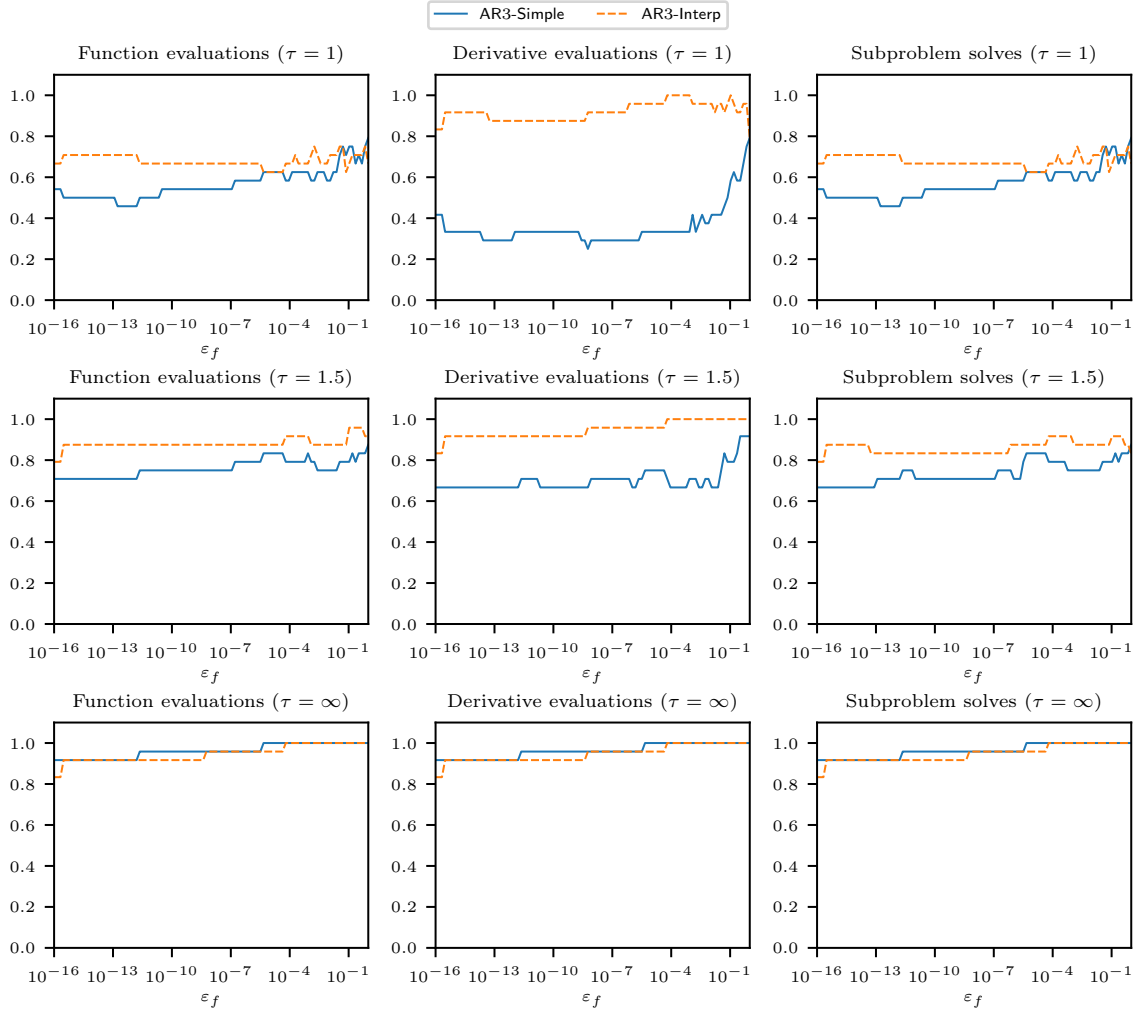


Figure 20: The performance profile plot illustrates the effectiveness of the interpolation-based strategy with respect to different τ .

C.3. A prerejection framework

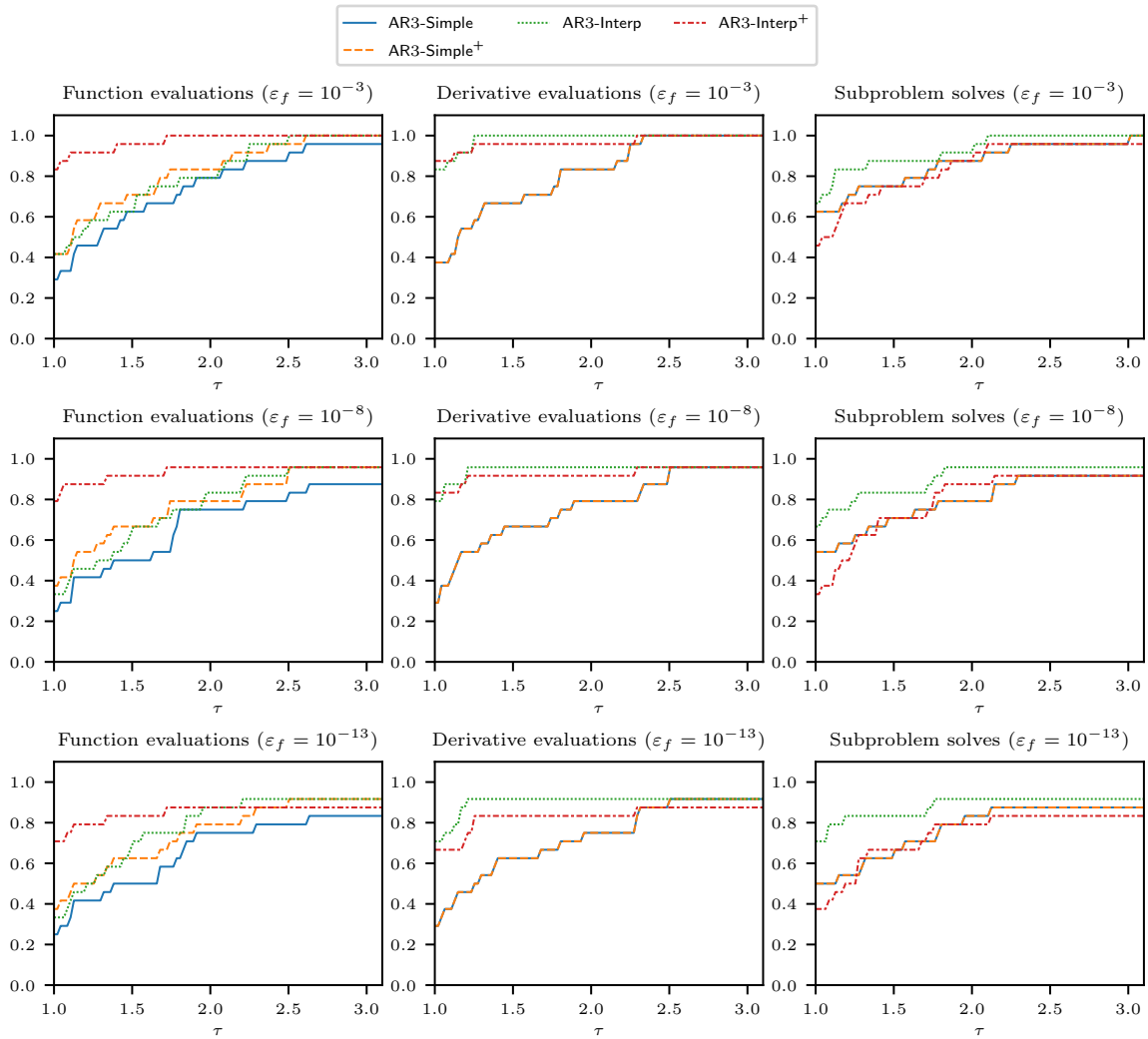


Figure 21: The convergence dot plot illustrates the impact of including prerejection with respect to different ϵ_f .

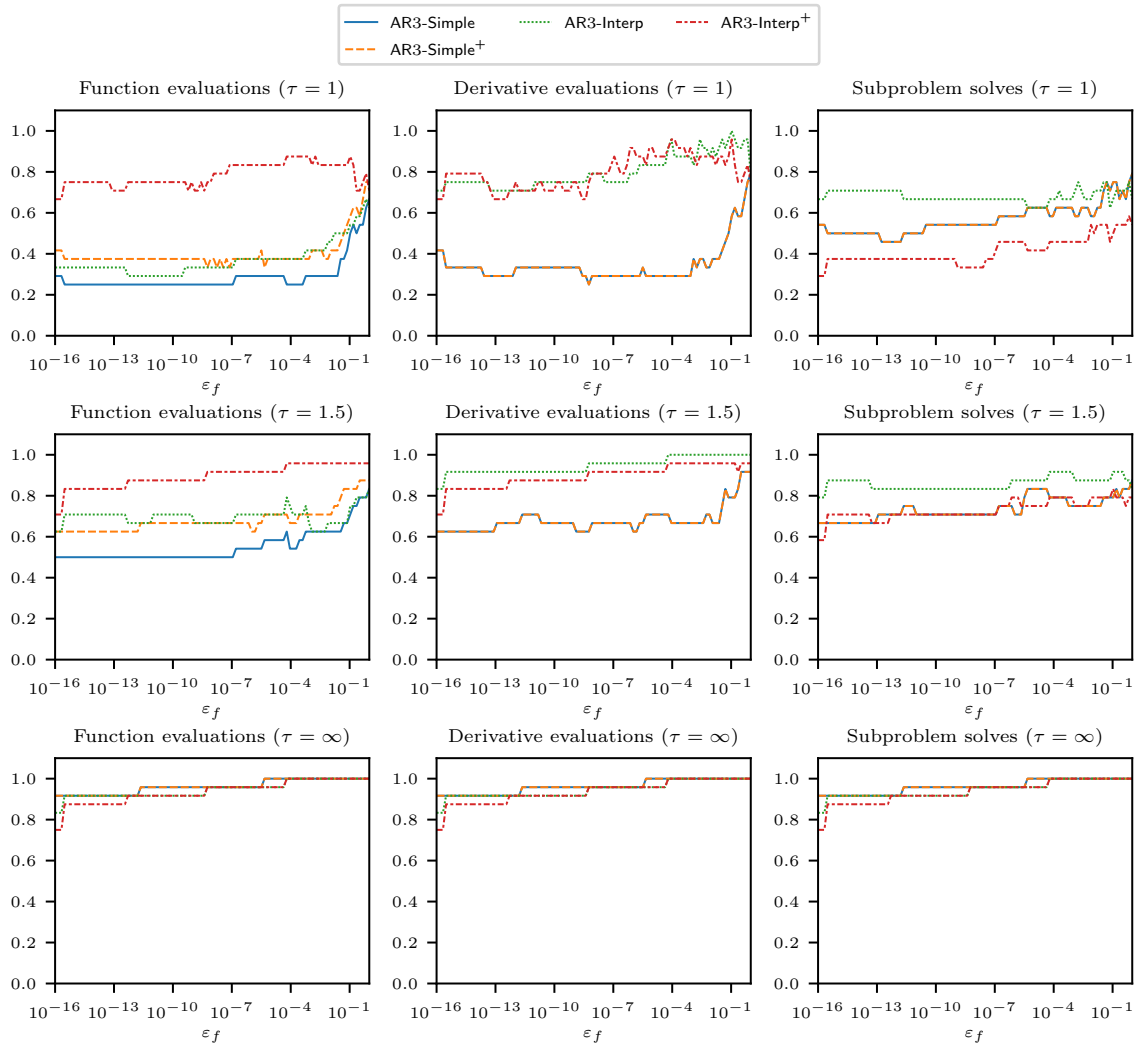


Figure 22: The performance profile plot illustrates the impact of including prerejection with respect to different τ .

C.4. Comparison with BGMS step control strategy

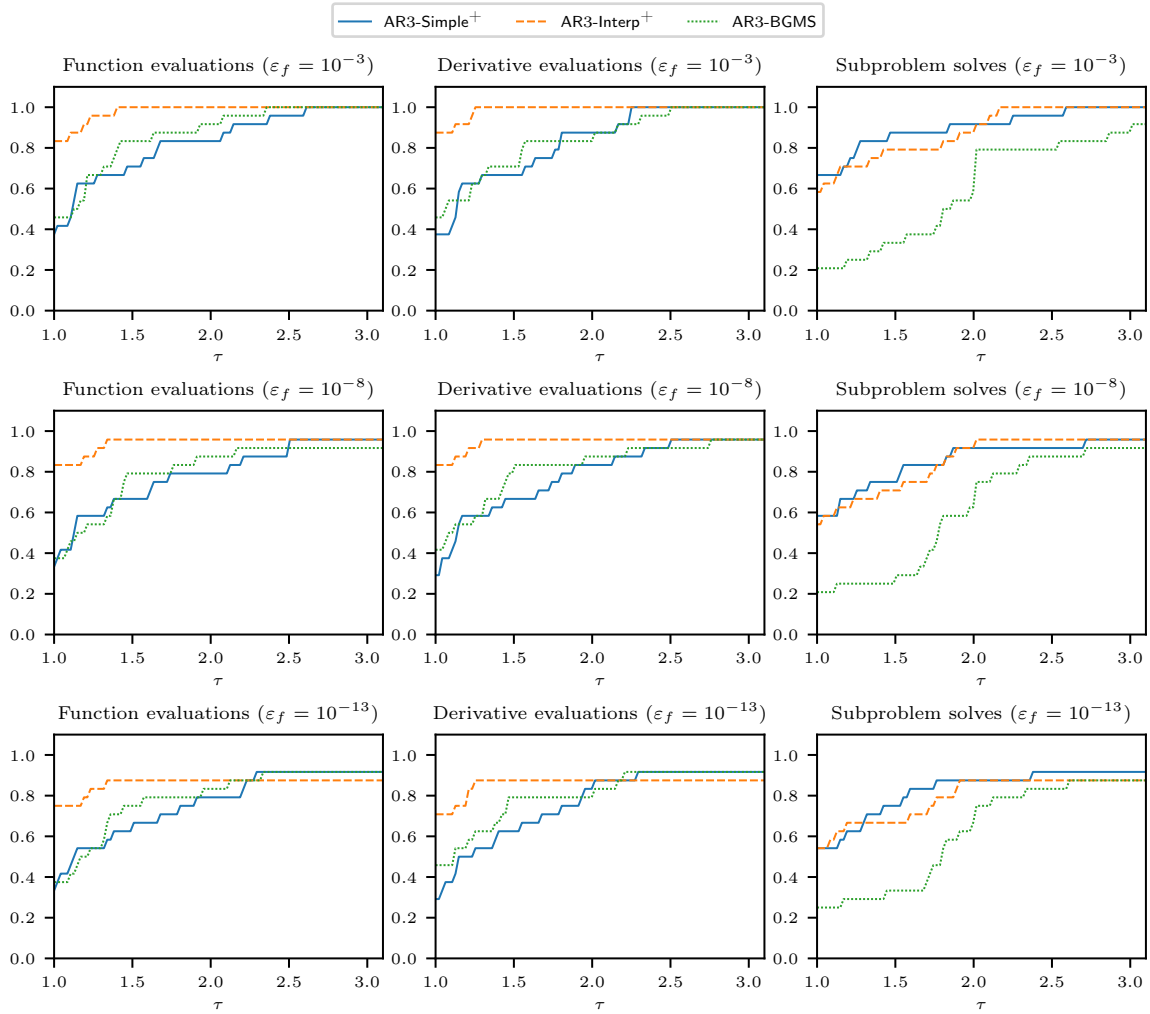


Figure 23: The convergence dot plot highlights the differences between the three update strategies with respect to different ε_f . Note that prerejection is enabled for all three methods.

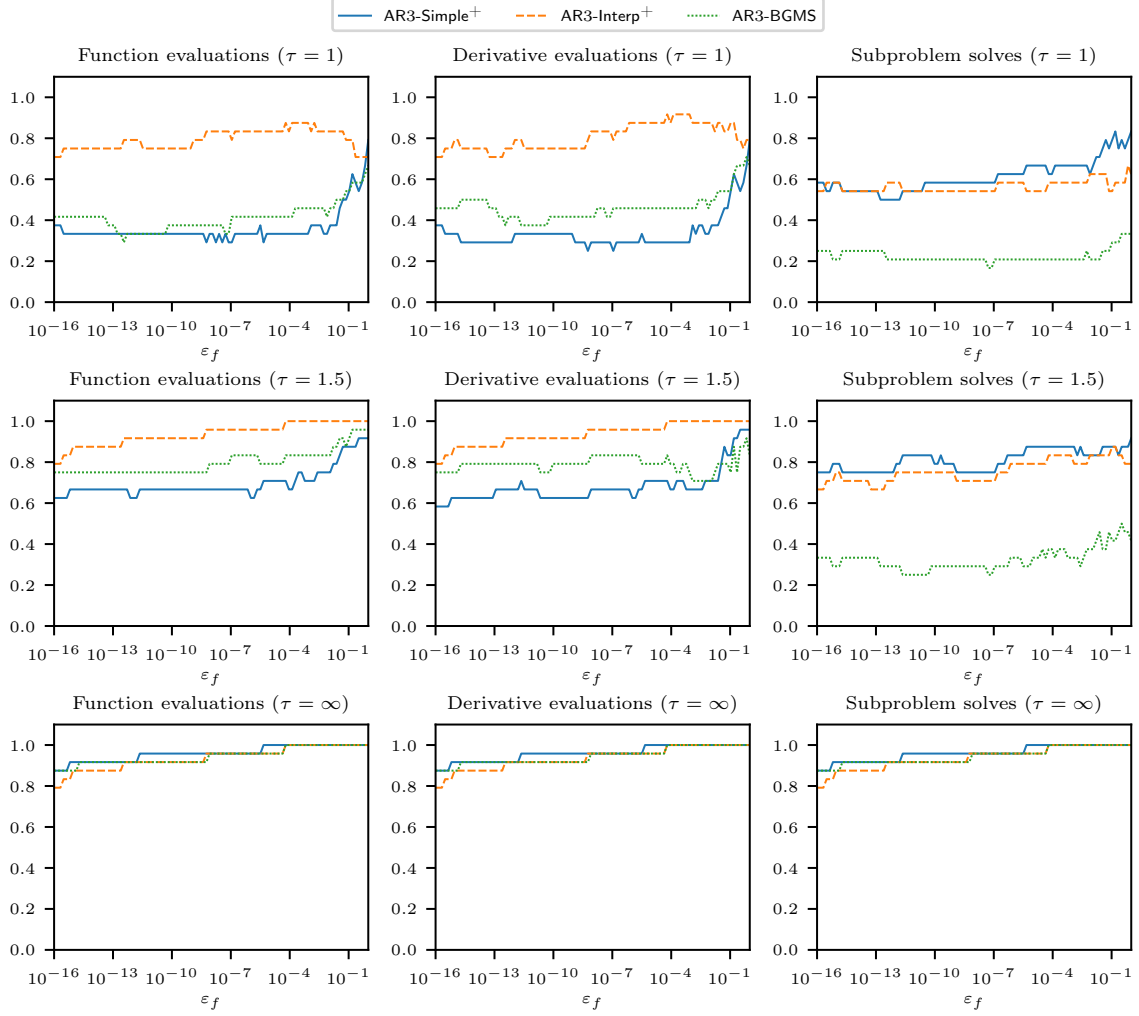


Figure 24: The performance profile plot highlights the differences between the three update strategies with respect to different τ . Note that prerejection is enabled for all three methods.

C.5. Subproblem termination condition

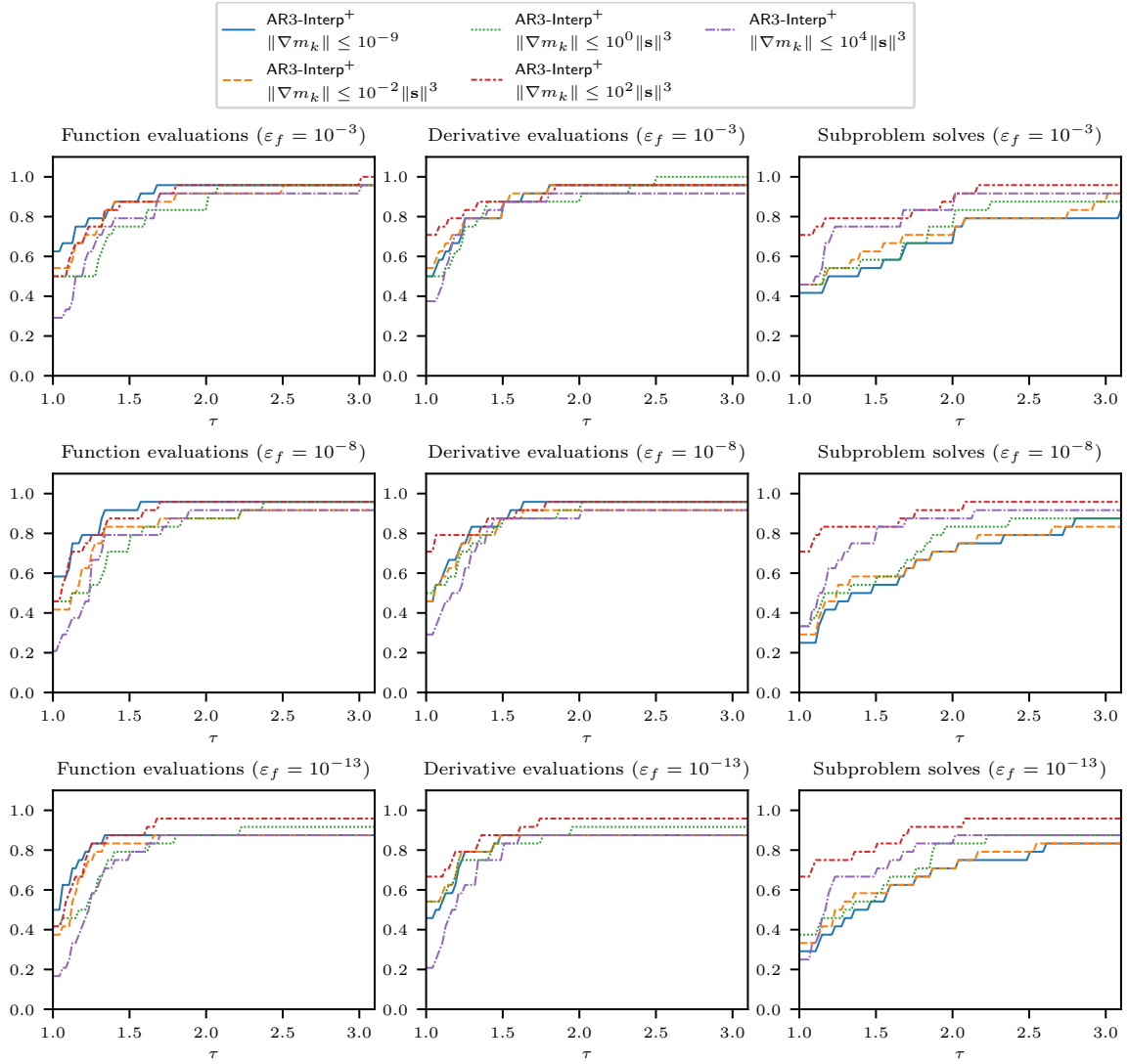


Figure 25: The convergence dot plot showing the differences between $\theta \in \{10^{-2}, 10^0, 10^2, 10^4\}$ in (TC.r) with $p = 3$ with respect to different ε_f .

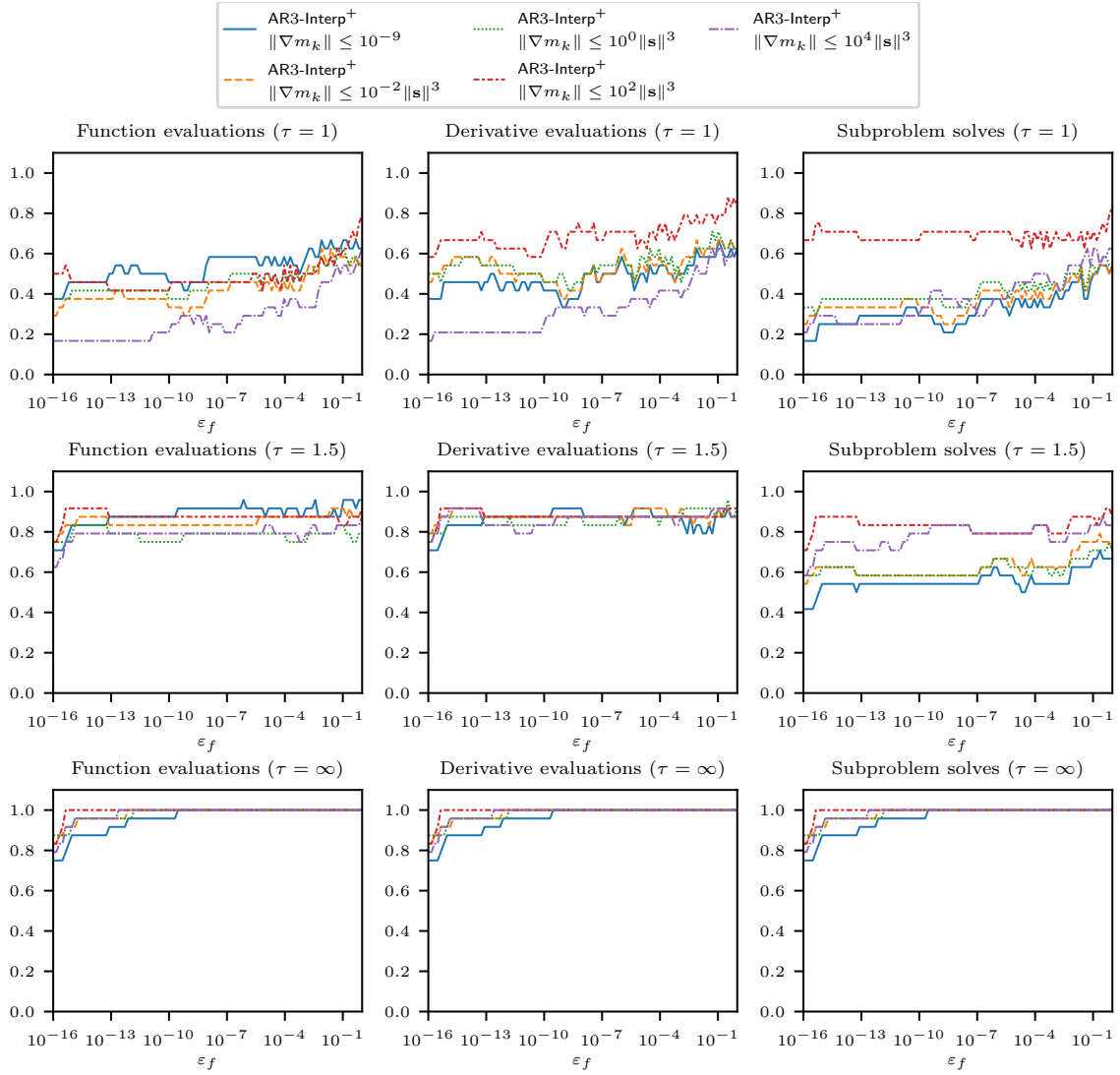


Figure 26: The performance profile plot showing the differences between $\theta \in \{10^{-2}, 10^0, 10^2, 10^4\}$ in (TC.r) with $p = 3$ with respect to different τ .

C.6. Benchmarking

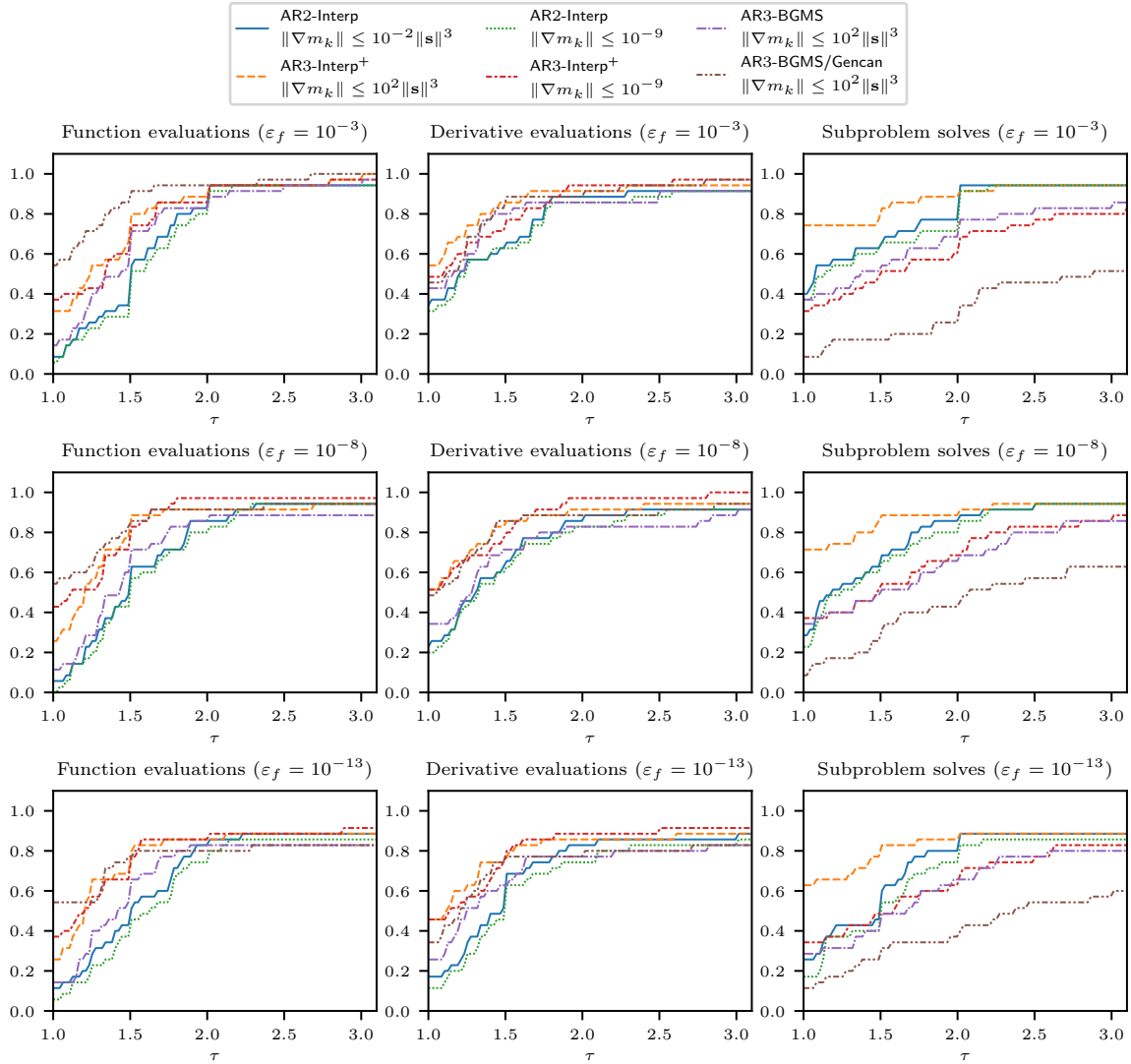


Figure 27: The convergence dot plot compares AR2-Interp, AR3-Interp+, AR3-BGMS and AR3-BGMS/Gencan using both (TC.a) and (TC.r) on full 35 MGH test set with respect to different ε_f .

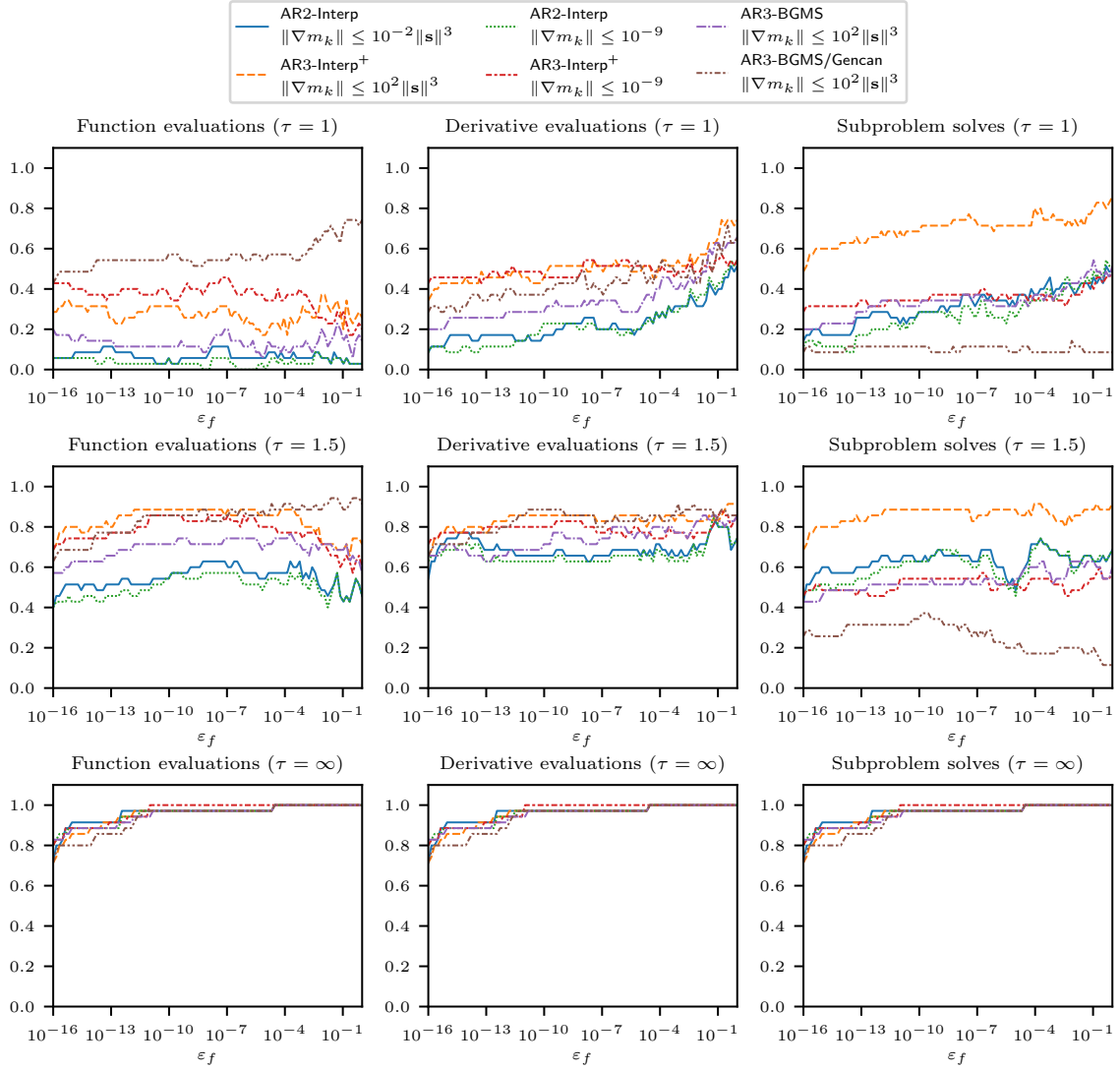


Figure 28: The performance profile plot compares AR2-Interp, AR3-Interp⁺, AR3-BGMS and AR3-BGMS/Gencan using both (TC.a) and (TC.r) on full 35 MGH test set with respect to different τ .

D. Relative termination condition for AR2

In this section, we provide the numerical illustrations for Section 5 for AR2. From Figures 29 and 30 we can conclude that the impact of the termination condition on AR2 is limited, with (TC.r) and $\theta = 10^{-2}$ being among the best with respect to function evaluations, derivative evaluations and subproblem solves.

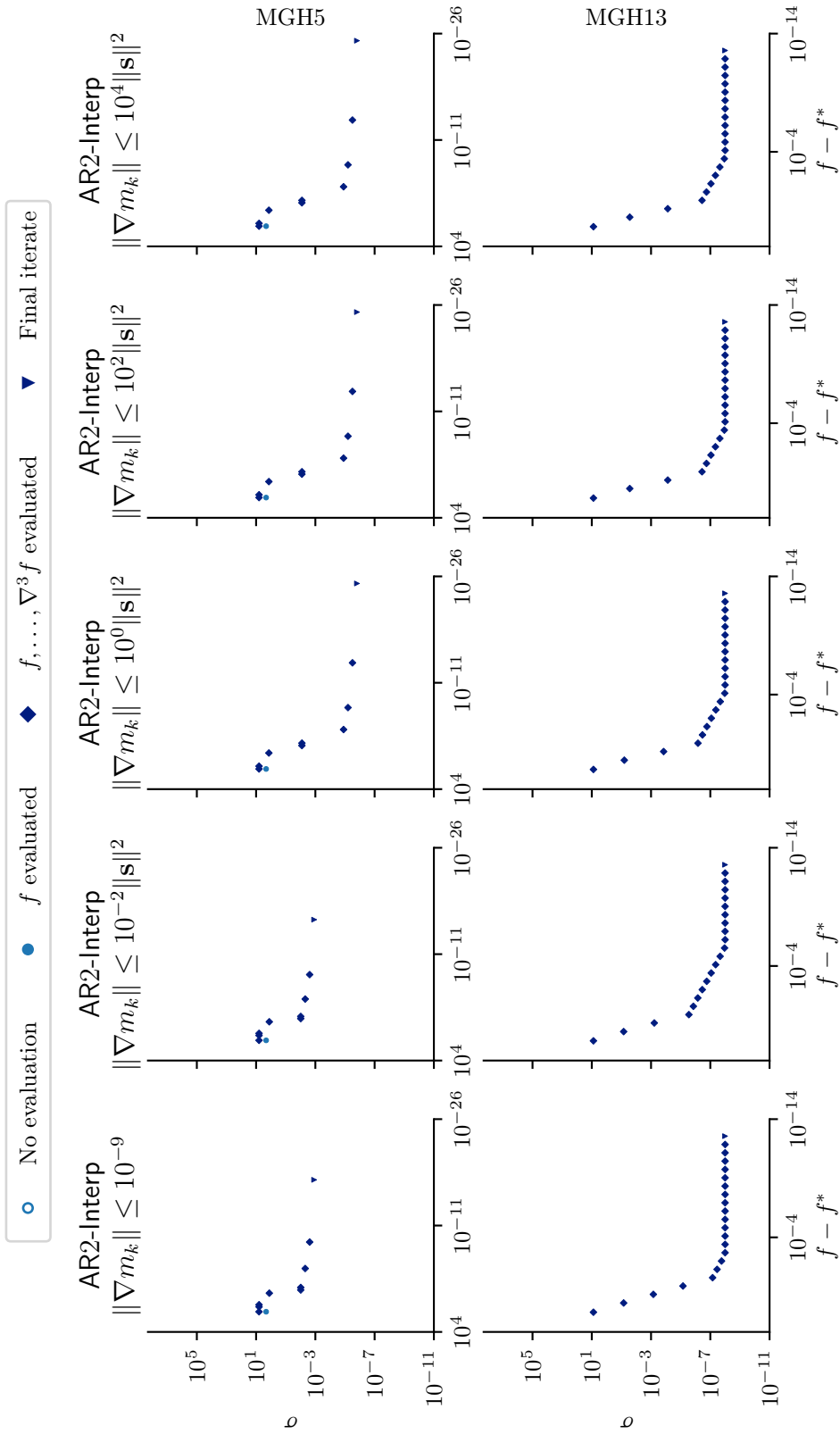


Figure 29: The convergence dot plot showing the differences between $\theta \in \{10^{-2}, 10^0, 10^2, 10^4\}$ in (TC.r) for AR2-Interp. An extra condition (TC.a) is provided as an approximation of an exact solve.

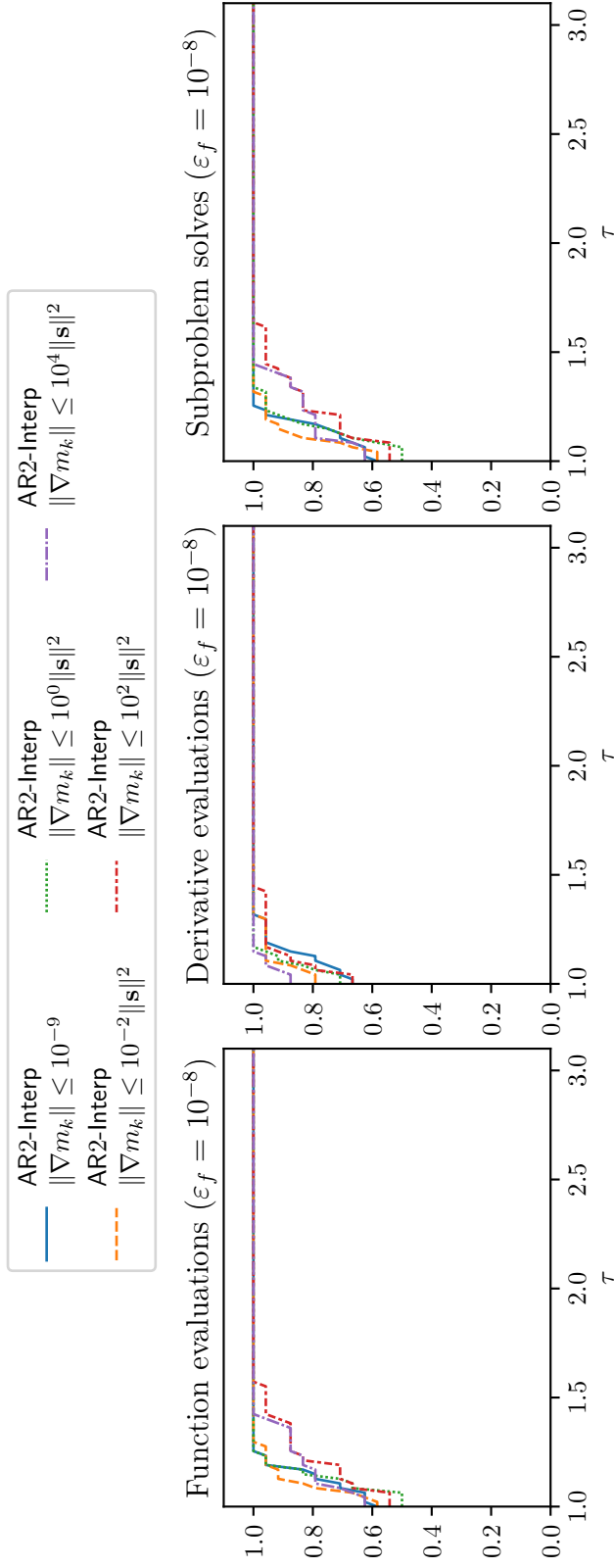


Figure 30: The performance profile plot showing the differences between $\theta \in \{10^{-2}, 10^0, 10^2, 10^4\}$ in (TC.r) for AR2-Interp. An extra condition (TC.a) is provided as an approximation of an exact solve

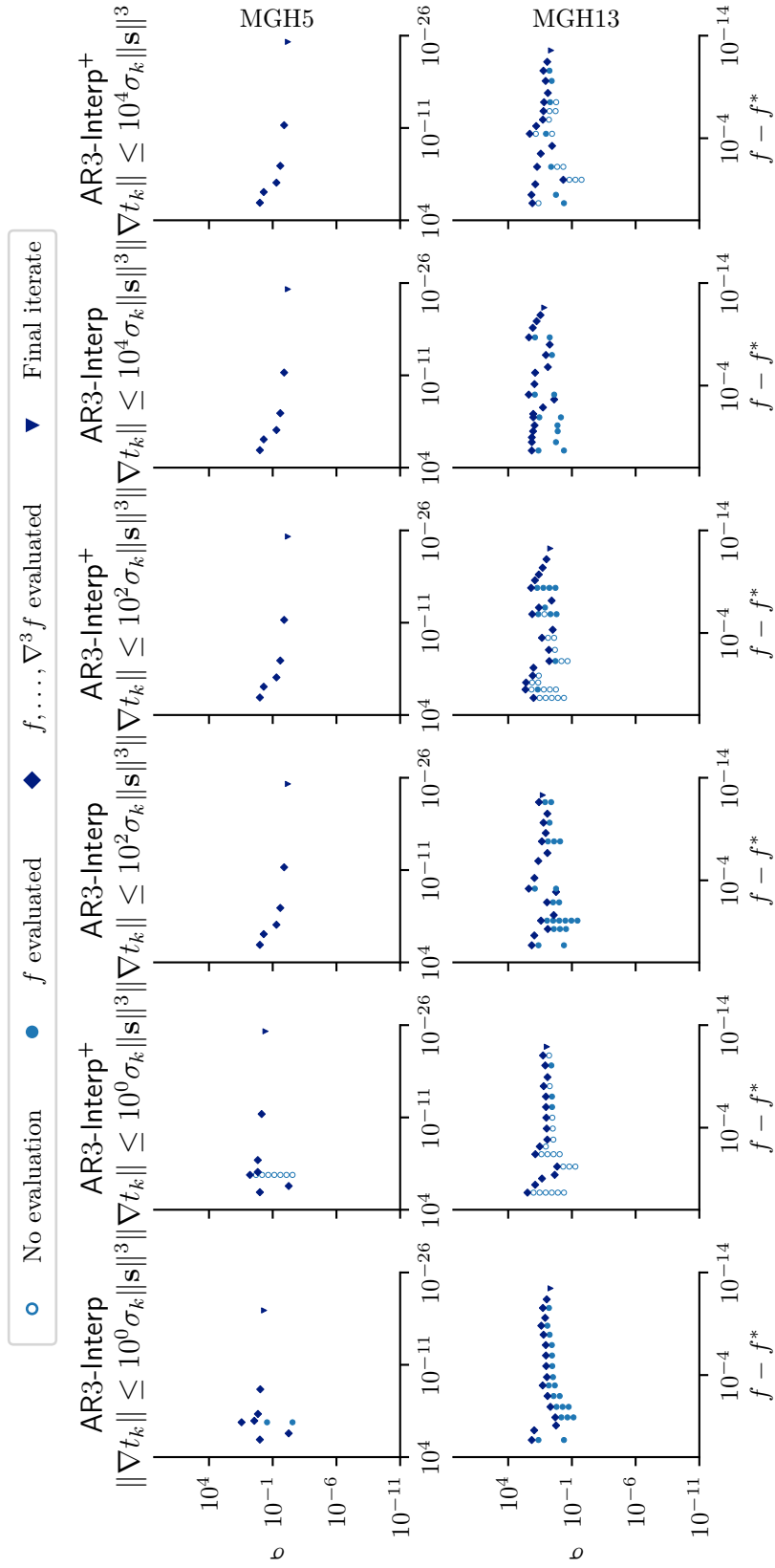


Figure 31: The convergence dot plot shows the differences between $\theta \in \{10^0, 10^2, 10^4\}$ in (TC.g) for both AR3-Interp and AR3-Interp⁺

E. Generalized norm termination condition

In this section, we consider the generalized norm termination condition [25], given by

$$\|\nabla t_k(\mathbf{s}_k)\| \leq \theta \sigma_k \|\mathbf{s}_k\|^p \quad (\text{TC.g})$$

where $\theta \geq 1$. We choose $\theta = \{1, 10^2, 10^4\}$. It has been shown in [25] that an exact solution to the subproblem satisfies (TC.g) with $\theta = 1$, however, the reverse is not necessarily true, which means that $\theta = 1$ still represents an inexact condition. From Figure 31, we observe similar performance compared to the results in Figure 13. The prerejection framework continues to work well with this termination condition. When $\theta = 1$, the performance of (TC.g) is very similar to that shown in the leftmost subplot in Figure 13. However, when θ increases, no drastic improvements are observed for MGH13.

Figure 32 demonstrates the overall performance for different values of θ . It is clear that the variant with $\theta = 1$ uses the least amount of function evaluations, whereas the variant with $\theta = 10^4$ requires the fewest subproblem solves.

Next, we maintain $\theta = 1$ in (TC.g) and provide the benchmark performance profile plot in Figure 33 to determine the best combination of AR3 variant and termination condition. All three AR3-Interp strategies outperform AR3-Simple and AR3-BGMS in both function and derivative evaluations. Furthermore, AR3-Interp using (TC.r) with $\theta = 100$ emerges as the most competitive candidate across all three measures.

Figures 34 to 36 present the results of the same experiments as above for AR2.

F. AR2 versus AR3

In this section, we focus on the comparison between AR2-Interp and AR3-Interp⁺ variants. We provide performance profile plots for different test sets, namely:

- For 18 odd MGH test problems and 6 additional problems in Figure 37,
- For the full 35 problems in the MGH test set in Figure 38,
- For the six additional problems in Figure 39,
- For the four regularized third-order polynomial problems Figure 40.

As shown in Figures 39 and 40, AR3-Interp⁺ with (TC.a) performed exceptionally well across all measures on the four regularized third-order polynomial problems, particularly in function evaluations. However, on a larger test set as in Figures 37 and 38, these advantages are less pronounced compared to AR3-Interp⁺ with $\theta = 100$. Nonetheless, it is evident by Figures 37 to 40 that AR2-Interp is less efficient compared to AR3-Interp⁺, which aligns with the observations in [6] and our example in Example 1.1.

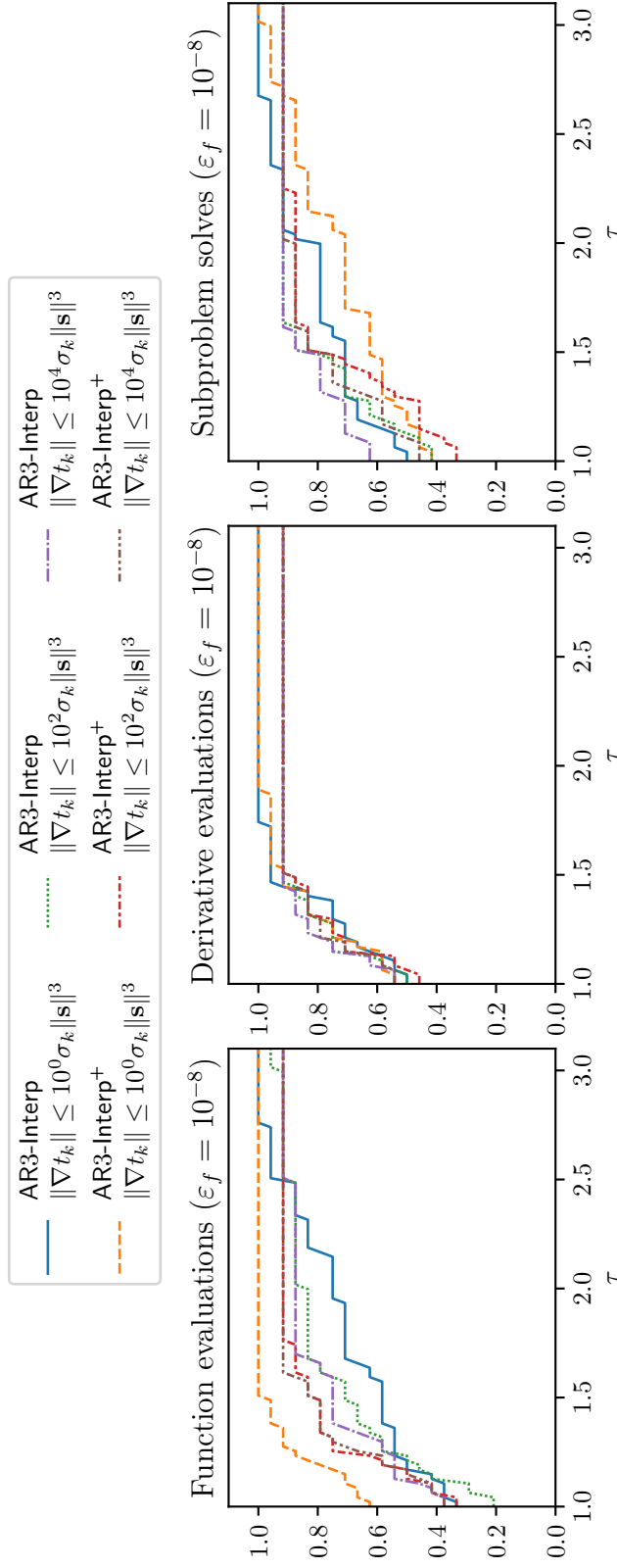


Figure 32: The performance profile plot shows the differences between $\theta \in \{10^0, 10^2, 10^4\}$ in (TC.g) for both AR3-Interp and AR3-Interp+.

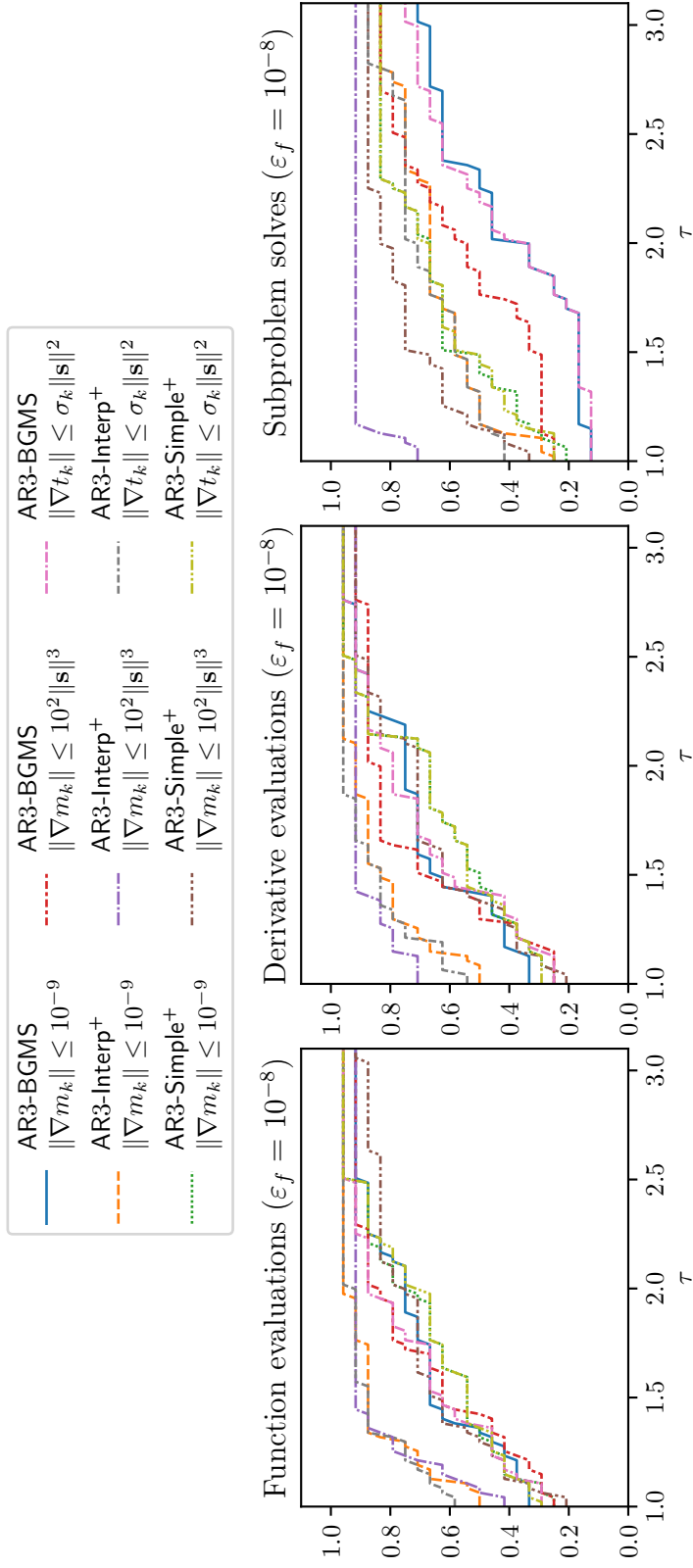


Figure 33: The performance profile benchmark plot shows the differences between AR3-Simple⁺, AR3-Interp⁺, and AR3-BGMS using three termination conditions: (TC.a) with $\varepsilon_{\text{sub}} = 10^{-9}$, (TC.r) with $\theta = 100$, and (TC.g) with $\theta = 1$. This experiment uses the full 35 MGH test set.

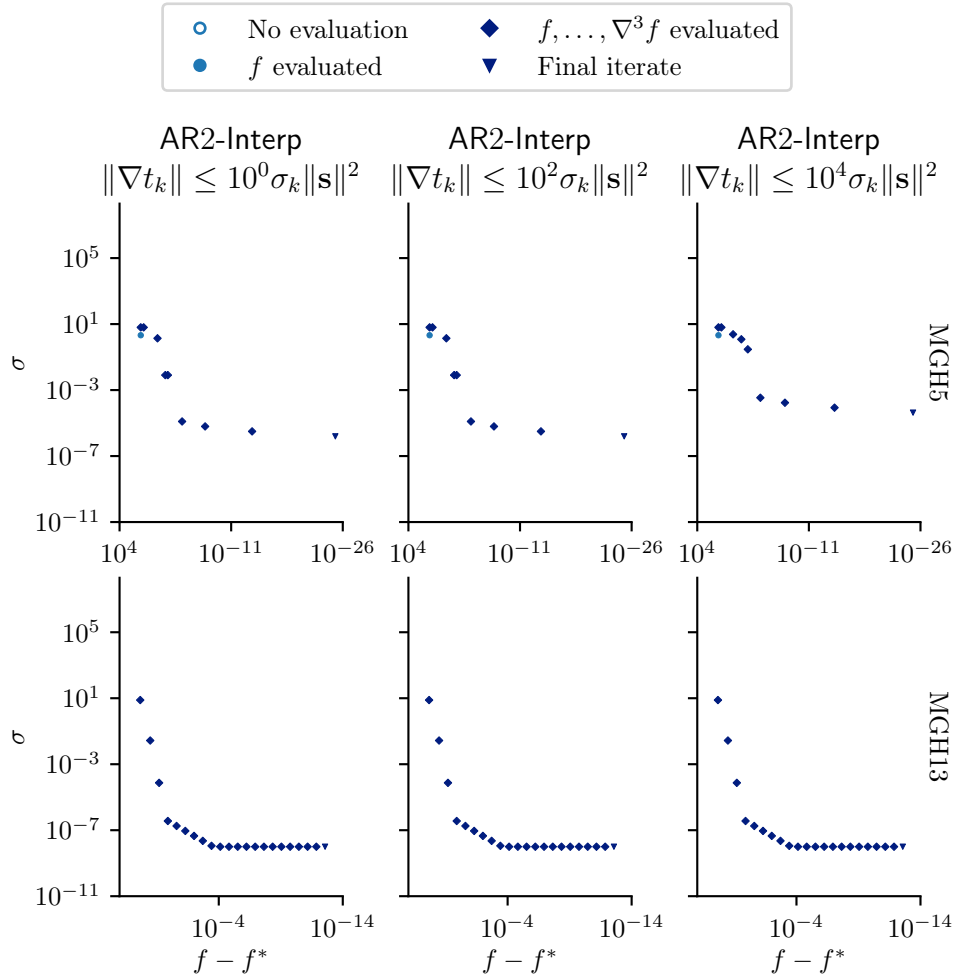


Figure 34: The convergence dot plot shows the differences between $\theta \in \{10^0, 10^2, 10^4\}$ in the subproblem termination condition (TC.g) for AR2-Interp.

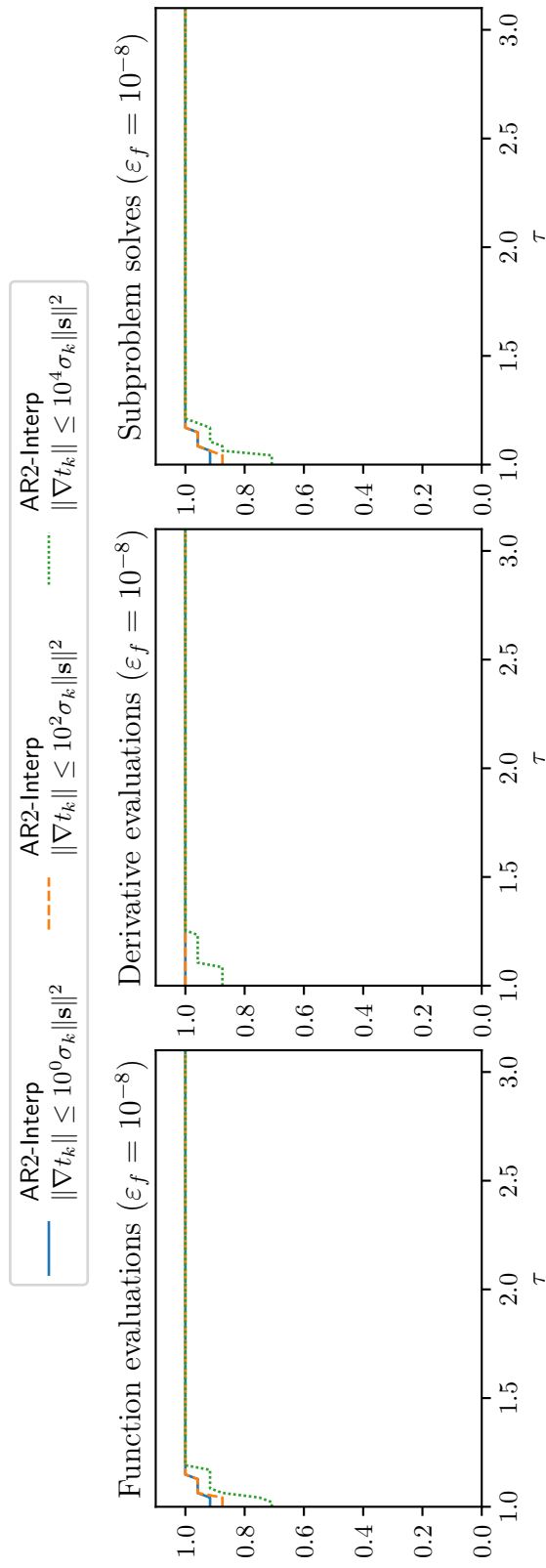


Figure 35: The performance profile plot shows the differences between $\theta \in \{10^0, 10^2, 10^4\}$ in the subproblem termination condition (TC.g) for AR2-Interp.

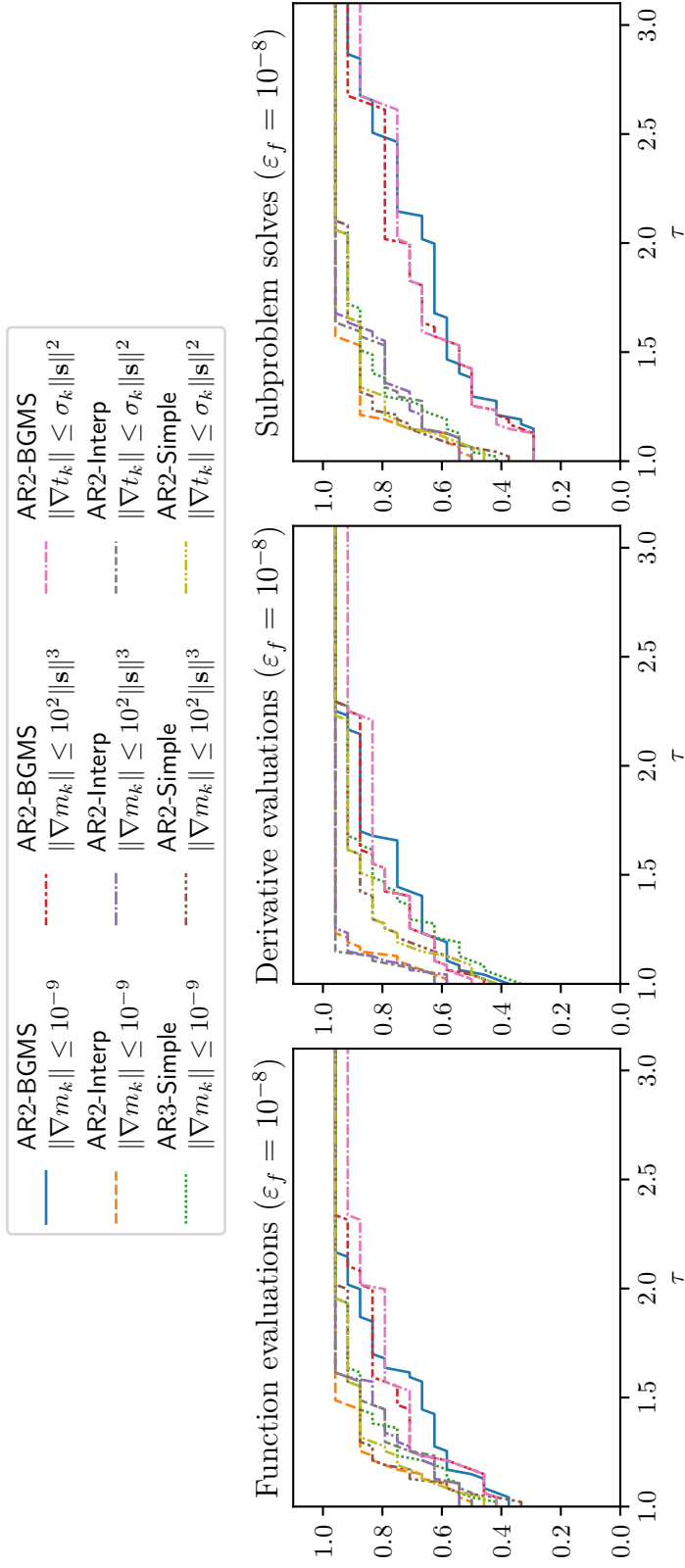


Figure 36: The performance profile benchmark plot shows the differences between AR2-Simple, AR2-Interp, and AR2-BGMS using three termination conditions: (TC.a) with $\varepsilon_{\text{sub}} = 10^{-9}$, (TC.r) with $\theta = 100$, and (TC.g) with $\theta = 1$. This experiment uses the full 35 MGH test set.

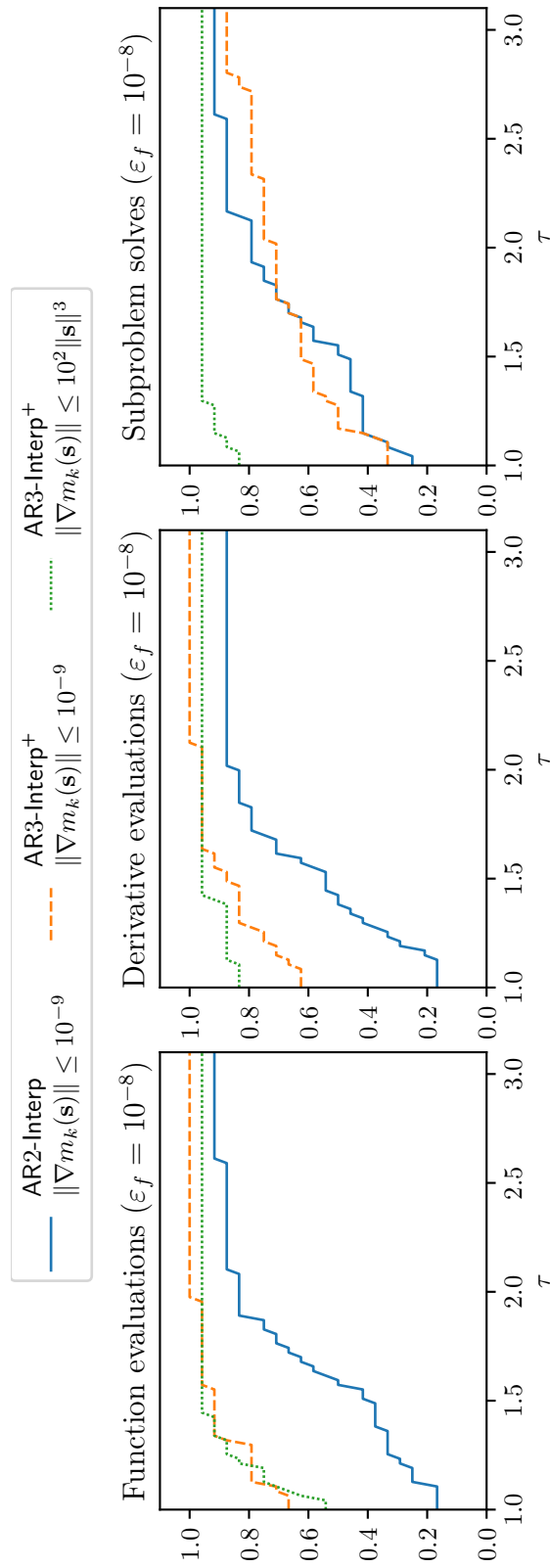


Figure 37: The performance profile plot compares the AR2-Interp and AR3-Interp+ variants using 18 odd MGH test problems and 6 additional test problems.

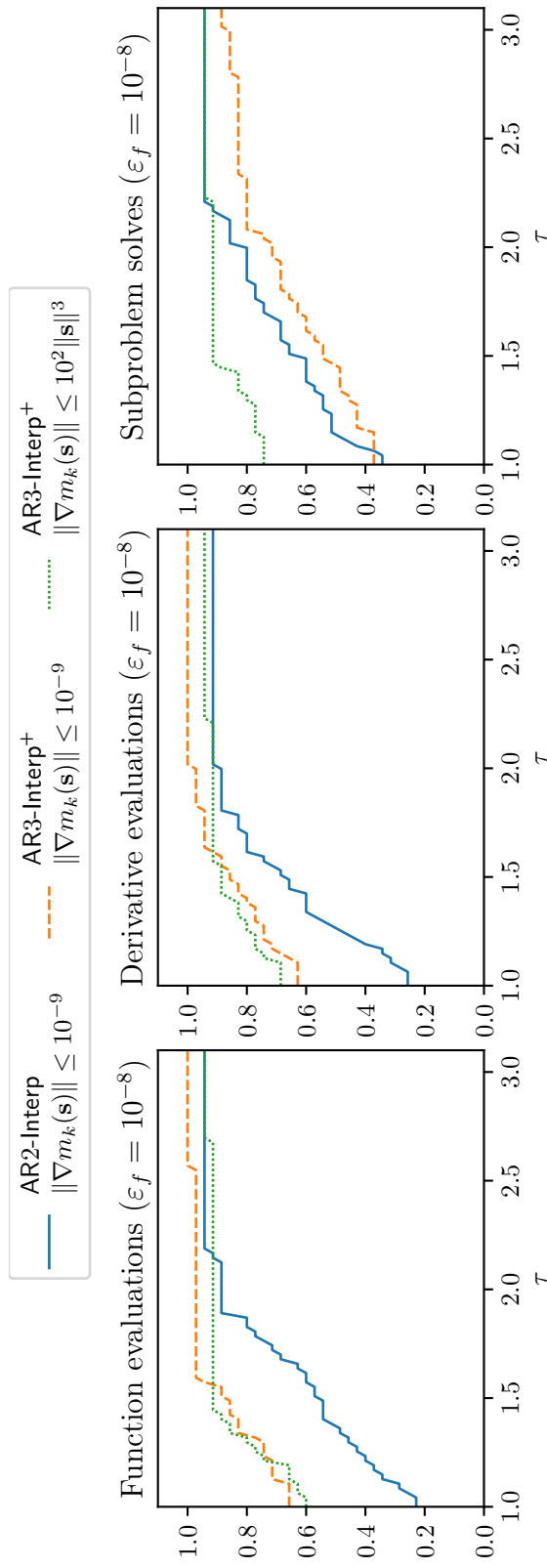


Figure 38: The performance profile plot compares the AR2-Interp and AR3-Interp+ variants using full 35 MGH test set.

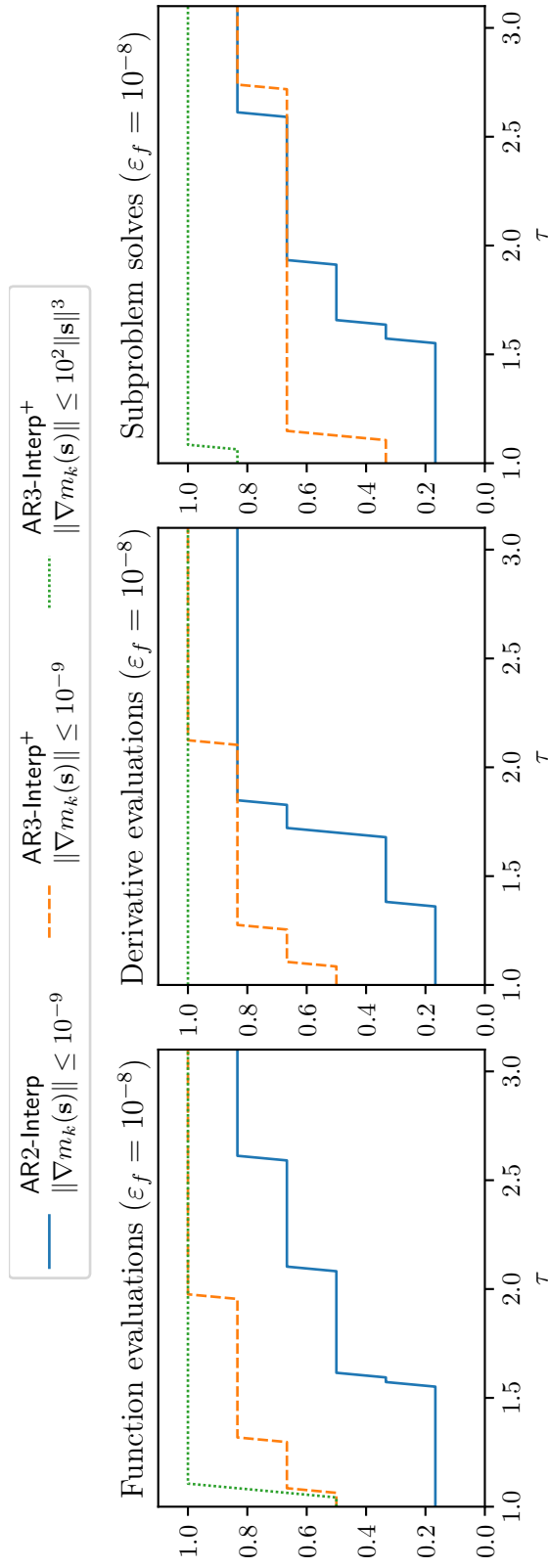


Figure 39: The performance profile plot compares the AR2-Interp and AR3-Interp⁺ variants using 6 additional test problems

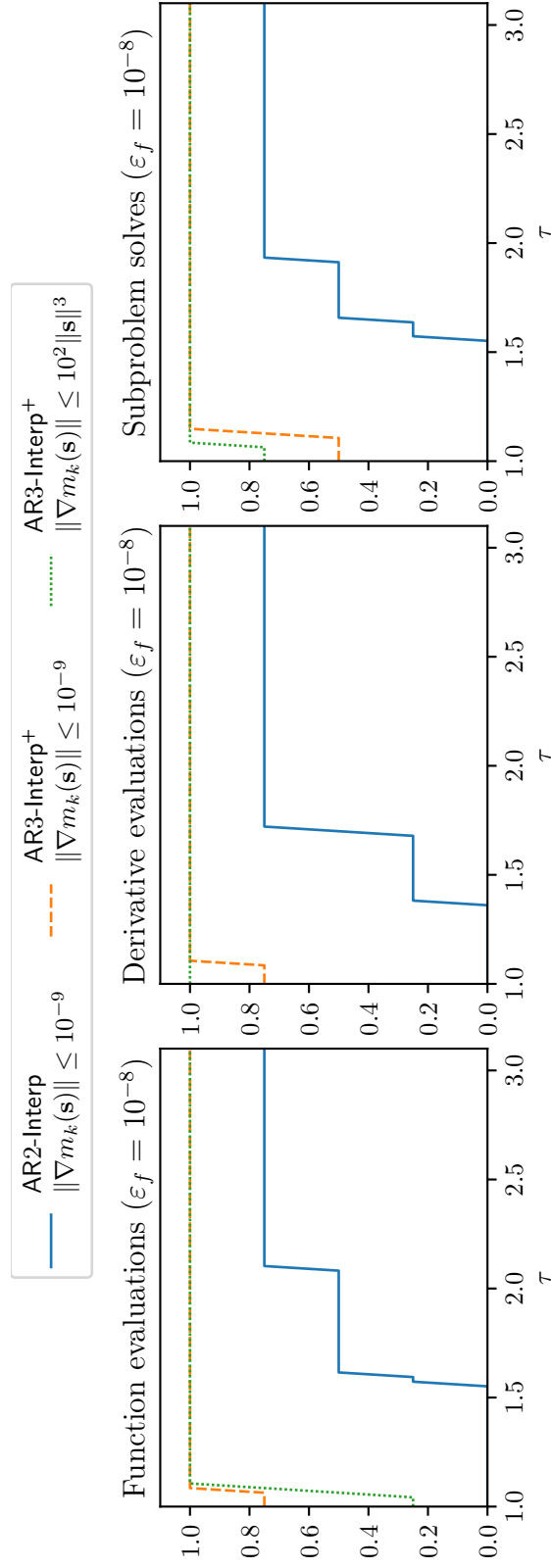


Figure 40: The performance profile plot compares the AR2-Interp and AR3-Interp+ variants using 4 regularized third-order polynomials test problems